

## ABSTRACT

Title of Document:           Blueprinting Self-Assembled Soft Matter: An ‘Easy’  
Approach to Advanced Material Synthesis in Drug  
Delivery and Wound Healing  
Matthew Dowling, Doctor of Philosophy, 2010

Directed By:                 Professor Srinivasa R. Raghavan, Department of Chemical  
and Biomolecular Engineering

From Jello to mayonnaise to silly putty to biological cells, our world is replete with “**soft matter**” – materials that behave as soft, deformable solids or highly viscoelastic liquids. Living systems, in particular, can be thought of as extremely sophisticated ‘soft’ machines, with each cellular unit representing a touchstone for the functional potential of soft materials built via self-assembly. Drawing inspiration from biology, we blueprint soft biomaterial designs which rely upon self-assembly to achieve enhanced functionality. As opposed to complex synthesis schemes often used to develop improved biomaterials, we take an ‘easy’ approach by allowing relatively simple molecules orchestrate themselves into advanced machines. In this dissertation, we describe four separate “soft” systems, all constructed by self-assembly of amphiphilic molecules under designed and/or triggered conditions in aqueous media. These systems revolve around a common theme: the structural tandem of (1) *vesicles* and (2) *biopolymers*, and the resulting interactions between the two. Our blueprints show promise in several important biomedical applications including controlled drug release, tissue engineering, and wound care.

In the first part of this study, we blueprint a biopolymer gel that entraps pH-sensitive vesicles. The vesicles are formed by the self-assembly of a single-tailed fatty acid surfactant. We show that the gel has pH-responsive properties imparted upon it via the embedded vesicle nanostructures. Specifically, when the gel is brought in contact with a high pH buffer, the diffusion of buffer into the gel disrupts the vesicles and transforms them into micelles. Accordingly, a vesicle-micelle front moves through the gel, and this can be visually seen by a difference in color. The disruption of vesicles means that their encapsulated solutes are released into the bulk gel, and in turn these solutes can rapidly diffuse out of the gel. Thus, we can use pH to tune the release rate of model drug molecules from these vesicle-loaded gels into the external solution.

In the second part, we have blueprinted hybrid biopolymer capsules containing drug-loaded vesicles by means of a one-step self-assembly process. These capsules are called “motherships” as each unit features a larger container, the polymer capsule, carrying a payload of smaller vesicular containers, or “babyships,” within its lumen. These motherships are self-assembled via electrostatic interactions between oppositely charged polymers/surfactants at the interface of the droplet. Capsule size is simply dictated by drop size, and capsules of sizes 200-5000  $\mu\text{m}$  are produced here. Lipid vesicles, i.e. the babyships, are retained inside motherships due to the diffusional barrier created by the capsule shell. The added transport barrier provided by the vesicle bilayer in addition to the capsule shell provides sustained drug release from the motherships. Furthermore, this one-step drop method allows for the rapid synthesis of soft materials exhibiting structural features over a hierarchy of length scales, from *nano-*, to *micro-* to *macro-*.

Thirdly, we have therapeutically functionalized biopolymer films by simply passing a solution of vesicles over the film surface. We deposit films of an associating biopolymer onto patterned solid substrates. Subsequently, these polymer films are able to spontaneously capture therapeutically-loaded vesicles from solution; this is demonstrated both for surfactant as well as lipid vesicles (liposomes). Importantly, it is verified that the vesicles are *intact* – this is shown both by direct visualization of captured vesicles (via optical and cryo-transmission electron microscopy) as well as through the capture and subsequent disruption of drug-filled vesicles. Such therapeutically-functionalized films may be of use in the treatment of chronic wounds and burns.

Lastly, we have demonstrated that the addition of a certain biopolymer transforms a suspension of whole blood into a gel. This blueprint is inspired from previous research in our group on the biopolymer-induced gelation of vesicles, which are structurally similar to cells. Upon mixture with heparinized human whole blood, this amphiphilic biopolymer rapidly forms into an “artificial clot.” These mixtures have highly elastic character, with the mixtures able to hold their own weight upon vial inversion. Moreover, the biopolymer shows significant hemorrhage-controlling efficacy in animal injury models. Such biopolymer-cell gelation processes are shown to be reversed via introduction of an amphiphilic supramolecule, thus introducing the novel concept of the “reversible hemostat.” Such a hemostatic functionality may be of large and unprecedented use in clinical the treatment of problematic hemorrhage both in trauma and routine surgeries.

BLUEPRINTING SELF-ASSEMBLED SOFT MATTER:  
AN 'EASY' APPROACH TO ADVANCED MATERIALS SYHNTHESES IN DRUG  
DELIVERY AND WOUND HEALING

Matthew B. Dowling

Dissertation Submitted to the Faculty of the Graduate School of the  
University of Maryland, College Park, in partial fulfillment  
of the requirements for the degree of  
Doctor of Philosophy  
2010

Advisory Committee:

Prof. Srinivasa R. Raghavan, Dept. of Chemical and Biomolecular Engineering, Chair

Prof. William E. Bentley, Fischell Dept. of Bioengineering

Prof. Philip R. DeShong, Dept. of Chemistry and Biochemistry

Prof. John P. Fisher, Fischell Dept. of Bioengineering

Prof. Gregory F. Payne, Dept. of Bioengineering

© Copyright by  
Matthew Dowling  
2010

## **Acknowledgements**

First and foremost, I would like to thank my advisor Dr. Srinivasa Raghavan. I simply cannot begin to thank him for the past five years. He has not only been the most influential person on my scientific career, but on my entire outlook in life. His influence has been massively positive on my graduate career and has provided an amazing foundation from which to advance my career. Being able to work in his group has been an unbelievable blessing. His inspiration, outlook and enthusiasm are infectious, and it indeed translates into the impressive production and attitude of his group members. I owe all of my successes in grad school to him. He is truly a model educator.

Next, I would like to thank my family for their unending support. I am particularly grateful to my parents, Tom and Sandy, who have instilled in me a priority of extremely high value on education. Only in graduate school have I been able to truly see why education really is the foundation for the future, and I thank them for force-feeding that to me early in life. Also, I thank my siblings, Laura, Chris, Tommy, Stephen and William, for their belief in me in whatever I pursue, and for their humor when I need a laugh. I believe in all them and I hope that I can inspire them in the way that they inspire me.

I would also like to thank my committee: Dr. William Bentley, Dr. John Fisher, Dr. Philip DeShong, and Dr. Greg Payne. I've collaborated with every one their labs at some point or another in the past five years. All of them have done world-class research that I could not help but be interested in learning more about during my time here at UMD. They have all developed some amazing grad students who share their advisors'

love of learning and collaborative spirit. This is a testament to what makes Clark School such a great place to do graduate research and why the Fischell Department, in particular, is moving up the national ranks so quickly. Thank you to my collaborators at University of Maryland, Baltimore, Dr. Hamid Ghandehari (now at Univ of Utah) and Dr. Anjan Nan in the Pharmacy School, and Dr. John Hess and Dr. Grant Bochicchio at the School of Medicine. Working with these researchers has allowed me to gain absolutely invaluable clinical insight into the problem that I frame from a basic materials development standpoint.

I am infinitely grateful to all of my past and present fellow labmates in Dr. Raghavan's lab: Jaeho Lee, Hee-Young Lee, Shihuang Tung, Bani Cipriano, Aimee Ketner, Rakesh Kumar, Kunshan Sun, Chao Zhu, Oluwatosin Ogunsola, Peter Thomas, George Chacko, Khyati Tiwari, Vishal Javvaji, Veidhes Basrur, Kunqiang Jiang, Neville Fernades and Charles Kuo. Without you guys, my research would amount to nothing. This is not to mention some outstanding undergrads I have had the pleasure of working with as a grad mentor including Mark Keibler, Patrick Kelleher, Nick Levy, Leigh Quang, Shelby Skoog, Datren Chiou, Gabrielle Galvez, Joe Bender, Jerry Wierwille and Alex Gedra. A number of them have gone on to top 10 graduate engineering programs, and that makes me truly proud.

I certainly have to give a great deal of special thanks to my Remedium Technologies co-founders, Peter Thomas, Oluwatosin Ogunsola, Bani Cipriano and Chao Zhu. In some sense, I feel like we have achieved the "impossible" by starting a biotech company as grad researchers. The undying enthusiasm of these colleagues has helped push me to achieve feats of which I thought I was not capable; not the least of which are

a number of instances of getting back “in the saddle” after some very frustrating failures. Furthermore, MTECH has been massively instrumental in supporting Remedium via the MIPS and VA programs. Special thanks to Martha Connelly, Jim Chung, Dean Chang, Akbar Dawood, John Shin, Herb Rabin and Karen Thornton. Without the support and guidance of these individuals, the company would simply be non-existent.

I have to acknowledge my great friends and fellow musicians/entrepreneurs, Daniel Scheurman, Brian Hospital, Dominic Campanaro and Chris Scheffey. I’ve learned so much from these guys and been through so many unforgettable experiences. Your insight into life is consistently inspiring. Your humor is addictive. Your talents are endless.

I deeply thank my girlfriend, Katie Horner, who has been my rock over the past many years. Without her support, I’d be nowhere. I’m excited for our future together and for her upcoming graduate career at NYU.

Last, but not least, I thank Dr. Robert Fischell for his support of my graduate research and entrepreneurship via the Fischell Fellowship in Biomedical Engineering. His inspiration and example has driven me over the years to work relentlessly in both science and business, and to learn how the two can work together to create real solutions for the improvement of human health. I’m forever indebted to his generosity and his spirit.



# TABLE OF CONTENTS

<b>Acknowledgements</b> .....	ii
<b>Table of Contents</b> .....	v
<b>List of Tables</b> .....	vii
<b>List of Figures</b> .....	viii
<b>1. Introduction and Overview</b> .....	1
1.1. Problem Description and Motivation.....	1
1.2. Our Approach .....	3
1.3. Significance of this Work.....	8
<b>2. Background</b> .....	11
2.1. Vesicles and Liposomes .....	11
2.2. Associating Polymers.....	17
2.3. Biopolymers .....	19
2.4 Cyclodextrins .....	24
2.5. Characterization Technique – I: Rheology.....	26
2.6. Characterization Technique – II: SANS .....	30
2.7. Characterization Technique – III: DLS.....	32
2.8. Characterization Technique – IV: Cryo-TEM.....	33
<b>3. Biopolymer Gels Containing pH-Sensitive Vesicles</b> .....	36
3.1. Introduction .....	36
3.2. Experimental Section .....	40
3.3. Results and Discussion .....	42
3.4. Conclusions .....	57

<b>4. Biopolymer Capsules Containing Vesicles</b> .....	58
4.1. Introduction .....	58
4.2. Experimental Section .....	65
4.3. Results and Discussion .....	70
4.4. Conclusions .....	80
<b>5. Vesicles Capture on Patterned Surfaces Coated with Amphiphilic Biopolymer..</b>	82
5.1. Introduction .....	82
5.2. Experimental Section .....	86
5.3. Results and Discussion .....	90
5.4. Conclusions .....	102
<b>6. Gelling Blood with an Amphiphilic Biopolymer.....</b>	104
6.1. Introduction .....	104
6.2. Experimental Section .....	108
6.3. Results and Discussion .....	112
6.4. Conclusions .....	122
<b>7. Conclusions and Recommendations.....</b>	124
7.1. Conclusions .....	124
7.2. Recommendations for Future Work .....	126
<b>8. References .....</b>	130

## LIST OF TABLES

**Table 2.1.** Properties of the three naturally occurring cyclodextrins 26

**Table 3.1.** Parameters obtained by fitting Peppas Equation to dye release curves 56

## LIST OF FIGURES

- Figure 1.1.** Overview of the Four Blueprinted Self-Assembled Soft Systems. (a) *Controlled-Release Jello*: pH-Sensitive Vesicles within Biopolymer Gels, (b) ‘*Mothership*’ *Drug Carriers*: Biopolymer Capsules Containing Vesicles; (c) *Band-Aids* for Chronic Wounds: Biopolymer Films Capturing Vesicles; (d) Self-Assembled *Hemostats*: Associating Biopolymers Gelling Vesicles/Cells 4
- Figure 2.1.** The structure of vesicles formed by the self-assembly of amphiphiles. The vesicle is formed by the folding of an amphiphilic bilayer that is about 2-5 nm in thickness. 12
- Figure 2.2.** Schematic illustration of the formation of vesicles by self-assembly of amphiphilic molecules in water. Due to their cylindrical geometry, lipids, which are two-tailed amphiphiles, can form vesicles in aqueous solution upon folding of lipid bilayers into spheroid structures represented in the cartoon above. Also, pairs of fatty acid surfactants can collectively take on a cylindrical geometries and, thus, form vesicles in the same way as lipids. 14
- Figure 2.3.** Preparation of unilamellar lipid vesicles of various sizes: (a) small or large vesicles (20 nm – 200 nm);<sup>20</sup> (b) giant vesicles by electroformation 17
- Figure 2.4.** Architecture of a telechelic associating polymer and the structures formed by its self-assembly in aqueous solution 18
- Figure 2.5.** Structures of the parent sugars in (a) chitin and (b) chitosan. The N-acetyl-D-glucosamine sugar in chitin is deacetylated to give the D-glucosamine sugar in chitosan. 21
- Figure 2.6.** Structure of hydrophobically-modified chitosan (hm-chitosan) with C<sub>12</sub> hydrophobic tails. 22
- Figure 2.7.** Structure of Gellan Gum 24
- Figure 2.8.** Truncated cone-shaped conformation of  $\beta$ -CD 25
- Figure 2.9.** Photograph of the Rheometer RDA-III strain-controlled rheometer being operated in a cone-and-plate geometry. 27
- Figure 2.10.** Schematic of a SANS experiment. 30
- Figure 2.11.** Photograph of the controlled environment vitrification system (CEVS) used for sample preparation in cryo-TEM. The schematics on the left show the various steps in the process. 35

**Figure 3.1.** Photographs and titration curve for 1% NaOA at 25°C. Increasing amounts of 1 M HCl are added to a micellar solution of NaOA (pH 10) and the corresponding solution pH at equilibrium is shown in the plot. Structural assignments are done in accordance with Ref. 10. Photographs of samples corresponding to different regions of the plot are shown above. 43

**Figure 3.2.** Photographs and schematics of (a) gelatin gel; (b) NaOA vesicles; (c) gelatin gel loaded with NaOA vesicles. The gelatin gel is a 3-D network of gelatin chains, with chain segments connected into triple helices at the crosslink points. When vesicles of diameter  $\sim 100$  nm are entrapped in the gelatin gel, the initially colorless gel assumes a bluish hue due to light scattering from the vesicles. 45

**Figure 3.3.** SANS data at 25°C for 0.5% NaOA vesicles at pH 8.3 (circles) and a 5% gelatin gel loaded with 0.5% NaOA vesicles (squares). In both cases, the intensity  $I$  follows a slope of  $-2$  at moderate  $q$ , which is characteristic of scattering from vesicles. 47

**Figure 3.4.** Movement of micellar front within a vesicle gel due to diffusion of pH 10 buffer. The buffer is introduced into the headspace above the gel at time zero. As the buffer diffuses into the gel, NaOA vesicles in the gel are converted into NaOA micelles, as indicated by the change in a portion of the gel from bluish to colorless. As time progresses, the micellar front travels deeper into the gel, indicating that more of the vesicles are converted into micelles. After 9 h, the micelle region covers most of the gel. The plot on the right shows the interface position (measured from the top of the vial) as a function of time. The line through the data is a fit to eq 1. 49

**Figure 3.5.** Patterning of vesicle gels by inducing localized vesicle to micelle transitions. (Top panel): core-shell structure with a vesicle-rich core surrounded by a micelle-rich shell. This is accomplished by immersing a spherical gel (41 mm diameter) in a pH 10 buffer. The photographs correspond to increasing incubation times in this buffer solution. (Bottom panel): gel in a petri dish with micelle-rich regions created at discrete points. This was done by sticking straws into the gel and subsequently filling the straws with the pH 10 buffer. The photographs again correspond to increasing times and show the expansion of the micelle-rich regions as the buffer diffuses into the gel. 51

**Figure 3.6.** Release profiles of calcein dye from a gelatin gel and from a vesicle-loaded gelatin gel. In the case of the vesicle-gel, the dye was encapsulated within the vesicles, which were then embedded within the gel. The data show a slower release of dye from the vesicle-gel relative to the control gelatin gel. After 10 h, Triton X-100 detergent was added to the external solution for both samples (this point is marked by the arrow). The detergent diffused in and disrupted the vesicles, which lead to an increase in the rate of dye release. 53

**Figure 3.7.** Tunable calcein release from a vesicle-loaded gel based on the pH of the external solution. The control is a gelatin gel surrounded by a pH 8.3 buffer and in this case (red circles), the dye is released rapidly. The same gel loaded with vesicles releases dye much more gradually at pH 8.3 (green hexagons): in this case, the vesicles are intact and the vesicle bilayer thus presents a transport resistance. On the other hand, if the same vesicle-loaded gel is placed in contact with pH 10 buffer, the dye release is more rapid (blue triangles): in this case, the high pH converts the vesicles into micelles, thereby eliminating the transport resistance due to the vesicle bilayers. All the data are fit to eq 2 and the fit parameters are shown in Table 1. 55

**Figure 4.1. Formation Chitosan ‘mothership’ capsules containing vesicles.** Capsules are formed by dropping a positively-charged amphiphilic biopolymer mixed with vesicles (~100 nm in size) into a solution of negatively charged SDBS surfactant or negatively charged gellan gum biopolymer. Spherical capsules are formed instantaneously. Capsule size is dictated by droplet size and sizes can range from ~100  $\mu\text{m}$  (*micro*) to 10,000  $\mu\text{m}$  (*macro*) 62

**Figure 4.2. Schematic of Chitosan ‘mothership’ capsules attacking a tumor.** In step (1), the microcapsule “motherships” would be docked at the tumor site using antibodies or magnetic targeting and thereafter release one drug from the capsule lumen (e.g. an anti-angiogenic drug). In step (2), capsule shell would become ruptured due to enzymatic degradation, and “babyship” vesicles carrying cytotoxic drug would escape freely into the tumor tissue. 64

**Figure 4.3. Controlled Release of Dye from ‘Mothership’ Capsules.** In (a), a sustained release is observed for chitosan-gellan capsules impregnated with carboxyfluorescein-loaded liposomes (red circles). Chitosan-gellan control capsules with dye freely dispersed inside the capsule lumen shows a “dosage dumping” release profile (blue circles). Addition of Triton X-100 at 3.25 h shows a spike in dye release for “mothership” capsules, indicating vesicle intactness. In (b), chitosan-SDBS capsules impregnated with CF-loaded liposomes show (blue circles) show a similar release profile to control capsules containing no liposomes (yellow triangles), suggesting potential liposome rupture during capsule formation. In contrast, hm-chitosan capsules formed in SDBS while retaining liposomes, shows a sustained release over a 2 hour interval. 72

**Figure 4.4.** Magnetically targeted ‘mothership’ capsules via encapsulated ferrite nanoparticles show their magnetic properties in response to a bar magnet. (a) magnet placed near capsules in a vial (b) magnet placed next to a tube in which the capsules are flowing along with the fluid (water) from left to right. 74

**Figure 4.5. Antibody targeted ‘Motherships.** (a) Fluorescently tagged primary IgG antibody (emission 600 nm) is covalently conjugated to the surface of a Chitosan-SDBS “mothership” capsule as shown by fluorescence micrograph. After incubation with a secondary anti-IgG antibody and subsequent rinsing, fluorescent signal at 520 nm is

observed, indicating that a significant amount of primary surface IgG is actively available for “lock-and-key” binding. 75

**Figure 4.6. Enzymatic Degradation of ‘Mothership’ Capsules.** (a) Phase contrast micrograph of Chitosan – Gellan capsules formed by standard drop method via 22G syringe needle; (b) 1h, 2d, and 5d micrographs of chitosan-gellan capsule after addition of 10 units/ml of chitosanase in external buffer solution. Capsule appears almost wholly degraded after the studied 5 day interval. Note that the chitosanase cannot degrade chitosan capsules formed with SDBS. 77

**Figure 4.7. Schematic of hierachical nano-micro-macro ‘motherships.’** By a simple one-step self-assembly process, structures displaying a hierchary of length scales, from nano (i.e. vesicles), to micro (microcapsules), to macro (large capsules) can be produced. These structures can package a wide variety of molecules and targeting agents either on their surface, or within their multi-level lumens. 78

**Figure 4.8. Phase Microscopy (2.5×) of Capsules-within-capsules.** Small Chitosan SDBS capsules were formed by the standard drop method via 22G syringe needle. After incubation, capsules were removed from SDBS solution and placed into a fresh chitosan solution. Chitosan solution containing capsules was uptaken by a wide-aperture fluid transfer pipet and dispensed dropwise into a solution of SDBS, thus forming capsule-within-capsule structures. 79

**Figure 4.9. Release of dye from capsules-within-capsules.** Release of carboxyfluorescein dye from smaller capsules packaged with larger capsules (red circles) is significantly sustained over a 24 period relative to the same number of small capsules freely dispersed in aqueous buffer (blue circles). 80

**Figure 5.1. Schematic showing the spatiotemporal capture of vesicles using hm-chitosan.** The structure of hm-chitosan as well as a schematic of its chain are shown in the top left. The chain has a hydrophilic backbone shown in blue and pendant hydrophobes ( $C_{12}$  tails) that are shown in red. In step (1), thin films of hm-chitosan are electrodeposited onto gold cathodes that are patterned on a silicon chip. Next, in step (2), the chip is incubated with a solution of vesicles. Intact vesicles become spontaneously anchored onto the polymer films. The inset shows the likely mechanism for such anchoring, which is via non-covalent interaction between the hydrophobes on the polymer and vesicle bilayers. 85

**Figure 5.2.** Photograph of micropatterned chips used in this study. The leads and electrodes are formed by depositing gold on a silicon wafer using lithographic techniques. On the left is a 2-electrode chip and on the right a 6-electrode chip. A US penny is shown for size comparison. 92

**Figure 5.3:** Comparison of hm-chitosan (H) and chitosan (C) films in terms of their ability to capture vesicles. *Top images:* Green-filtered fluorescence micrographs showing deposition of NHS-tagged hm-chitosan on the left electrode and NHS-tagged chitosan on the right electrode of a two-electrode chip. The chips are then incubated with vesicles for 10 min, followed by rinsing with DI water. *Bottom images:* Red-filtered fluorescence micrographs showing the presence of DiI-tagged vesicles on the electrodes. The results in (a) (left-column) are obtained with cationic surfactant vesicles, while those in (b) (right-column) are obtained with liposomes. In both cases, the vesicles are anchored preferentially to the hm-chitosan film than to the chitosan one. 94

**Figure 5.4:** Variation in the extent of vesicle capture based on the time of chip incubation with a vesicle solution. Hm-chitosan (H) and chitosan (C) are deposited on the left and right electrodes, respectively. The chip is incubated with a solution of surfactant vesicles for different lengths of time and then imaged by fluorescence microscopy. The images are red-filtered fluorescence micrographs showing DiI-tagged vesicles on the electrodes. A constant exposure time of 20 s at the excitation wavelength was used to obtain each image. The results show increasing capture of vesicles on the H side and negligible capture on the C side. 96

**Figure 5.5:** Immobilization of giant unilamellar vesicles (GUVs) on an hm-chitosan film. After 10 min incubation with DiI-tagged GUVs, multiple red-fluorescent ‘hot spots’ appear on the electrode bearing hm-chitosan. A zoomed-in image of a ‘hot-spot’ shows an intact GUV of ca. 20  $\mu\text{m}$  diameter. 97

**Figure 5.6:** Evidence for intact capture of liposomes on hm-chitosan films. (a) Green-filtered fluorescence image showing preferential binding of liposomes (filled with the hydrophilic dye CF) to the hm-chitosan (H) side relative to the chitosan (C) side. The chip is then exposed to the detergent Triton X-100 and rinsed. The detergent disrupts the liposomes into micelles, as shown by the schematics, and the encapsulated dye is thus released and washed away. (b) Fluorescence image of the rinsed chip shows nearly complete loss of fluorescent signal, confirming disruption of originally intact liposomes. 98

**Figure 5.7:** Cryo-TEM image of vesicles on an hm-chitosan film. The hm-chitosan was deposited on the TEM grid and then used to capture surfactant vesicles from solution. The image shows numerous spherical objects of  $\sim 100\text{--}150$  nm diameter, which are presumably intact vesicles. 99

**Figure 5.8:** Patterning of vesicles on 6-electrode chips. (a) NHS-tagged hm-chitosan (H) and chitosan (C) are electrodeposited in an alternating pattern, HCHCHC. (b) Following contact with DiI-tagged surfactant vesicles and rinsing, the red fluorescence indicative of vesicles is found only on the H electrodes. (c) H and C are electrodeposited in an ‘outside-inside’ pattern, HCHHCH. (d) Once again, DiI-tagged surfactant vesicles are found anchored only on the H electrodes. 100



**Figure 5.9:** Protein sensing via vesicles anchored to an hm-chitosan film. (a) Schematic of the experiment: biotin-decorated liposomes are first immobilized, then the chip is contacted with the fluorescently labeled protein, FITC-streptavidin. The binding of the protein is then detected by fluorescence microscopy. (b) Fluorescence image showing a strong signal from the hm-chitosan (H) electrode compared to the chitosan (C) electrode. The strong signal is indicative of protein binding to the biotins on the anchored liposomes. (c) Analysis of the intensities in (b). The average gray values for each electrode area are listed above the corresponding regions. 102

**Figure 6.1. Schematic of hydrophobically-modified (hm)-chitosan as a self-assembling hemostat.** When adding hm-chitosan to a whole blood cell suspension, the resulting mixture self-assembles into a 3-dimensional network. This self-assembly is driven by insertion of hydrophobes into blood cell membranes and the subsequent physical crosslinking of adjacent cells. 107

**Figure 6.2. Comparison of the native and hydrophobically-modified polymers with regard to their physical influence on blood.** In (a), photographs show hm-chitosan at 0.25 wt% mixed with heparinized human whole blood (50 wt %) is able to hold its weight upon test tube inversion, whereas unmodified chitosan at 0.25 wt% mixed with heparinized human whole blood (50 wt %) remains as a liquid. A cartoon of the proposed “bridging” effect of hm-chitosan on blood cells is shown above the left photograph; a contrasting schematic of unmodified chitosan mixed with blood is above the right photograph. In (b), steady shear rheology displays a dramatically increased ( $\sim O(10^5)$ ) zero-shear viscosity of the hm-chitosan-blood mixture (red circles), relative to both hm-chitosan (0.25 wt%) with no blood (cyan hexagons) and chitosan-blood (yellow triangles) controls. In (c), dynamic rheology of the hm-chitosan blood mixture ( $G'$ , closed red circles,  $G''$  closed green triangles) is that of gel-like elastic material which relaxes slightly over time, whereas rheology of the unmodified chitosan/blood mixture ( $G''$ , open green triangles,  $G'$ , open red circles) is that of a viscous sol 112

**Figure 6.3. Time-to-gelation of hm-chitosan/blood mixtures.** In (a), a time-sweep of an hm-chitosan (0.25%)/blood (50%) mixture displays the characteristics of an elastic material ( $G'$  [red triangles]  $>$   $G''$  [green triangles]) over the studied interval of 11 min.  $G' > G''$  immediately at  $t = 0$  min for this sample. In (b), unmodified chitosan (0.25%)/blood (50%) mixture shows that the sample remains as a viscous sol ( $G''$  [green triangles]  $>$   $G'$  [red triangles]) over the same interval. Lastly, in (c), a sample comparison in a rat femoral vein injury model demonstrates that hm-chitosan (HM-CS) solution (0.5%) significantly decreases bleeding time relative to saline buffer (SAL) and native chitosan (CS) solution (0.5%) controls. 114

**Figure 6.4. Application of an hm-chitosan sponge to a porcine femoral artery puncture.** In (a) the injury was created in the femoral artery, resulting in high-pulsatile flow. An hm-chitosan is then applied to the injury in (b) by direct compression. After 2 min of compression, the bandage is observed in (c) to be attached to the wound site and providing hemostasis. The bandage is removed after 180 min (d) with no rebleeding during the studied interval. 117

**Figure 6.5. Dynamic rheology of hm-polymer mixed with separated blood hematocrit and plasma.** The hm-chitosan concentration is maintained at 0.25%. Hematocrit was resuspended in isotonic buffer after centrifugation; plasma was removed and stored for use. Visual observation of an hm-chitosan-hemotacrit mixture shows that the sample can hold its weight upon vial inversion, whereas an hm-chitosan-plasma mixture flows freely as a viscous liquid. Dynamic rheology confirms the visual evidence, as the hematocrit mixed with polymer ( $G'$  [closed red circles] and  $G''$ [closed green circles]) is that of a gel-like elastic material which relaxes slightly over long times. In contrast, the rheology of the plasma mixed with polymer ( $G'$  [open red triangles] and  $G''$ [open green triangles]) is close to that of a sol-gel transition. 119

**Figure 6.6. Reversal of blood-gelation via  $\alpha$ -cyclodextrin (CD).** In (a), a cartoon of  $\alpha$ -CD displays its supramolecular barrel-shaped structure, with hydrophobic core and hydrophilic exterior. A schematic hypothesis shows that by adding these molecules together with hm-chitosan-blood mixtures, the samples become liquefied due to “capping” of hydrophobes by the  $\alpha$ -CD molecules. In (b), dynamic rheology confirms this hypothesis as a hm-chitosan (0.25%)/blood (50%) displays gel-like characteristics ( $G'$  [closed red circles] and  $G''$ [closed green triangles]), whereas a hm-chitosan (0.25%)/blood (50%)/ $\alpha$ -CD (3%) mixture displays the rheology of a freely-flowing liquid ( $G'$  [open red circles] and  $G''$ [open green triangles]). 121

**Figure 7.1. Photolysis of MGC, a photobase generator (PBG).** Upon UV irradiation, the molecule dissociates and releases  $\text{OH}^-$ . 127

# Chapter 1

## Introduction and Overview

---

### 1.1 Problem Description and Motivation

In the current age of micro- and nanotechnology, there is a great deal of interest in making structures, machines, and robots at smaller scales.<sup>3</sup> While processing techniques for metals or plastics are well-established at the macroscale (e.g., > 10 cm), the same techniques can be difficult to implement at smaller scales. For example, the machining or molding of a small (~ 5–10 mm) robot made of metal or plastic is not an easy task. This problem has an important context particularly within the field of nanomedicine. The popularized vision of nanomedicine is to create nano-sized robots, “nano-bots,” which patrol through the body, responding to environmental cues to repair tissue and cure disease when and where required.<sup>4</sup> Despite the fact that such an intriguing and ambitious goal has driven an enormous amount of research over the past 20 years,<sup>5</sup> it is important to take a step back and carefully consider some of the key points Edward Purcell made in his popular 1977 article “Life at Low Reynold’s Number.”<sup>6</sup> Purcell emphasized that everything at the nano-scale essential becomes “sticky,” and, as such, it is very difficult to design hard nanoscale mechanical structures which move and function in a manner uniquely independent from Brownian motion. In plainer terms, building a robot is hard enough....building a robot to operate within a world of sticky, slimy, and grimy “muck” approaches the impossible.

In this context, it is useful to look to nature for inspiration to our nano-machine blueprints, as opposed to simply down-sizing successful macro- or micro-mechanical designs. Nature's equivalents to crawling mini-robots are creatures such as geckos, earthworms, and ants. It is worth noting that these creatures are generally "soft", i.e., they are not hard like metal or plastic, but gooey and pliable like jello or silly putty. Rather than building hard nano-bots to achieve a rigid endpoint, a more sensible approach would be to learn the inner-workings and conditions of these soft biological systems and, subsequently, build structures which complement or cleverly manipulate them in therapeutically beneficial ways.

An excellent system to first study as a means to improved nanomaterial design is the biological cell. No machinery in the history of mankind has ever come close to rivaling its complex set of functionalities and wonderfully robust design. The cell is truly a 'soft machine' which is able to perform such tasks as rapidly build AND disassemble rods and trusses (actin filaments, intermediate filaments, microtubules), periodically replenish its outer shine (synthesis and transport of phospholipids to cell membrane), and reliably respond to myriad electrical and molecular signals from the external environment ( $\text{Na}^+/\text{K}^+$  membrane-associated ion channels). These cellular processes occur via self-assembly (i.e. they are thermodynamically driven,  $\Delta G < 0$ ) within a soft environment. Note that from a materials characterization standpoint, the cell is not a bag of water, but rather a lump of jello. Understanding how the cell's machination works within this 'squishy' and 'sticky' environment is key to making progress in almost any given sub-discipline of nanomedicine including targeted delivery of drugs or genes, controlled release, tissue repair and engineering, and wound healing.

## 1.2 Proposed Approach

We take inspiration from biology to build self-assembled materials which are able to function as soft machines for improved therapies in nanomedicine. In this dissertation, we explore the **integration of polymers with vesicles** as a route to creating new and useful classes of soft materials. Vesicles, of course, are reminiscent of cells in a few key ways: (1) they have a very similar bilayer structure to cell membranes, (2) they have an aqueous core which can hold proteins and/or small molecules and (3) they are able to split/fuse based on particular environmental cues.<sup>7-8</sup> Additionally, the cell uses actual nano-scale ~100 nm vesicles to transport molecules into and out of the cell. The polymers used in our studies are reminiscent of many of the structural polymers which interact with cell membranes and assist in the assembly and transport of vesicles within cells.

Using these 2 key ingredients, (1) **vesicles** and (2) **biopolymers**, we blueprint self-assembled systems in which the polymer plays an active role in creating a carrier or matrix for the vesicles. The resulting hybrid structures impart increased stability, or functional restraint of the self-assembled vesicles. Conversely, the vesicles impart enhanced functionality to the biopolymer. Such “easy” approaches to building materials involve dialing up conditions and environmental triggers such that vesicles and biopolymers build and/or disassemble themselves within aqueous environments. Hence, these approaches are not labor intensive. However, we are indeed able to achieve high-levels of functionality from these systems simply by understanding and appropriately manipulating the factors which drive key self-assembly events. Four specific classes of such systems are investigated. These are depicted in Figure 1.1 and briefly described below.

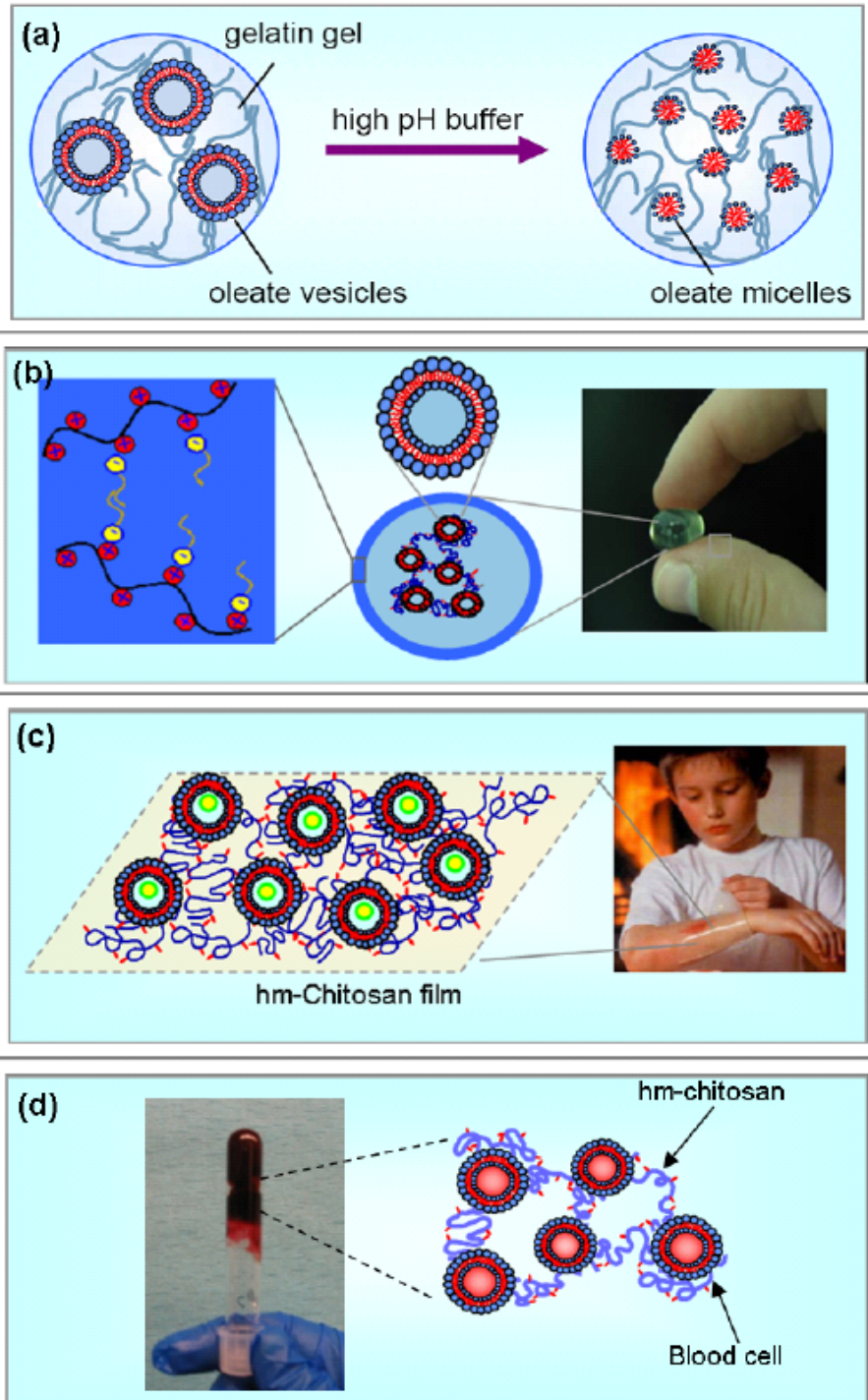


**Figure 1.1.** Overview of the Four Blueprinted Self-Assembled Soft Systems. (a) *Controlled-Release Jello*: pH-Sensitive Vesicles within Biopolymer Gels, (b) *'Mothership' Drug Carriers*: Biopolymer Capsules Containing Vesicles; (c) *Band-Aids for Chronic Wounds*: Biopolymer Films Capturing Vesicles; (d) *Self-Assembled Hemostats*: Associating Biopolymers Gelling Vesicles/Cells

### ***1.2.1 pH-Sensitive Vesicles within Biopolymer Gels***

Vesicles which undergo a self-assembled transition into micelles upon increase in pH will be embedded within a gelatin gel. Here, we anticipate that a biopolymer gel network will form “around” a solution of vesicles, without disrupting the vesicles (Figure 1.1a). The presence of intact vesicles would presumably enhance the functionality of the gel by protecting encapsulated molecules and providing a sustained release of model drug. Presence of intact vesicles within the gel will be tested by a few different experimental methods. Next, a high pH-buffer solution will be placed in contact with the gel. As the high pH buffer diffuses into the gel, we will track the movement of a vesicle-micelle front through the gel as a function of time, and we will also explore the types of vesicle-micelle patterns created by varying the gel geometry and the buffer-gel contact points. Lastly, we will attempt to characterize the vesicle-to-micelle transitions within the gel by packaging dye molecules within the vesicles and attempting to use pH as a trigger for their release. The experimental design and complementing results for this system are explained in detail in Chapter 3.

### ***1.2.2 Vesicles Loaded into Biopolymer Capsules***

Next, we plan to entrap vesicles inside microcapsules made from biopolymers. We call these structures “motherships” as smaller containers, i.e. “babyships,” are protected within a larger container until degradation of the mothership capsule shell. Motherships are formed when droplets of a cationic biopolymer solution mixed with vesicles are added to a solution of anionic biopolymer or surfactant.<sup>5-7</sup> A physical crosslinking occurs at the interface of the drop, leading to an interfacial shell (Figure 1.1b) and this shell

protects the contents of the drop from external stimuli. Capsule size is determined solely by the size of the drop and can be varied from a few millimeters to a few microns. Our goal is to trigger the release of vesicles by tailoring the capsule surface to degrade in response to specific pH transitions. Also, we hope to develop structures displaying features on hierarchy of length scales (from macro to micro to nano) using this single-step drop method by placing micro-scale mothership capsules containing nano-scale vesicles within macro-scale capsules. Details on the results of this proposed approach are explained in Chapter 5.

### ***1.2.3 Vesicles Captured Onto Biopolymer Films***

A challenging problem in materials science is the ability to anchor “soft” biomolecular nanostructures such as vesicles to “hard” surfaces such as gold. For our 3rd blueprint, we approach a simple method to accomplish this kind of anchoring using an amphiphilic biopolymer as an soft “interconnect”. The polymer is hydrophobically-modified chitosan (hm-chitosan), which is obtained by covalently attaching alkyl tails to the backbone of chitosan. We plan to electrodeposit films of hm-chitosan onto microscale gold cathodes formed by lithography on a silicon wafer. Such hm-chitosan films could potentially capture drug-loaded vesicles from solution (Figure 1.1c). If the vesicles remain strongly bound to the films, a method of therapeutically functionalizing the film with multiple agents which are protected from degradation would be achieved in a quick one-step process. We envision such films being used for protection and controlled release of drug to accelerate the healing of chronic wounds of diabetics and burn victims. Additionally,



the immobilized vesicles could also be use for biosensing applications. The results of this approach in explained in Chapter 5.

#### ***1.2.4 Gelling Cells with Biopolymers***

Lastly, we blueprint a system involving biopolymers and *cells*, instead of vesicles. The ability to rapidly self-assemble into a flow-impeding barrier on demand is an ideal feature of hemostat, i.e. a material which controls hemorrhage. Indeed, the self-assembly of fibrinogen into fibrin, the hemostatic “plug” which is naturally observed in mammalian organisms in response to bleeds, is a rapid process regulated by a highly nuanced cascade of previous events. Here, we aim to achieve an equally effective set of coordinated via interactions between hm-chitosan and the blood hematocrit. We anticipate based on previous work done in our lab with vesicles the biopolymer will form an “artificial clot,” via interaction of hydrophobes and the hydrophobic bilayers of the blood cells (Figure 1.1d). In this way, the biopolymers would act as bridges between adjacent cells, thus forming an elastic 3-dimensional network with the cells themselves acting as physical crosslinks. Additionally, we plan to utilize the amphiphilic supramolecule,  $\alpha$ -cyclodextrin (CD), which is a barrel-shaped molecule featuring a hydrophobic interior, so as screen the hydrophobic interactions and, in this way, reverse the mechanism of gelation. Detailed explanations of the designed experimental and results on such “reversible hemostats” are given in Chapter 6.

### 1.3 Significance of this Work

The studies described in this dissertation are potentially significant from two different standpoints: (a) *they provide fundamental insight into self-assembly processes, such as in biological systems*; and (b) *the studies provide a foundation for new therapeutic concepts in the field of nanomedicine*.

Firstly, from a scientific standpoint, the interactions between vesicles and biopolymers are crucial to the behavior of cell membranes and membrane-bound organelles within a cell. As is well known, every biological membrane consists of a combination of lipids as well as biopolymers (proteins or polysaccharides) either spanning the membrane or tethered on one side of the membrane. Our studies on cells mixed with amphiphilic biopolymers presented in Chapter 6 can certainly provide some immediate “hands-on” insights into these sorts of interactions. Additionally, our controlled release studies in Chapters 3 (gels) and 4 (capsules) can potentially give indirect information on vesicle-polymer interaction at the nano-scale. Chapter 4 gives some important scientific insights into building hierarchical structures via self-assembly which have interesting implications for biomimetic organelles, cells or tissues. Furthermore, the results shown on the interactions between ‘soft’ vesicles and ‘hard’ surfaces as discussed in Chapter 5 is of fundamental importance in the physical sciences.

From the standpoint of utility, all four systems display either proof-of-concept level or immediate application to an existing biomedical need. The vesicle gels and

vesicle-loaded capsules described in this dissertation may be useful for controlled release applications. Compared to vesicles alone, the above vesicle-bearing hybrid materials present some benefits. For starters, the stability of vesicles is enhanced by embedding them in the soft biopolymer matrix. Moreover, the presence of an additional transport barrier enables a slower and more extended rate of release for molecules encapsulated in the vesicles. As an added benefit, encapsulation within vesicles may also help in maintaining the bioactivity of drugs and proteins.<sup>9</sup> Vesicles may also be useful as storage depots for hydrophobic drugs that cannot be loaded otherwise into gels or capsules. Finally, we will show that it is relatively easy to confer targeting capabilities (either by magnetic fields or via antibodies) to the capsules, in comparison to the vesicles.

The vesicles on biopolymer films may also be useful in controlled release, but more specifically for the application to chronic wound treatment. Biopolymer films presented in Chapter 5 can be fabricated in a variety of sizes. As such, we can envision a larger macro-sized film functionalized with therapeutically-loaded vesicles that can completely cover up a chronic wound or burn injury. The vesicles would provide protection and sustained release of the therapeutics, while the anti-microbial chitosan film both prevents fluid exudation and bacterial invasion. These films would also allow for ample oxygen transfer to the injury during administration, which is very important for the outcome of the underlying tissue.

Amphiphilic biopolymers for the gelation of cells have an immediate utility in hemorrhage control. Chapter 6 presents some important *in vitro* and *in vivo* work on these

materials for treating bleeding injuries. The material used in those studies, hm-chitosan, is very low cost, and it achieves similar efficacies to hemostats 3 orders of magnitude higher in cost. Furthermore, the use of cyclodextrin in that work as an “anti-clotting” complement system offers a functionality which no other hemostatic material has achieved. The reversibility of this system via self-assembly is highly clinically significant for two key reasons. First, it allows for the surgeon treating the patient to easily clean out the hemostatic material and identify the injury under controlled circumstances so as to plan the optimal regimen of treatment for the patient for full recovery. Secondly, the anti-clotting aspect of the system provides a mitigation against unwanted clotting, a problem which is a major concern for any new hemostat undergoing clinical trials.

# Chapter 2

## Background

---

In this chapter, we describe some of the basic properties of vesicles, associating polymers, and biopolymers. We then briefly describe the techniques that we will use to study these resulting “soft” systems, specifically: rheology, neutron scattering, and cryo-TEM. The aspects discussed here are of a general nature; literature dealing with more specific aspects are discussed in the Introduction sections of succeeding Chapters 3-6.

### 2.1 Vesicles and Liposomes

Vesicles are self-assembled capsules formed in water by lipids, surfactants, or block copolymers.<sup>10-11</sup> The molecules that form vesicles are amphiphilic, with a hydrophilic head (depicted as a blue sphere in Figure 2.1) and hydrophobic tail(s) (shown in red). The shell of the vesicle is a bilayer (*ca.* 2-5 nm in thickness) of these amphiphilic molecules, with the hydrophilic heads on both sides of the bilayer and thereby exposed to water, while the hydrophobic tails inside the bilayer are shielded from water. A vesicle can be considered to form by the folding of amphiphilic bilayers, as shown in Figure 2.1. Vesicles with only a single bilayer (or lamella) are called unilamellar vesicles (ULVs), while vesicles with several concentric bilayers are called multilamellar vesicles (MLVs) and these are also referred to as “onions”.

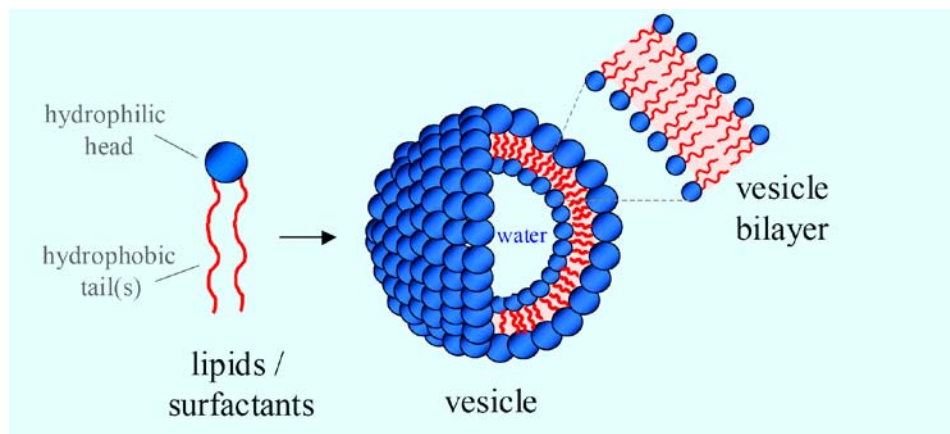


**Figure 2.1.** The structure of vesicles formed by the self-assembly of amphiphiles. The vesicle is formed by the folding of an amphiphilic bilayer that is about 2-5 nm in thickness.

The folding of bilayers into vesicles tends to occur only when the bilayers are present at low concentration; at high concentrations, bilayers form a lamellar phase.<sup>10</sup> The tendency for bilayers to fold is driven by a desire to minimize contact of the hydrophobes with water at the bilayer ends. Also, the formation of many vesicles from a single extended bilayer sheet increases the entropy of the system. Nevertheless, it is useful to remember that, at equilibrium, the amphiphiles usually exist as a lamellar phase; so, the vesicle state is often of limited stability. In other words, given sufficient time, vesicles will get disrupted and form a dilute lamellar phase. An important exception to this rule exists in the case of mixed surfactants, where vesicles can exist as equilibrium structures.<sup>12</sup>

Vesicles formed from lipids are referred to as “liposomes”. The term lipid usually refers to amphiphiles that have a biological origin and typically, such molecules have two hydrophobic (acyl) tails. Lipid bilayers constitute the membranes found at the boundary

of every living cell as well as many intracellular organelles. The classification of lipids is done based on their headgroup type – for example, phospholipids have a phosphate moiety in their headgroup. Among the phospholipids, the phosphatidylcholines or lecithins are a common variety. Lipids tend to have a very low solubility in water because they have two hydrophobic tails. As a result, an organic solvent is usually employed in preparing lipid vesicles.

The tendency of lipids to form bilayers or vesicles can be rationalized from the geometry of these molecules. Generally speaking, the role of molecular geometry in dictating the self-assembly of amphiphiles can be understood by a term called the critical packing parameter or CPP, which is defined as follows:<sup>13</sup>

$$\text{CPP} = \frac{a_{\text{tail}}}{a_{\text{hg}}} \quad (2.1)$$

where  $a_{\text{hg}}$  is the effective area of the amphiphile headgroup and  $a_{\text{tail}}$  is the average area of the amphiphilic tail. Amphiphilic molecules having  $a_{\text{tail}} \approx a_{\text{hg}}$ , i.e.,  $\text{CPP} = 1$ , tend to assemble into bilayers or vesicles (Figure 2.2). Note that the shape of these molecules resembles that of a cylinder. In contrast, molecules with a larger headgroup area than tail tend to favor curved structures, specifically micelles. A CPP of 2 corresponds to spherical micelles while a CPP of  $\frac{1}{2}$  corresponds to cylindrical (rodlike or wormlike) micelles.

In addition to lipids (2-tailed amphiphiles), mixtures of single-tailed amphiphiles, one cationic and the other anionic, can also form vesicles.<sup>12</sup> The formation of such “catanionic” vesicles can also be understood via the CPP concept (Figure 2.2). In this

case, each individual surfactant molecule resembles a cone because of the electrostatic repulsion from its headgroup. When mixed together, however, the cationic and anionic headgroups mutually mitigate their repulsive electrostatic effects, leading to a significant reduction in headgroup area. The combination of these molecules thus resembles a cylinder, and consequently leads to vesicle structures. Interestingly, these surfactant vesicles tend to spontaneously form when the two individual surfactants are mixed. Moreover, the vesicles are indefinitely stable, which suggests that they may actually be equilibrium structures.

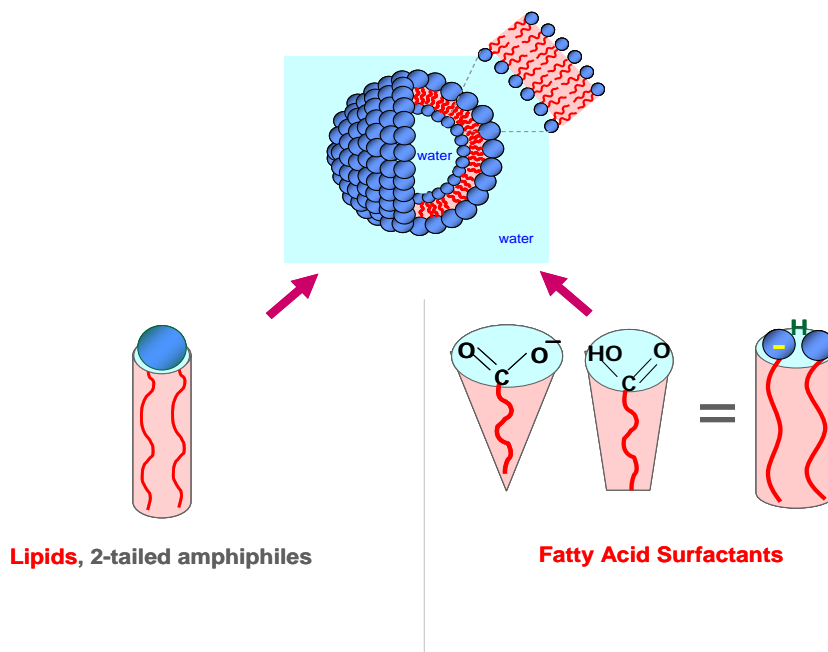


**Figure 2.2.** Schematic illustration of the formation of vesicles by self-assembly of amphiphilic molecules in water. Due to their cylindrical geometry, lipids, which are two-tailed amphiphiles, can form vesicles in aqueous solution upon folding of lipid bilayers into spheroid structures represented in the cartoon above. Also, pairs of fatty acid surfactants can collectively take on a cylindrical geometries and, thus, form vesicles in the same way as lipids.

Vesicles can also be formed from single surfactants in some rare cases.<sup>14-15</sup> Single ionic surfactants usually form micelles, but in the case of fatty acids and their soaps,



vesicles can form over a limited pH range around the pKa of the acid.<sup>15</sup> Fatty acids are among the simplest types of amphiphiles that exist and there is speculation that their self-assembly into vesicles could have occurred in pre-biotic earth, eventually culminating in the origin of life.<sup>14</sup> The mechanism for vesicle formation from fatty acids is not fully understood; however, it is significant that vesicles form only at intermediate pH values at which the acid is partially ionized. Thus, fatty acid molecules in vesicles tend to exist as pairs of ionized and unionized molecules, and presumably such pairs self-assemble into structures exhibiting geometries required to form bilayers (see Figure 2.2).

### ***2.1.1 Vesicle Preparation from Lipids***

As mentioned, lipids are insoluble in water and at equilibrium they tend to form a lamellar phase. Therefore, preparation of lipid vesicles calls for the use of an organic solvent and some input of energy.<sup>1,11</sup> First, the lipid(s) are dissolved in an organic solvent such as chloroform. Thereafter, the solvent is removed by evaporation to yield a dry lipid film. This film is then hydrated by adding water (or a buffer solution) at a temperature above the gel-to-liquid crystal transition of the lipid (Figure 2.3a). The solution is gently stirred during this process and the result is the formation of large multi-lamellar vesicles (MLVs) in solution. To convert the MLVs to unilamellar vesicles (ULVs), the lipid solution is either sonicated or extruded through a polycarbonate filter of given pore size. Sonication tends to produce small unilamellar vesicles (15 – 50 nm in diameter), whereas extrusion is typically used to produce unilamellar vesicles with a diameter on the order of 100 nm (Figure 2.3a).

While the above methods yield nanometer-sized vesicles, it is also possible to obtain giant unilamellar vesicles (GUVs, or giant vesicles in short) that are several microns in diameter.<sup>2</sup> Giant vesicles can be seen directly by optical microscopy, typically in phase contrast mode. A popular method to form giant vesicles in the size range 5 – 200  $\mu\text{m}$  is by *electroformation* (Figure 2.3b). This involves application of an AC voltage across lipid-coated electrodes spanning a water-filled chamber. In this process, the giant vesicles break off from the lipid film and their size is controlled by the AC voltage and frequency.

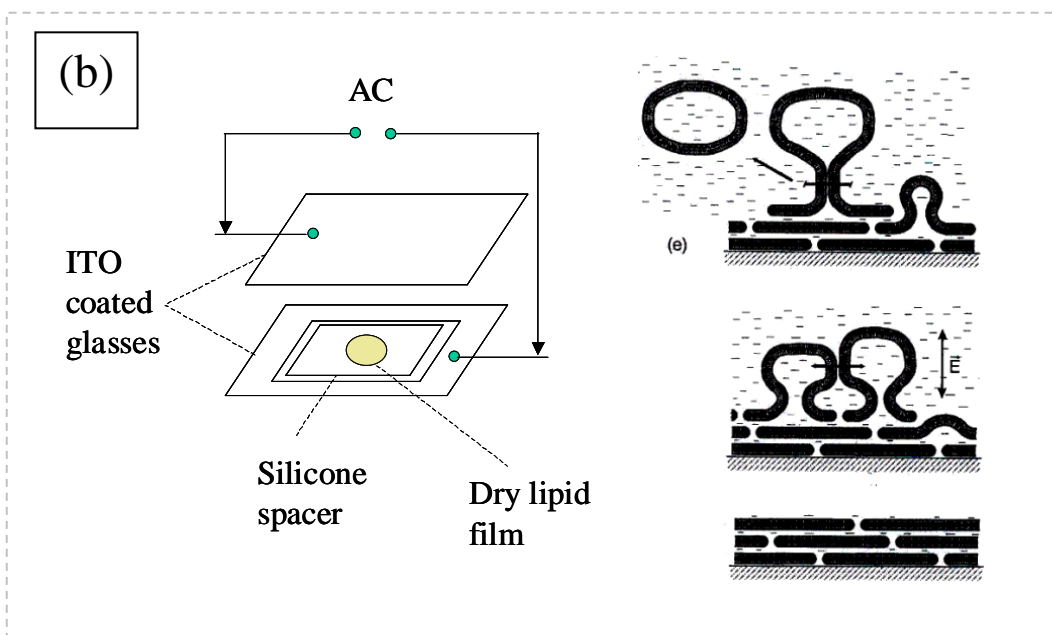
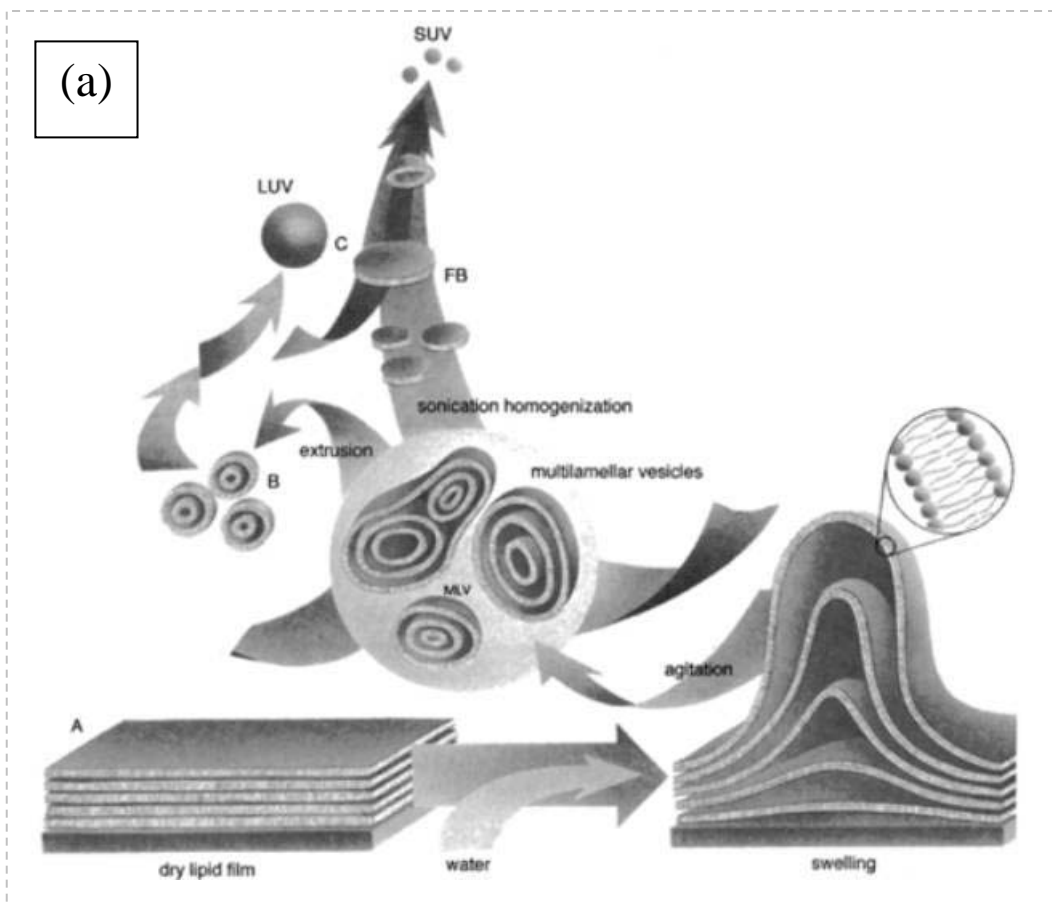


**Figure 2.3.** Preparation of unilamellar lipid vesicles of various sizes: (a) small or large vesicles (20 nm – 200 nm);<sup>1</sup> (b) giant vesicles by electroformation.<sup>2</sup>

## 2.2 Associating Polymers

The term associating polymer refers to a water-soluble polymer that has an amphiphilic character.<sup>16</sup> Typically, the polymer backbone is hydrophilic, while hydrophobic groups are either present at the ends of the chain (this is called a telechelic structure) or the hydrophobes are tethered by chains to the polymer backbone (this is referred to as a comb-graft structure). Associating polymers have been synthesized by attaching hydrophobes to a range of water-soluble polymers, including polyethylene oxide (PEO) and polyacrylamide (PAAm) as well as to biopolymers such as cellulose and chitosan.<sup>16-17</sup> We will work with chitosan-based associating polymers in this study.

When added to water, hydrophobes on the polymer associate or self-assemble in

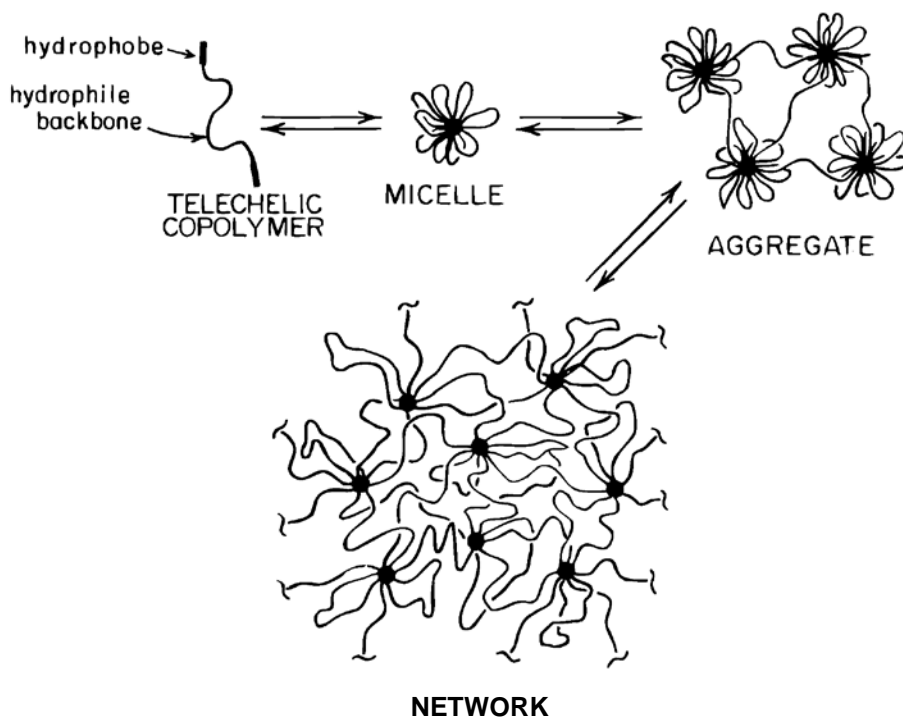


**Figure 2.4.** Architecture of a telechelic associating polymer and the structures formed by its self-assembly in aqueous solution

much the same way as surfactant hydrophobes.<sup>16,18</sup> In analogy to the micelles formed by surfactants, polymer association is believed to result in “flower micelles” (shown in Figure 2.4 for the case of the telechelics), with hydrophobes from many chains present at the center of these micelles. Note that at low polymer concentrations, there is significant *intra*-polymer association, while at higher concentrations, there is a shift to *inter*-polymer associations. Thus, at high polymer concentrations, the flower micelles function as crosslinks in a transient network, thereby enhancing the solution viscosity. For high molecular weights, the polymer will both associate as well as entangle with other chains.

## **2.3 Biopolymers**

Macromolecules of biological origin fall broadly under three classes: polypeptides or proteins; polynucleotides; and polysaccharides.<sup>19</sup> For the purposes of this study, we will focus on polysaccharides. The polysaccharide that is of especial interest to us is chitosan and we describe its properties below in more detail. The common theme with the chosen biopolymers is their ability to render viscosity to water by forming entangled networks or gels.

### **2.3.1 Gelatin**

Gelatin is protein produced by the partial hydrolysis of collagen extracted from the bones and connective tissues of animals such as cattle, pigs and horses. The natural molecular bonds between individual collagen strands are broken down into a form that rearranges more easily. Gelatin forms a solution of high viscosity in water, which sets to a gel upon cooling, and its chemical composition is similar to that of its parent molecule collagen.<sup>19</sup>

The same triple helical Gly-X-Y domains abundant in collagen fibers, where X is typically proline and Y is typically hydroxyproline, form the physical crosslinks below the phase transition temperature of 32°C which cause gelatin to form an elastic gel in water.

### ***2.3.2 Chitosan***

Chitosan is a linear polysaccharide obtained by the deacetylation of chitin.<sup>20</sup> Chitin, in turn, is a natural polysaccharide that constitutes the hard exterior shell of insects and crustaceans. Among biological polymers, chitin is next only to cellulose in abundance. However, while chitin is insoluble in water, its deacetylated derivative, chitosan, is water-soluble under acidic conditions ( $\text{pH} < 6.5$ ). Under these conditions, the amine groups along the chitosan backbone are ionized and chitosan acts as a cationic polyelectrolyte. Note that chitosan is strictly a copolymer of mostly D-glucosamine ( $\beta$ -(1,4)-2-deoxy-2-amino-D-glucopyranose) sugars and a few of the N-acetyl-D-glucosamine ( $\beta$ -(1,4)-2-deoxy-2-acetamido-D-glucopyranose) sugars from the parent chitin. The structures of these sugars are shown in Figure 2.5.

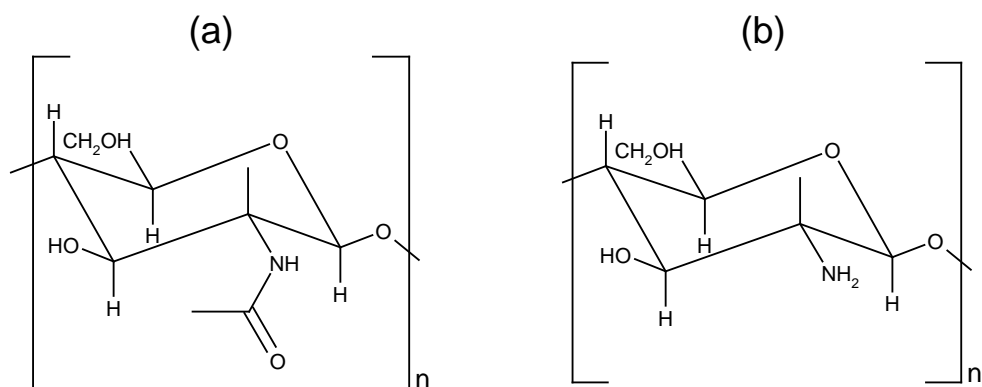


**Figure 2.5.** Structures of the parent sugars in (a) chitin and (b) chitosan. The N-acetyl-D-glucosamine sugar in chitin is deacetylated to give the D-glucosamine sugar in chitosan.

Current scientific and technological interest in chitosan is motivated by a number of factors.<sup>20</sup> First, chitosan is a biocompatible and biodegradable polymer. It is one of the few cationic biopolymers, and as a result, it can interact with anionic cell membranes. Second, chitosan confers anti-bacterial properties to substrates. As a result, chitosan finds application in tissue regeneration, artificial skin constructs, wound dressings and sutures, drug delivery, antibacterial coatings, and bioseparation membranes.<sup>20-24</sup> Third, there is an

environmental benefit to using chitosan since the parent chitin is usually obtained from food-processing wastes (e.g., crab, shrimp or lobster shells). For these reasons, there is ample interest in chitosan and many researchers have also attempted to modify the parent polymer to confer it unique properties.<sup>22,25-27</sup> One such modification is to attach hydrophobic groups to chitosan, and this is discussed below.

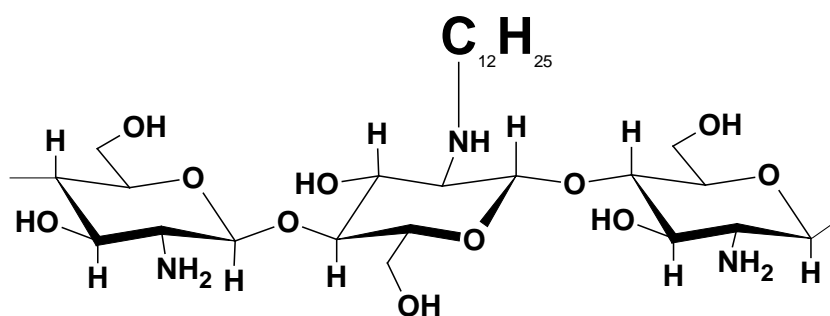


**Figure 2.6.** Structure of hydrophobically-modified chitosan (hm-chitosan) with C<sub>12</sub> hydrophobic tails.

### 2.3.3 Chitosan Modification

Chitosan can be modified easily due to its amine groups as well as its primary and secondary hydroxyls. Modifications have been done to improve chitosan solubility in water, to increase its chelating ability, and to modify its antibacterial effect.<sup>17,22,28</sup> Our particular interest is in attaching hydrophobic groups to the chitosan backbone to alter its association behavior in water. The synthesis of hydrophobically-modified chitosan (hm-chitosan) is rather straightforward and can be performed under mild conditions.<sup>17</sup> The procedure involves reacting the chitosan with an *n*-alkyl aldehyde and a typical recipe is described below. In the process, the amine (NH<sub>2</sub>) groups are converted into



NH-R groups, where R is the *n*-alkyl moiety. The structure of hm-chitosan containing C<sub>12</sub> hydrophobic tails is shown in Figure 2.6. Note that this is a comb-graft type of associating polymer.

A typical procedure for synthesizing hm-chitosan with C<sub>12</sub> tails involves the following steps.<sup>17-18</sup> First, *n*-dodecyl aldehyde is added to an acidic chitosan solution in a water-ethanol mixture, followed by addition of sodium cyanoborohydride. The molar ratio of aldehyde to chitosan monomer(s) is fixed at a certain value (e.g. 2.5%). The reaction yields the hm-chitosan, which is then precipitated by raising the pH and adding ethanol. Next, the precipitate is purified by washing with ethanol followed by deionized water. The final hm-chitosan precipitate is re-dissolved in acetic acid solution and the concentration is recalibrated. This solution tends to be viscous due to associations between the hydrophobes (this is a qualitative indication that the synthesis has been successful). The degree of hydrophobic substitution in the final product can be compared to the value expected from stoichiometry using <sup>1</sup>H NMR.

Hydrophobically modified chitosans with *n*-alkyl pendant chains can also be synthesized by alternate routes, e.g., by reacting with alkyl carboxylic acids,<sup>29</sup> or alkyl acid anhydrides,<sup>30</sup> or alkyl acid chlorides.<sup>31</sup> High substitution levels (> 10%) have been reported via the acid chloride method. These alternate routes are not attempted in the present study.

### 2.3.4 Gellan Gum

Gellan Gum is a polysaccharide produced extracellularly by a microorganism (*Pseudomonas elodea*); it is a straight-chain heteropolysaccharide and it is constituted of a repeating unit of four monosaccharide molecules, i.e. glucose, glucuronic acid, glucose, and rhamnose, thus have one carboxyl group in the repeating unit. This carboxyl group allows the biopolymer to carry a negative charge in aqueous media. A schematic of the biopolymer is shown below:

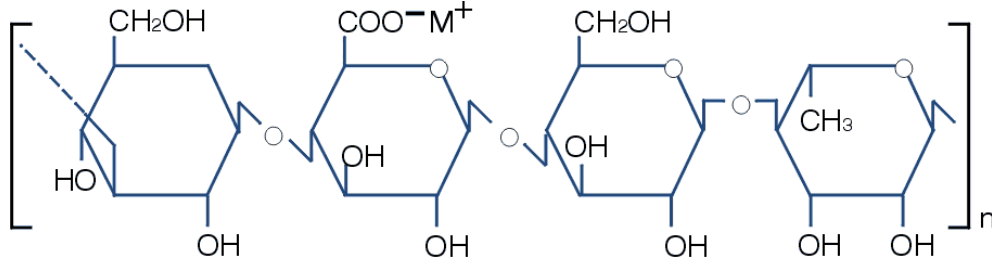


**Figure 2.7.** Structure of Gellan Gum

## 2.4 Cyclodextrins

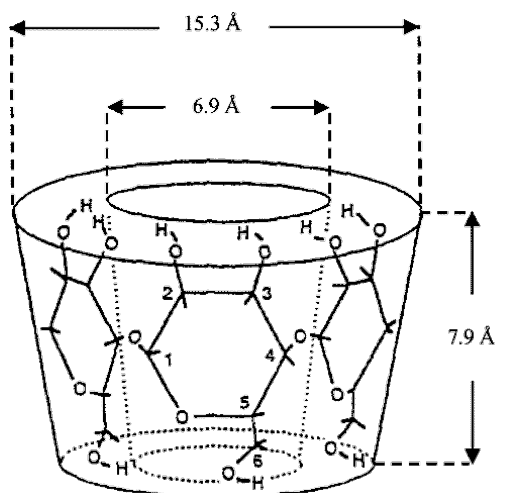


**Figure 2.8.** Truncated cone-shaped conformation of  $\beta$ -CD.<sup>32</sup>

Cyclodextrins (CDs) are cyclic oligosaccharides containing D-(+) glucopyranose units attached by  $\alpha$ -(1,4) glucosidic bonds, as shown in Figure 2.7.<sup>33</sup> They are rigid, truncated cone-shaped structures, with an internal cavity of size 5 to 8 Å depending upon the number of glucopyranose units. The wide side of the truncated cone is bordered by the secondary hydroxyl groups (2-OH and 3-OH), while the primary hydroxyl groups (6-OH) are on the narrow side. The molecule is stiffened by hydrogen bonding between the 2-OH and 3-OH groups around its outer rim. Note that all hydroxyl groups are located on the outside of the molecular cavity, thereby making the outer surface hydrophilic. On the other hand, no hydroxyl groups are located in the inner cavity, which is thus hydrophobic. CDs thus have hydrophilic outer surfaces and hydrophobic inner cavities. Because of their unique structure, CDs can form host-guest inclusion complexes with various hydrophobic guest molecules or hydrophobic parts of these molecules.<sup>32-38</sup> Note

that the bonding between the CD and the guest is through non-covalent interactions. Table 2.1 lists the properties of the three naturally occurring CDs, which are labeled  $\alpha$ -,  $\beta$ -, and  $\gamma$ -CDs.<sup>39</sup> These natural CDs are produced from starch by enzymatic degradation. In our research, we will use CDs to create new TR fluids, as described in Chapter 5.

Type of CD	Number of glucose units	Cavity diameter Å	Molecular Weight	Solubility in water (g/L)
$\alpha$	6	4.7-5.3	972	145
$\beta$	7	6-6.5	1135	18.5
$\gamma$	8	7.5-8.3	1297	232

**Table 2.1.** Properties of the three naturally occurring cyclodextrins.

## 2.5 Characterization Technique – I: Rheology

Rheology is formally defined as the study of flow and deformation in materials.<sup>40</sup> Rheological measurements provide important information on soft materials, specifically on the relation between microstructure and macroscopic properties. These measurements are typically performed on a rheometer (Figure 2.9) under steady or dynamic oscillatory shear. Typical geometries used in rheometers are the cone-and-plate, the parallel plate, and the concentric cylinder or Couette.



**Figure 2.9.** Photograph of the Rheometer RDA-III strain-controlled rheometer being operated in a cone-and-plate geometry.

In *steady shear rheology*, the sample is subjected to a constant shear-rate  $\dot{\gamma}$  (e.g. by applying a continuous rotation at a fixed rate on a rotational instrument), and the response is measured as a shear-stress  $\sigma$ . The ratio of shear-stress  $\sigma$  to shear-rate  $\dot{\gamma}$  is the (apparent) viscosity  $\eta$ . A plot of the viscosity vs. shear-rate  $\dot{\gamma}$  is called the flow curve of the material.

In *dynamic or oscillatory rheology*, a sinusoidal strain  $\gamma = \gamma_0 \sin(\omega t)$  is imposed on the sample. Here,  $\gamma_0$  is the strain-amplitude (i.e. the maximum applied deformation) and  $\omega$  is the frequency of the oscillations. The sample response will be in the form of a sinusoidal stress  $\sigma = \sigma_0 \sin(\omega t + \delta)$  which will be shifted by a phase angle  $\delta$  with respect to the strain waveform. Using trigonometric identities, this stress waveform can be decomposed into two components, one in-phase with the strain and the other out-of-phase by  $90^\circ$ :

$$\sigma = G' \gamma_0 \sin(\omega t) + G'' \gamma_0 \cos(\omega t) \quad (2.2)$$

where  $G' = \mathbf{Elastic}$  or  $\mathbf{Storage Modulus}$

and  $G'' = \mathbf{Viscous}$  or  $\mathbf{Loss Modulus}$

The elastic modulus  $G'$  is the in-phase component and provides information about the elastic nature of the material. Since elastic behavior implies the storage of deformational energy, this parameter is also called the storage modulus. The viscous modulus  $G''$ , on the other hand, is the out-of-phase component and characterizes the viscous nature of the material. Since viscous deformation results in the dissipation of

energy,  $G''$  is also called the loss modulus. For these properties to be meaningful, the dynamic rheological measurements must be made in the “*linear viscoelastic*” (LVE) regime of the sample. This means that the stress must be linearly proportional to the imposed strain (i.e., moduli independent of strain amplitude). In that case, the elastic and viscous moduli are only functions of the frequency of oscillations  $\omega$ , and are true material functions. A log-log plot of the moduli vs. frequency, i.e.  $G'(\omega)$  and  $G''(\omega)$ , is called the frequency spectrum or *dynamic mechanical spectrum* of the material. Such a plot represents a signature of the material microstructure.

The important advantage of dynamic shear is that it allows us to characterize microstructures without disrupting them in the process. The net deformation imposed on the sample is minimal because the experiments are restricted to small strain amplitudes within the LVE regime of the sample. As a result, the linear viscoelastic moduli reflect the microstructures present in the sample at rest. This is to be contrasted with steady shear, where the material functions are always obtained under flow conditions corresponding to relatively drastic deformations. We can therefore correlate dynamic rheological parameters to static microstructures, and parameters under steady shear to flow-induced changes in microstructure.

## 2.6 Characterization Technique – II: Small Angle Neutron Scattering (SANS)

Scattering techniques are invaluable probes of the micro- and nanostructure in soft materials.<sup>41</sup> The basic principle underlying all scattering techniques is that the intensity of scattered radiation is a function of the size, shape, and interactions of the “particles” present. For aqueous systems, small-angle neutron scattering (SANS) is the technique of choice because contrast between the “particles” and the solvent can be easily achieved by switching H<sub>2</sub>O with D<sub>2</sub>O. Also, the incident radiation in SANS is composed of neutrons having a wavelength  $\sim 7 \text{ \AA}$ , and as a result, SANS is useful in probing size scales on the order of a few nm. SANS experiments require a nuclear reactor to generate neutrons and we are fortunate to have one of the premier SANS facilities in the world close to UMD at NIST in Gaithersburg, MD.

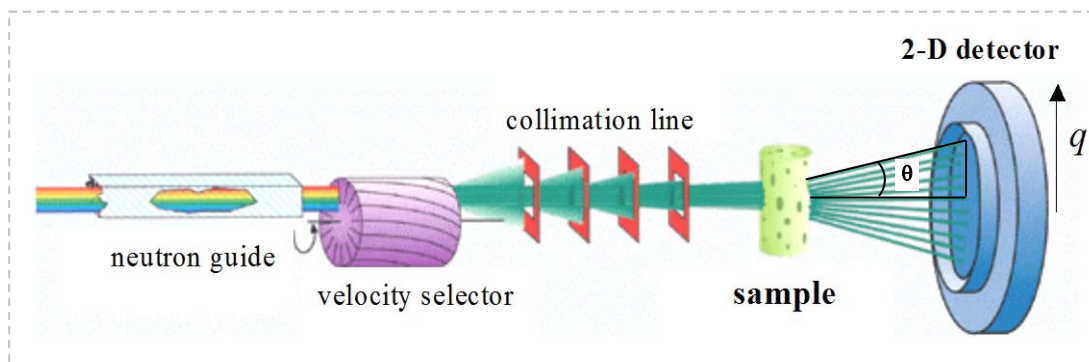


**Figure 2.10.** Schematic of a SANS experiment.

The basic geometry of a SANS experiment is illustrated in Figure 2.10. Neutrons emitted from a nuclear reactor are selected at a particular wavelength and wavelength spread using a velocity selector, collimated by several lenses, and passed through a sample chamber. The neutrons scattered by the sample are collected on a 2-D detector. This 2-D data is corrected and placed on an absolute scale using calibration standards. It



is then converted into a plot of scattered intensity  $I$  vs. scattering or wave vector  $q$  by spherical averaging. The wave vector  $q$  is related to the scattering angle and wavelength by: <sup>41</sup>

$$q = \frac{4\pi}{\lambda} \sin\left(\frac{\theta}{2}\right) \quad (2.3)$$

Here,  $\lambda$  is the wavelength of the incident radiation and  $\theta$  is the scattering angle. Thus,  $q$  can be considered an inverse length scale, with high  $q$  corresponding to small structures, and vice versa.

The SANS intensity  $I(q)$  from a structured fluid containing  $n_p$  particles per unit volume can be expressed in the following manner:<sup>41</sup>

$$I(q) = n_p \cdot P(q) \cdot S(q) \quad (2.4)$$

where  $P(q)$  is called the form factor and  $S(q)$  the structure factor.  $P(q)$  is the scattering that arises from intraparticle interference, which is a function of the particle size and shape.  $S(q)$  arises from interparticle interactions and thereby reflects the spatial arrangement of particles in the sample. When the particles are in dilute solution or are non-interacting, the structure factor  $S(q) \rightarrow 1$  and the SANS intensity  $I(q)$  can then be modeled purely in terms of the form factor  $P(q)$ . Different expressions exist for the form factor  $P(q)$  for various particle geometries. By fitting the appropriate  $P(q)$  to the SANS data, one can obtain the characteristic sizes of the particles present.

## 2.7 Characterization Technique – III: Dynamic Light Scattering (DLS)

Static scattering techniques such as SANS provide important information about the quiescent structure in complex fluids. Dynamic scattering techniques have a complementary role in that they probe structural relaxations and dynamics. In particular, dynamic light scattering (DLS) probes the Brownian motion of particles in the fluid. This method can give a reliable estimate of particle size under certain limiting conditions. In a DLS experiment, the fluctuating intensity of light scattered from the sample is recorded at a certain angle  $\theta$ . The fluctuations are then correlated to yield the intensity autocorrelation function  $g^{(2)}(q, \tau)$  vs. the correlation time  $\tau$ .<sup>42</sup>

$$g^{(2)}(q, \tau) = \frac{\langle I(q, t)I(q, t + \tau) \rangle}{\langle I(q, t)^2 \rangle} \quad (2.5)$$

Note that in light scattering, the definition of the wave vector is slightly modified as:

$$q = \frac{4\pi n}{\lambda} \sin\left(\frac{\theta}{2}\right) \quad (2.6)$$

where  $n$  is the refractive index of the medium. The relevance of  $q$  in DLS is that structural relaxations are probed over length scales on the order of  $q^{-1}$ .

The measured intensity autocorrelation function  $g^{(2)}(q, \tau)$  can be converted into an electric field autocorrelation function  $g^{(1)}(q, \tau)$  through the Siegert relation:

$$g^{(2)}(q, \tau) = 1 + f \left| g^{(1)}(q, \tau) \right|^2 \quad (2.7)$$

Here,  $f$  is an adjustable parameter called the coherence factor that depends on the instrument geometry. For a dilute solution of monodisperse spherical particles, the

electric-field autocorrelation function is a single exponential whose time decay is determined by the translational diffusion coefficient of the particle  $D$ :

$$g^{(1)}(q, \tau) = \exp(-Dq^2\tau) \quad (2.8)$$

From the measured diffusion coefficient, the particle size can be obtained by the Stokes-Einstein equation:

$$D = \frac{k_B T}{6\pi\eta R_h} \quad (2.9)$$

where  $k_B$  is the Boltzmann constant,  $T$  the absolute temperature and  $\eta$  the viscosity of the solvent (assumed to be a Newtonian liquid). The size obtained from DLS is the *hydrodynamic radius*  $R_h$ . The hydrodynamic size is the bare particle size along with any solvation layer.

## **2.8 Characterization Technique – IV: Cryo-Transmission Electron Microscopy (Cryo-TEM)**

While scattering techniques provide indirect information about the nanostructure in a sample, an alternate technique that would allow direct visualization of the structure in real space would be extremely useful. Transmission electron microscopy (TEM) can potentially reveal structural detail with sub-nanometer resolution. However, the use of TEM for self-assembled fluids and soft materials is problematic. For imaging under TEM, the solvent must be completely removed, and the process of solvent removal can alter or destroy fragile structures such as micelles and vesicles. Also, to achieve contrast, structures usually have to be stained with heavy metal salts – again, the staining process might degrade the structures present.

The above deficiencies of conventional TEM techniques have led researchers to develop an alternative that is particularly suited for aqueous nanostructured fluids. This technique is called **cryo-TEM**, and it involves the rapid freezing of the aqueous sample such that the water is vitrified instead of forming ice crystals. In the process, the structural details are preserved, and the sample can be imaged under conventional TEM at low electron doses. Sample preparation for cryo-TEM is conducted using a controlled environment vitrification system (CEVS), illustrated in Figure 2.11. In the CEVS, the sample is equilibrated at conditions of controlled temperature and humidity prior to plunge vitrification. First, a drop of the sample is placed on a holey carbon film supported on a TEM grid. A filter paper is then used to blot the drop, so as to create a thin film of the sample spanning the grid holes. The grid is then plunged into the cryogen, liquid ethane, thereby rapidly vitrifying the sample. Subsequently, the grid has to be transferred to the electron microscope in a dedicated cold stage. Typically, the grid is maintained at  $-170^{\circ}\text{C}$  at all times, to ensure that there is no formation of ice crystals nor condensation of atmospheric water.

As with any other technique, care has to be taken in interpreting cryo-TEM data. One frequent source of artifacts is that the sample blotting process (used to spread a thin film) involves a substantial amount of shear. This shear may distort the structures present, and one has to take this into account while interpreting images. Despite these artifactual concerns, cryo-TEM has now developed into a powerful tool for directly probing the structures of various complex fluids. A variety of self-assembled structures including micelles, vesicles and liquid crystalline phases have been successfully imaged by cryo-

TEM. Also, the use of cryo-TEM in biology has provided unique insights into phenomena such as endocytosis and vesicle fusion.

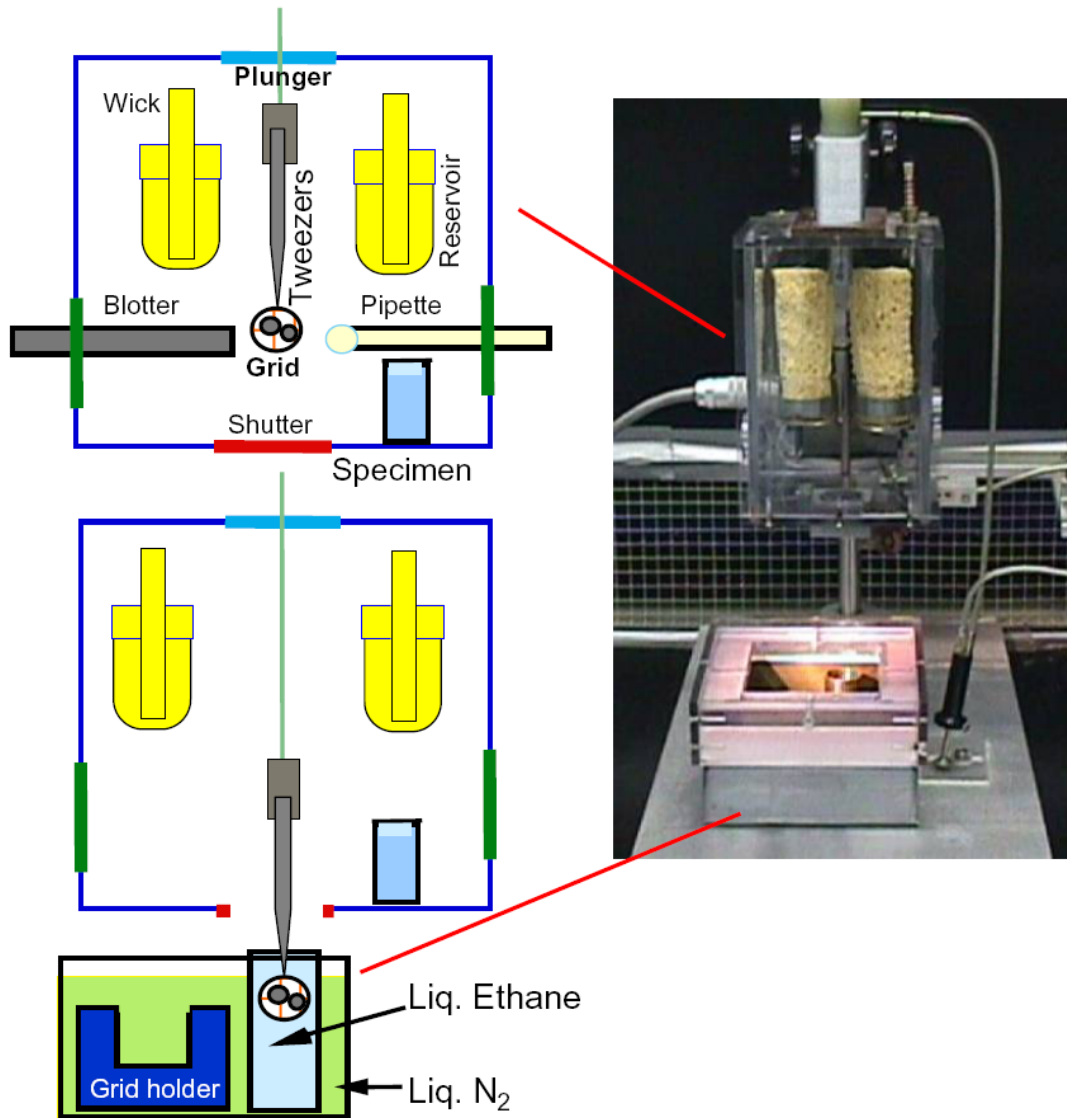


**Figure 2.11.** Photograph of the controlled environment vitrification system (CEVS) used for sample preparation in cryo-TEM. The schematics on the left show the various steps in the process.

## Chapter 3

# Biopolymer Gels Containing pH-Sensitive Vesicles

---

The results presented in this chapter have been published in the following journal article:  
Matthew Dowling, Jae-Ho Lee, and Srinivasa R. Raghavan, “*pH-Responsive Jello: Gelatin Gels Containing Fatty Acid Vesicles*” *Langmuir*, 25 (15), 8519-8525 (2009).

### 3.1 Introduction

In recent years, there has been immense interest in creating smart materials, i.e., materials that can change their properties in response to external stimuli such as light, temperature, pH, or biological targets.<sup>43-46</sup> In particular, stimuli-responsive polymer hydrogels have attracted much attention, and a stimulus of interest in this context has been pH.<sup>43-45</sup> Polymers having ionizable groups (acid or base) tend to form gels with pH-responsive swelling properties. Such gels generally tend to be swollen when the groups are ionized, while they revert to a collapsed or shrunken state when the same groups lose their charge. Examples include gels of poly(acrylic acid), poly(methacrylic acid) etc. and their copolymers, and these have proven attractive for controlled release and drug delivery applications.<sup>43-45</sup>

An alternate way to impart pH-dependent properties to polymer gels is by embedding pH-responsive nanoparticles or nanostructures in their interior.<sup>46</sup> In this scenario, the polymeric framework itself is unaffected by pH (e.g., there is no change in the degree of gel swelling with pH). This approach may be attractive for a variety of

reasons. For instance, one may wish to modulate the release of a drug from a gel while maintaining a constant gel volume. Secondly, by embedding nanostructures, *pH-responsiveness can be conferred to materials that by themselves do not have such properties*. For example, consider hydrogels of gelatin and poly(N-isopropyl acrylamide) (NIPAAm).<sup>44,47</sup> Both gels have thermoresponsive properties: gelatin gels melt upon heating while NIPAAm gels shrink when heated beyond a critical temperature. While these polymers are workhorses in many applications, they are not pH-responsive (at least not at moderate pH values). One could modify the chemistry of these polymers to make the gels pH-sensitive, but that is generally a tedious process. The addition of nanostructures to impart pH-responsiveness is generally a much simpler alternative.

In this study, we explore the addition of pH-responsive *vesicles* into gelatin gels and investigate the resulting vesicle-gel hybrids. Unlike “hard” nanoparticles, vesicles (or liposomes) are “soft” self-assembled structures formed from lipids or surfactants.<sup>48</sup> Unilamellar vesicles of ca. 100 nm diameter can be essentially considered as nanocontainers, with a bilayer membrane enclosing an aqueous core.<sup>48-50</sup> Vesicles thus have the ability to encapsulate hydrophilic solutes in their core, and for this reason they are of great interest for drug delivery applications.<sup>48-50</sup> In the present context, we are interested in embedding vesicles within a polymer hydrogel network. Vesicle-gel hybrids have been investigated in the past by several researchers.<sup>51-56</sup> The motivation for past studies has been the use of these hybrid materials in tissue engineering or drug delivery. For example, drug delivery from a vesicle-loaded gel has been shown to occur in a prolonged manner compared to that from either the vesicles themselves or the bare gel

alone.<sup>51-56</sup> To our knowledge though, pH-responsive vesicles have not been combined with hydrogels previously – this is the first study to explore such a combination.

The pH-responsive vesicles we have chosen to examine are those made from sodium oleate (NaOA), the sodium salt of a single-tailed fatty acid, oleic acid. It has been known for many years that fatty acids can self-assemble into unilamellar vesicles at pH values close to their pKa.<sup>14-15,57-59</sup> Fatty acid vesicles have been investigated particularly by researchers in the field of prebiotic chemistry – these researchers believe that fatty acids and by extension their vesicles may have been components in the prebiotic soup of ancient earth (indeed, fatty acids have even been isolated from meteorites).<sup>14,58-59</sup> In the present study, we exploit the well-known pH-dependence of fatty acid self-assembly.<sup>15,57</sup> For example, NaOA forms vesicles at a pH around its pKa of 8.3, but these vesicles transform into spherical micelles at pH values much higher than the pKa, e.g., at pH > 10 (see the phase diagram in Figure 1).<sup>57</sup> We were interested to see whether such a pH-induced vesicle-to-micelle transition would occur even if the NaOA vesicles were entrapped within a gel. As the results in this paper show, this is indeed the case. The above concept can be extended to other pH-dependent vesicles (e.g., those formed from certain lipids<sup>60</sup>). Also, instead of gelatin, a variety of polymer and biopolymer-based hydrogels can also be used as the matrix for the vesicles.<sup>45,61</sup>

Finally, it is worthwhile to discuss some applications for gels loaded with pH-responsive vesicles. An obvious one would be in pH-controlled release of hydrophilic solutes.<sup>43-45</sup> Consider solutes encapsulated within the vesicles, which in turn are loaded



into a gel. If such a gel is immersed in an aqueous bath, the solute will slowly diffuse out of the gel. We can then use the pH in the bath to modulate the solute release rate. For example, at a pH corresponding to intact vesicles, the solute will face two barriers to transport, one from the vesicle bilayer and the other from the gel matrix.<sup>51-56</sup> On the other hand, consider a pH at which the vesicles are disrupted into micelles: in this case, the solute will only face resistance from the gel matrix and should therefore be able to diffuse out faster. In our studies, we have tested the above concept using a dye, calcein, as a model solute, and our findings confirm a pH-tunable release rate.

A vesicle-loaded gel could also serve as a simplistic model for a functional organ, with the vesicles as the cellular component and the gel as the extracellular matrix.<sup>45,62</sup> The overall functionality of an organ depends on the ability of cells to communicate with neighboring cells.<sup>62</sup> Cells of different types may be localized at different parts of the organ, e.g. they may be organized into distinct layers, with their location being strongly correlated with cellular function. In this context, it is useful to be able to dictate the spatial organization of vesicles within a gel, i.e., to have only certain regions filled with vesicles while adjoining regions would not contain any. We show that pH-responsive vesicles offer one way to accomplish such a design: specifically, we demonstrate how vesicle-to-micelle transitions can be achieved in localized regions within a gel. This opens up the prospect of creating a “biomimetic organ” by placing pockets of vesicles loaded with specific molecules at prescribed locations within a gel matrix.

## 3.2 Experimental Section

**Materials.** Sodium oleate (NaOA) (note: oleate = C18 chain with a 9-cis unsaturation) was purchased from TCI. Gelatin (Type A, from porcine skin, ~ 300 Bloom), calcein, Triton-X100 and Tris-base were purchased from Sigma. Carbonate buffer solution (potassium carbonate-potassium borate-potassium hydroxide) corresponding to a pH of 10 was purchased from Fisher Scientific. All experiments were performed using deionized (DI) water.

**Preparation of Vesicles and Vesicle-Loaded Gels.** 1 wt% (32.8 mM) NaOA was dissolved in DI water by heating for 2-3 h at 65°C. The pH of the solution was then adjusted to ~ 8.5 by dropwise addition of 1 M HCl. In order to generate unilamellar vesicles of consistent size, the vesicle solution was subjected to 5 freeze-thaw cycles, followed by passing the sample 10 times through a 100 nm polycarbonate membrane using the Mini-extruder® (Avanti Lipids). To prepare vesicle-loaded gels, an NaOA vesicle solution of given concentration was combined with a warm (50°C) solution of gelatin, with the overall pH adjusted to 8.5 using 1 M NaOH. The resulting mixtures were cooled to room temperature to form the vesicle-loaded gels. Further details are discussed in the Results section.

**Dynamic Light Scattering (DLS).** DLS was used to characterize the sizes of vesicles in solution. A Photocor-FC light scattering instrument with a 5 mW laser source at 633 nm was used at a scattering angle of 90°. A logarithmic correlator was used to measure the

intensity autocorrelation function. The hydrodynamic size of the vesicles was extracted from the data using the Stokes-Einstein equation.

**SANS.** SANS measurements were made on the NG-3 (30 m) beamline at the National Institutes of Standards and Technology (NIST) in Gaithersburg, MD. Samples were prepared in D<sub>2</sub>O and studied at 25°C in 2 mm quartz cells. The scattering spectra were corrected and placed on an absolute scale using calibration standards provided by NIST. Data are shown for the absolute intensity  $I$  versus the scattering vector  $q = (4\pi/\lambda)\sin(\theta/2)$ , where  $\lambda$  is the wavelength of incident neutrons and  $\theta$  is the scattering angle.

**Controlled Release Experiments.** NaOA vesicles were combined with 15 mM calcein dye. To separate unencapsulated dye, the vesicle-dye mixture was passed through a Sephadex G-50 size-exclusion chromatography (SEC) column. The vesicle fraction (with encapsulated dye) was collected and used in preparing the vesicle-loaded gels. To examine the release of dye, 4 g of aqueous buffer solution was added above 6 g of gel in the headspace of the containing vials. The concentration of calcein in the buffer was measured by UV-Vis spectrometry (Cary Bio 50) as a function of time. Release experiments were also done with a control gel (no vesicles). The dye concentration in the control gel was kept identical to that in the vesicle-loaded gel. To determine the latter, 2 mL of the vesicle fraction from SEC was combined with 50  $\mu$ L of 10% Triton-X100 detergent, thereby disrupting the dye-loaded vesicles and releasing the dye into the bulk solution. The dye absorbance (and thereby concentration) could then be measured accurately by UV-Vis, and this concentration was used in preparing the control gel.

### 3.3 Results and Discussion

**Creation of Vesicle-Loaded Gelatin Gels.** We first describe the creation of vesicle-loaded gelatin gels by blending NaOA vesicles and gelatin. We will also address the stability of the vesicles within the gels. As mentioned in the Introduction, NaOA vesicles are made by adjusting the pH of an NaOA solution. The variation in NaOA solution structure as a function of pH is depicted in Figure 3.1, which is an equilibrium titration curve. To obtain this data, increasing amounts of 1 M HCl were added to a micellar solution of NaOA at pH 10 and the samples were studied by visual observations and light scattering. Phase assignments were done in accordance with our observations and these are fully in accord with the phase diagram reported previously for oleate solutions by Cistola *et. al.*<sup>57</sup> Photographs of selected samples corresponding to different regions in the phase diagram are shown in Figure 3.1.

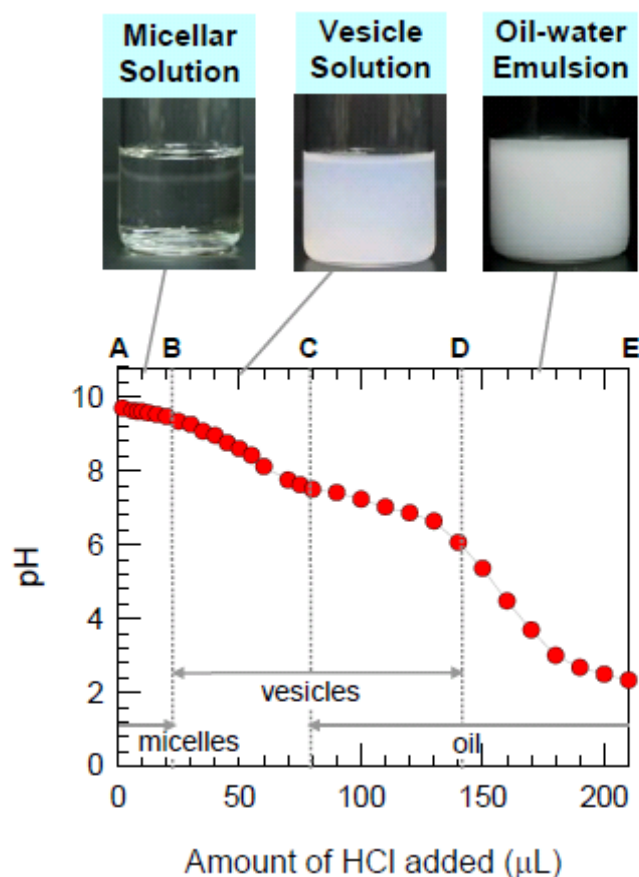


**Figure 3.1.** Photographs and titration curve for 1% NaOA at 25°C. Increasing amounts of 1 M HCl are added to a micellar solution of NaOA (pH 10) and the corresponding solution pH at equilibrium is shown in the plot. Structural assignments are done in accordance with Ref. 10. Photographs of samples corresponding to different regions of the plot are shown above.

Let us consider the data starting from the origin. At high pH (9.5 or above), NaOA forms solutions of spherical micelles and these samples are colorless and transparent, as shown by the photograph. As concentrated HCl is added, the solution pH drops from about 9.5 to 7.0, a range that spans the pKa of NaOA (which is 8.3). Samples in this pH range (interval BC on the plot) are homogeneous and have a strong bluish color, as shown by the photograph. These samples are vesicle solutions and the bluish

hue is a manifestation of light scattering from the vesicles (Tyndall effect). With further decrease in pH, the NaOA samples become unstable and inhomogeneous due to the formation of an oil phase (undissociated NaOA). The low pH samples are turbid, milky emulsions of the oil and water phases, as seen from the photograph.

The aspect to note from Figure 3.1 is the continuous and reversible transition from NaOA micelles at high pH ( $> 9.5$ ) to NaOA vesicles at moderate pH ( $\sim 8.3$ ). The mechanism for this transition (which occurs for all long-chain fatty acids) has been discussed in a number of studies and the central factor is believed to be the change in the degree of ionization of the fatty acid.<sup>15,57</sup> At high pH, the carboxylate groups on NaOA are fully ionized and the headgroups of the amphiphile thus bear a strong negative charge. The repulsions of these headgroups lead to the formation of spherical micelles. Because the micelle size is only around 5 nm, the solutions scatter light weakly and therefore appear transparent. When the pH is lowered to a value close to the pKa, approximately half the NaOA groups are no longer ionized. The charge may then be considered to be shared by two adjacent fatty acid molecules, one ionized and the other unionized: i.e., the molecules are effectively paired into dimers.<sup>15,57</sup> The net amphiphile geometry then becomes conducive to formation of vesicles rather than micelles. The vesicles typically range from 50 to 150 nm in diameter (much larger than the micelles), and therefore the solutions scatter light strongly, leading to the bluish color.

Having ascertained the pH-sensitive nature of NaOA vesicles, we now proceed to discuss their encapsulation within gelatin gels (Figure 3.2). For this purpose, we first

made a 1 wt% NaOA solution at a pH of 8.3 and extruded the vesicles through 100 nm pores to finally obtain vesicles of an average diameter around 100 nm. We then made a solution of 10 wt% gelatin in DI water and adjusted its pH to 8.3. Both the gelatin and NaOA solutions were warmed to 50°C and then mixed in a 1:1 ratio by weight. As is well-known, gelatin undergoes a sol to gel transition when cooled below 35°C.<sup>47</sup> Upon cooling to room temperature, we obtained a bluish gelatin gel, as shown by the photograph in Figure 3.2c, with an overall concentration of 5 wt% gelatin and 0.5 wt% NaOA vesicles. Note that gelatin gels not containing vesicles are colorless (Figure 2a), so the bluish color of the gel in Figure 3.2c is a visual indication that vesicles are indeed intact in the gel. This is further discussed below. Figure 3.2 depicts the microstructure of the vesicle-gel: it consists of vesicles entrapped in a 3-dimensional network of gelatin chains. The crosslinks in the gelatin gel are known to be triple helical domains where three adjacent chains are linked together.<sup>47</sup>

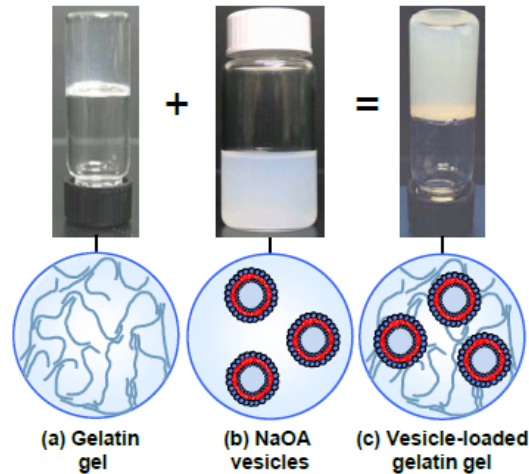


**Figure 3.2.** Photographs and schematics of (a) gelatin gel; (b) NaOA vesicles; (c) gelatin gel loaded with NaOA vesicles. The gelatin gel is a 3-D network of gelatin chains, with chain segments connected into triple helices at the crosslink points. When vesicles of diameter ~ 100 nm are entrapped in the gelatin gel, the initially colorless gel assumes a bluish hue due to light scattering from the vesicles.

How can we be sure that the vesicles are intact in the gel? One should note that stable encapsulation of vesicles in gels has already been demonstrated in a number of earlier studies.<sup>51-56</sup> In the present case, we cannot do a DLS experiment with the vesicle-loaded gel itself because the Stokes-Einstein formulation applies only for vesicles in a liquid medium. However, we can put the thermoreversibility of gelatin gels to use here. Specifically, we can heat the gelatin gel till it melts (~ to ca. 45°C) and becomes a sol and then check for the vesicle size in the sol by DLS. This can be compared with the DLS results on an NaOA vesicle solution at 45°C. For 0.5% NaOA vesicles in a 5% gelatin sol at 45°C, we measured a mean radius of  $46 \pm 3$  nm from DLS. In comparison, for 0.5% NaOA vesicles at the same temperature with no gelatin added, we obtained a similar mean radius of  $44 \pm 1$  nm. These results point to the presence of intact NaOA vesicles in gelatin gels. Incidentally, both the vesicle-gel and its corresponding sol retain the bluish hue of the original vesicle solution.

In addition to DLS, we have also conducted small-angle neutron scattering (SANS) experiments at room temperature on both NaOA vesicle solutions and gelatin gels containing NaOA vesicles. Figure 3.3 shows a plot of the scattered intensity  $I$  vs. wave-vector  $q$  for two samples: 0.5% NaOA vesicles and the corresponding vesicle gel made with 5% gelatin. In both cases, the data follow a slope of  $-2$  at low to moderate  $q$ , which is a qualitative indication for the presence of bilayered structures (vesicles).<sup>63</sup> By plotting the above data on cross-sectional Guinier plots (not shown),<sup>64</sup> we can extract the thickness of the vesicle bilayer, which is found to be  $3.2 \pm 0.2$  nm in both cases. Further modeling of the SANS data to compare vesicle sizes is beyond the scope of this paper



because, for the vesicle-gel, one would need to account for the contribution from the gelatin network to the scattering intensity. In any case, the SANS data are clearly consistent with the presence of vesicles inside the gel. It is also worth mentioning that in addition to NaOA vesicles, we have also been able to encapsulate phospholipid-based giant unilamellar vesicles (GUVs) in gelatin gels. These vesicles have diameters exceeding 10  $\mu\text{m}$  and so their presence in the gel is easily confirmed using phase-contrast and fluorescence microscopy (data not shown).

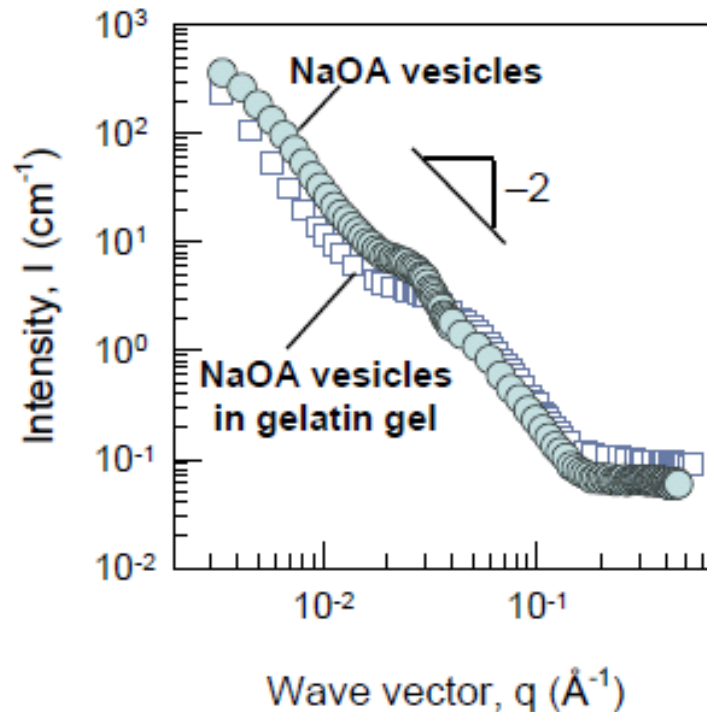


**Figure 3.3.** SANS data at 25°C for 0.5% NaOA vesicles at pH 8.3 (circles) and a 5% gelatin gel loaded with 0.5% NaOA vesicles (squares). In both cases, the intensity  $I$  follows a slope of  $-2$  at moderate  $q$ , which is characteristic of scattering from vesicles.

**Inducing Vesicle-Micelle Transitions Within Gels.** The above data confirm that NaOA vesicles can be entrapped within gels. The next question is whether these vesicles still retain their pH-responsive properties. To test the pH response of the vesicle-gels, we initially did the following experiment. We placed a 5% gelatin gel loaded with 0.5% NaOA vesicles in a vial and filled the headspace above the gel with a pH 10 buffer solution (Figure 3.4). Initially, the entire gel had the bluish color characteristic of vesicles. Within 1 h, we could observe that a portion of the gel closest to the buffer solution had cleared up – it was no longer bluish. As time progressed, the clear front advanced through the gel and by about 9 h, almost the entire volume of the gel had become clear. We also did a control experiment with a pH 8.3 buffer instead of a pH 10 buffer – in this case, no perceptible visual changes were observed in the gel over more than 48 h. These results imply that in the case of the pH 10 buffer the diffusion of the buffer into the gel disrupts the vesicles and transforms them into micelles. Due to the weaker light scattering of micelles, the micellized region of the gel shows up as practically clear. Incidentally, the photographs in Figure 4 were taken after removing the buffer solution from the vial headspace – this was necessary to clearly visualize the gel in the vial. Also, the vial is shown inverted in all the photographs – this is to indicate that the gelatin gel retains its integrity and mechanical strength during the pH-induced transition (there is no change in gel volume either).

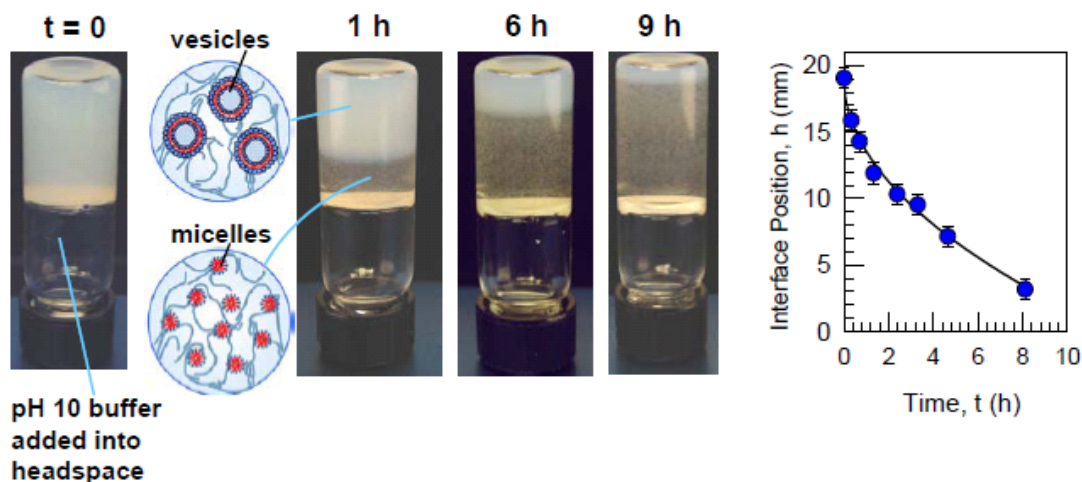


**Figure 3.4.** Movement of micellar front within a vesicle gel due to diffusion of pH 10 buffer. The buffer is introduced into the headspace above the gel at time zero. As the buffer diffuses into the gel, NaOA vesicles in the gel are converted into NaOA micelles, as indicated by the change in a portion of the gel from bluish to colorless. As time progresses, the micellar front travels deeper into the gel, indicating that more of the vesicles are converted into micelles. After 9 h, the micelle region covers most of the gel. The plot on the right shows the interface position (measured from the top of the vial) as a function of time. The line through the data is a fit to eq 1.

The above result is reproducible and can be replicated in other geometries (see below). More quantitative results were gathered from a second experiment in the same vial geometry and are shown in the right-hand panel of Figure 3.4. In this case, the vesicle-gel was loaded in a cylindrical vial of diameter 7 mm and up to a height of 19 mm. The remaining volume of the vial was filled with pH 10 buffer. The setup was monitored by a camera over the duration of the experiment. From photographs at different instants of time, we were able to monitor the movement of the micelle-vesicle front (i.e., the interface between the micelle-rich and vesicle-rich regions) within the gel. The data (Figure 4) follow the classic diffusive scaling with  $\sqrt{t}$ .<sup>65-67</sup> In other words, the

progression of the front is apparently limited by the rate of diffusion of buffer into the gel; in comparison, the vesicle-to-micelle transition occurs much faster.

We can then model the time-dependent position of the vesicle-micelle interface  $h(t)$  by the 1-dimensional diffusion equation:<sup>66</sup>

$$h(t) = h_0 - \sqrt{2Dt} \quad (3.1)$$

where  $D$  is the diffusivity of the buffer and  $h_0$  is the position at  $t = 0$  (which equals the total height of the gel). By fitting this equation to the data in Figure 3.4, we obtain a diffusivity  $D$  of  $4.2 \times 10^{-5} \text{ cm}^2/\text{s}$  for the buffer (hydroxide) ions from the external bath into the gelatin gel. This value is quite comparable to the bulk diffusivity of hydroxide ions in water ( $5.6 \times 10^{-5} \text{ cm}^2/\text{s}$ ).<sup>68</sup> In other words, the ions diffuse in the gel much like they would in water; this is not surprising since the hydrated size of the ions should be much smaller than the mesh size of the gel. The latter value is estimated from the literature to be about 5 nm for a 5% gelatin gel.<sup>69-70</sup>

We have seen from Figure 3.3 that it is possible to create a cylindrical gel with different microstructures over different regions. For example, half of the cylinder could contain vesicles and the other half micelles. If the gel is removed from the buffer solution and stored separately, this “pattern” is retained for several days. Similar patterning can also be done with gels of other geometries. For example, we made a vesicle-loaded gel (5% gelatin, 0.5% vesicles) into a spherical ball, 41 mm in diameter. This ball was then immersed in a bath of pH 10 buffer. As the vesicle-micelle front moved radially inward, the vesicles in the outer shell were transformed into micelles whereas the core remained

intact. This is evident from Figure 3.5 (top panel) where we see the clear micellar shell surrounding the bluish vesicle core. With increasing time, the shell becomes thicker and eventually the entire gel contains only micelles. Thus, we can easily create core-shell patterns with a vesicle core of given size surrounded by a micellar shell.

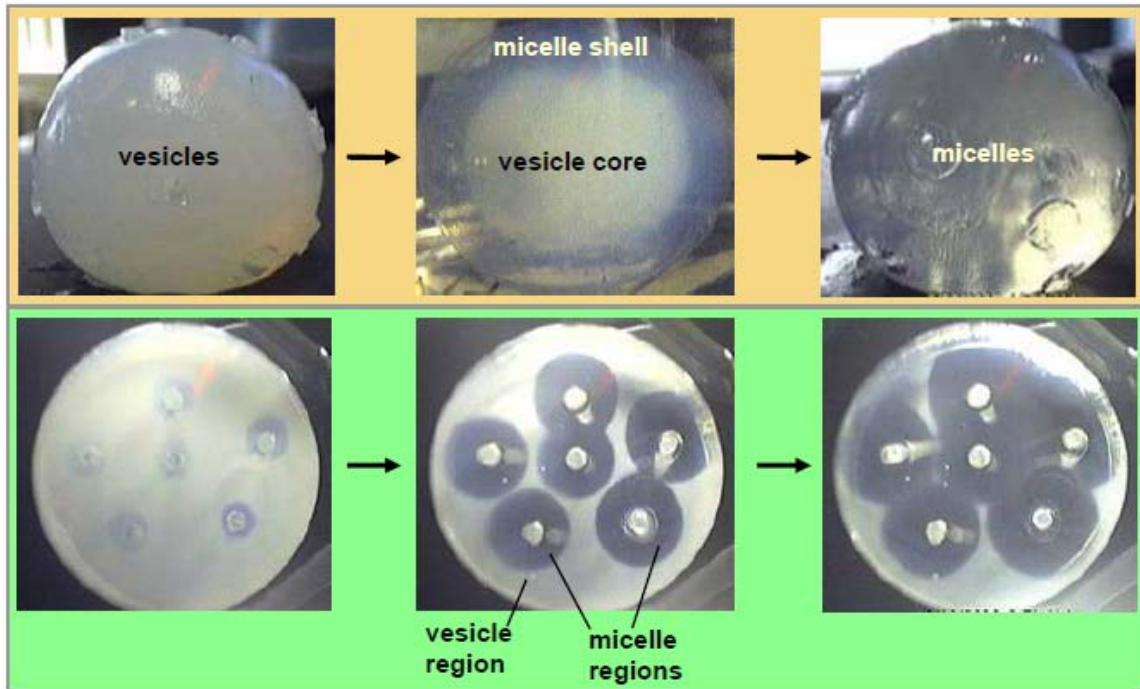


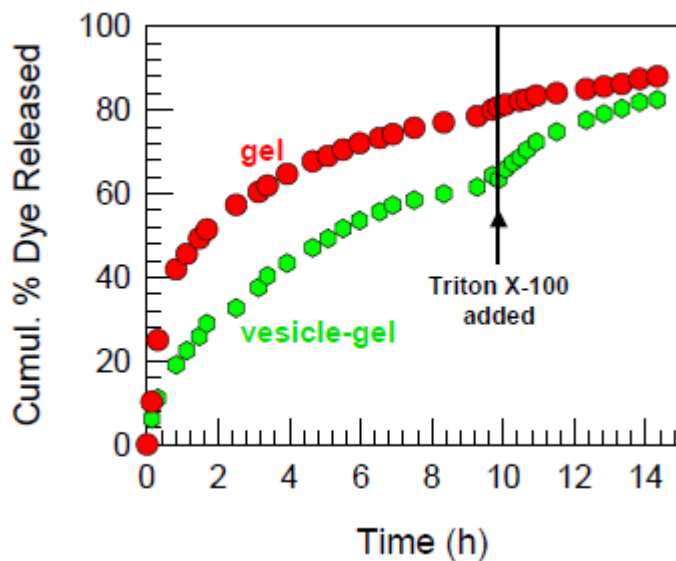
**Figure 3.5.** Patterning of vesicle gels by inducing localized vesicle to micelle transitions. (Top panel): core-shell structure with a vesicle-rich core surrounded by a micelle-rich shell. This is accomplished by immersing a spherical gel (41 mm diameter) in a pH 10 buffer. The photographs correspond to increasing incubation times in this buffer solution. (Bottom panel): gel in a petri dish with micelle-rich regions created at discrete points. This was done by sticking straws into the gel and subsequently filling the straws with the pH 10 buffer. The photographs again correspond to increasing times and show the expansion of the micelle-rich regions as the buffer diffuses into the gel.

Another patterning experiment was carried out with the above vesicle-gel in a Petri dish of diameter 90 mm and with the gel thickness being ~ 10 mm. We then stuck 6 drinking straws loosely into the gel at several locations. The straws were then filled with

pH 10 buffer. As the buffer diffused into the gel, the regions surrounding the straws became clear, indicating that the vesicles in those regions had been converted into micelles. This is shown in Figure 3.5, bottom panel. The clear regions are roughly circular in cross-section, and as time progresses, the circles grow radially outward from the straw positions. Eventually, the clear regions merge with one another and at this stage most of the vesicles in the gel have been transformed into micelles. Variations of the above experiments can be used to create more complex patterns. As mentioned in the Introduction, an ability to create gels containing pockets of vesicles at precise locations within the bulk structure could have applications in areas such as tissue engineering.

One comment needs to be made regarding the reversibility of the transition, i.e., back from micelles to vesicles. While a vesicle to micelle transition can be readily induced by high pH buffer, the vesicles *cannot* be subsequently re-formed in the gel if it is brought into contact with a low pH buffer. The reason has to do with the mesh size of the gel, which was estimated above to be  $\sim 5$  nm. Vesicles of NaOA are thus large enough to be trapped within the gel mesh, but spherical micelles of NaOA, which have a size around 4-5 nm can “leak” out of the gel and into the external buffer, thereby depleting the NaOA in the interior of the gel. Moreover, for vesicles to be re-formed within the gel matrix, several micelles will need to approach and fuse: again, the mesh is too dense to facilitate such fusion. To re-form vesicles, one would thus have to melt the gel and then combine it with NaOA at the appropriate pH.

**Controlled Release from Vesicle-Gels.** Finally, we study the controlled release of a dye (calcein) from vesicle-loaded gels and we examine whether the release kinetics are influenced by pH. First, Figure 3.6 compares the release of dye from a control gel (no vesicles) and from a vesicle-loaded gel, both containing the same amount of dye. In this experiment, the pH of both the gel and the external solution is at 8.3. In the case of the vesicle-gel, the dye is encapsulated in the vesicles before the vesicles are embedded in the gel (i.e., most of the dye is *inside* the vesicles at time zero). Figure 3.7 shows that the vesicle-gel releases dye at a slower rate than the control gel. The slower kinetics are evidently due to the additional transport barrier presented by the vesicle bilayers, which the dye molecules must first traverse before releasing into the gel and thereafter into the external solution. Similar results have been found in other studies.<sup>51-56</sup>



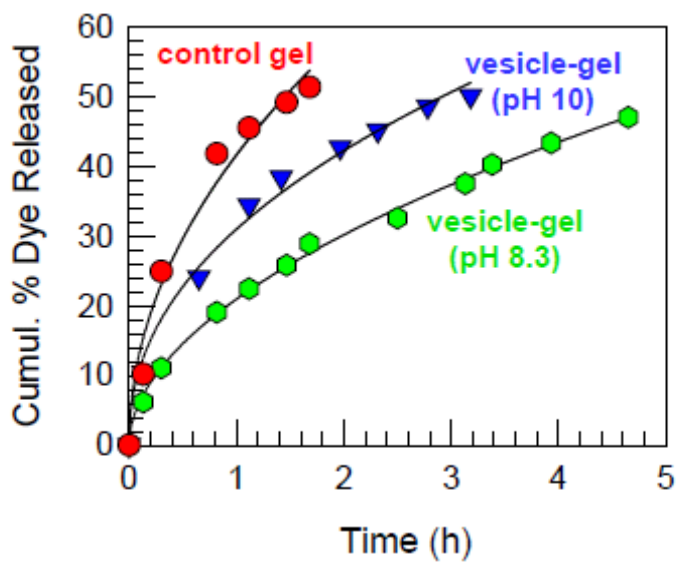
**Figure 3.6.** Release profiles of calcein dye from a gelatin gel and from a vesicle-loaded gelatin gel. In the case of the vesicle-gel, the dye was encapsulated within the vesicles, which were then embedded within the gel. The data show a slower release of dye from the vesicle-gel relative to the control gelatin gel. After 10 h, Triton X-100 detergent was added to the external solution for both samples (this point is marked by the arrow). The detergent diffused in and disrupted the vesicles, which lead to an increase in the rate of dye release.

Figure 3.6 also shows the effect of Triton X-100 detergent on the release profiles. This detergent is known to disrupt vesicle bilayers and thereby convert vesicles into micelles.<sup>56</sup> We added Triton to the external solution at the 10 h mark. This had no significant effect on dye release from the control gel, but the release curve from the vesicle-gel shows a sharp increase in slope. Evidently, the Triton molecules diffuse into the vesicle-gel and disrupt the vesicles, causing the encapsulated dye to spill out into the external gel and thus exit the gel at a faster rate; similar results have been reported previously.<sup>56</sup> Eventually, the vesicle-gel release profile catches up with that from the control gel (4 h after Triton addition). The overlap of the two curves confirms that the two gels contain approximately the same overall amount of dye. The Triton experiment is also an indirect proof for the existence of intact vesicles in the vesicle-gel. In addition, the experiment shows how the release rate from a vesicle-gel can be tuned by addition of certain molecules to the external solution.

We now discuss the effect of external pH on the calcein release profiles. The results are shown in Figure 3.7, where data from three experiments are displayed. Two of these are identical to those in Figure 3.6, namely a control gel (no vesicles) and a vesicle-loaded gel. For these two cases, both the gel and the external solution are at a pH of 8.3. Comparing the results, again the vesicle-gel releases dye much more slowly than the control gel, consistent with the data in Figure 3.6. The third case is the vesicle-gel placed in contact with a pH 10 buffer at time zero: in this case, the release rate is *higher* compared to the same gel at pH 8.3. This result agrees with our expectations and is similar to the effect of Triton in Figure 3.6. We expect the pH 10 buffer to diffuse into the



vesicle-gel and transform the vesicles into micelles, as shown earlier by the moving front in Figure 3.3. In turn, the dye encapsulated in the vesicles will be released into the gel matrix and these molecules would no longer have to contend with the vesicle bilayer as a transport barrier. This explains the net faster release of dye molecules out of the gel. In effect, the dye release kinetics for the pH 10 case gradually begins to resemble that of the control gel (i.e., a gel with no vesicles). Figure 3.7 thus conceptually demonstrates the use of pH as a trigger to accelerate the release rate of dye from our vesicle-gels.



**Figure 3.7.** Tunable calcein release from a vesicle-loaded gel based on the pH of the external solution. The control is a gelatin gel surrounded by a pH 8.3 buffer and in this case (red circles), the dye is released rapidly. The same gel loaded with vesicles releases dye much more gradually at pH 8.3 (green hexagons): in this case, the vesicles are intact and the vesicle bilayer thus presents a transport resistance. On the other hand, if the same vesicle-loaded gel is placed in contact with pH 10 buffer, the dye release is more rapid (blue triangles): in this case, the high pH converts the vesicles into micelles, thereby eliminating the transport resistance due to the vesicle bilayers. All the data are fit to eq 2 and the fit parameters are shown in Table 1.

The dye release curves in Figure 3.7 can be quantitatively treated using the following equation due to Peppas:<sup>65-67</sup>

$$\frac{M_t}{M_\infty} = kt^n \quad (3.2)$$

where  $M_t/M_\infty$  is the fractional dye release,  $k$  is a rate constant, and  $n$  is an exponent characteristic of the transport mechanism. This equation is only valid for short times such that  $M_t/M_\infty < 0.6$ . Fits of eq 2 to the data are shown in Figure 3.7 and the fit parameters are shown in Table 3.1 (in all cases, the quality of the fit was very good, with  $R^2 > 0.99$ ). The exponent  $n$  is determined to be 0.49 for the control gel and 0.53 for the vesicle-gel at pH 8.3; both are close to the value of 0.5 expected for Fickian diffusion in a slab geometry.<sup>66</sup> For the vesicle-gel at pH 10 the value of  $n$  is 0.45. The slight discrepancy in this case is probably because two processes are occurring simultaneously: the vesicles being disrupted into micelles and thus releasing dye into the gel, and the free dye in the gel diffusing out into the solution. Note that the rate constant  $k$  is highest for the control gel and lowest for the vesicle-gel with intact vesicles (pH 8.3). The acceleration of dye release due to the increase in pH is reflected in a 50% increase in the magnitude of  $k$  (from 0.2 at pH 8.3 to 0.3 at pH 10).

Sample	$k$	$n$
(1) Gel, no vesicles	0.4	0.49
(2) Vesicle gel, pH 8.3	0.2	0.53
(3) Vesicle gel, pH 10	0.3	0.45

**Table 3.1.** Parameters obtained by fitting eq 2 to dye release curves in Figure 7.

### **3.4 Conclusions**

We have shown that nanoscale vesicles of NaOA can be entrapped within gelatin hydrogels. The resulting vesicle-gel hybrids exhibit the pH-responsive properties of the NaOA vesicles. Specifically, when exposed to a pH 10 buffer, the vesicles within the gel become transformed into micelles. Vesicle disruption can be done in a controlled manner at specific locations within a gel. Gels can thus be “patterned” to have vesicle-rich and micelle-rich domains in predetermined arrangements. The utility of entrapping pH-responsive structures within the gel is in the area of controlled release of hydrophilic solutes. We show that the release of calcein dye out of a vesicle-gel into the external solution is accelerated when the solution pH is raised to 10. This increase is attributed to a pH-induced vesicle to micelle transition within the gel, which reduces the transport resistance to dye diffusion.

## Chapter 4

# Biopolymer Capsules Containing Vesicles: “Motherships” for Controlled Drug Release

---

### 4.1 Introduction

Two major classes of drug delivery vehicles are (1) microcapsules and (2) liposomes. Polymer microcapsules, which can range from a few  $\mu\text{m}$  to  $>1,000 \mu\text{m}$  are particularly interesting due to the wide range of packaging, targeting, and tunable release mechanisms they offer.<sup>71</sup> However, they are often avoided during pharmaceutical formulation as many methods of preparing them involve heat or organic solvents, which may destroy labile therapeutic molecules.<sup>72-73</sup> These common, yet labor-intensive and/or drug damaging methods of microcapsule synthesis include layer-by-layer polymer deposition (involving burning or harshly dissolving away an inorganic core),<sup>74</sup> oil-in-water emulsion polymerization,<sup>75</sup> and organic solvent evaporation.<sup>76</sup> In addition to the directly negative potential effects on the drug payload during processing, it can be difficult to develop uniformly sized populations of microcapsules, resulting in unpredictable drug release and biodistribution profiles.<sup>77</sup>

Liposomes, the other major class of drug carrier, are generally much smaller in size at  $\sim 100 \text{ nm}$ . These structures have also been suggested for numerous drug delivery applications, especially those involving the targeting and uptake of the liposome directly into cells.<sup>78-79</sup> These self-assembled spheroid structures, with lipid bilayers reminiscent of

cell membranes, are excellent for packaging a wide range of therapeutic molecules and are highly biocompatible. While PEGylation technology has greatly improved the parenteral administration of liposomes,<sup>80</sup> these structures still face unfavorable destabilization due to absorbed proteins from the bloodstream or from roaming phospholipases in soft tissue applications.<sup>81</sup>

Hybrids of these 2 structures, i.e. capsules containing vesicles, are attractive because they may potentially retain the advantages of both, while simultaneously mitigating some of the disadvantages of each separately. For example, capsules may protect vesicles from external stimuli, such as low or high pH, and from destruction by biological “watchdogs,” e.g. macrophages. Conversely, vesicles may extend the functionality of capsules, since they are generally more effective at encapsulating hydrophobic drugs (such as many anti-cancer formulations)<sup>82-83</sup> than the capsules themselves. Finally, the combination of transport resistances from the vesicle bilayer and the capsule shell can again prolong the release of encapsulated drug.

In recognition of this potential, such hybrid structures have been synthesized in a number of previous studies. The Langer group were the first to show that vesicles could be trapped within alginate microcapsules and that dye encapsulated in the vesicles could be released slowly under certain conditions.<sup>84</sup> Subsequent studies from the same group showed that micro-encapsulated vesicles could extend the *in vivo* drug release time and minimize immune responses.<sup>85</sup> The concept of “vesicles in capsules” has been used thereafter by other researchers.<sup>86-88</sup> Cohen et al. encapsulated vesicles into alginate-PLL

capsules.<sup>88</sup> Additionally, Feng et al have demonstrated stable liposome-in-microsphere structures which are able to achieve sustained release of drug.<sup>89</sup>

More recently, Dhoot et al. have studied the effect of crosslinking ions on release rates of fluorescein-isothiocyanate labeled bovine serum albumin (FITC-BSA) from vesicle-loaded alginate capsules.<sup>90</sup> A rapid initial burst of the FITC-BSA protein was observed when alginate beads were ionically crosslinked with  $\text{Ca}^{2+}$ ,  $\text{Al}^{3+}$ , and  $\text{Ba}^{2+}$ . The release rate of the protein was found to differ based on the type of ions used in generating the capsules. Additionally, Ramadas et al. have used vesicle-loaded alginate-chitosan capsules for oral delivery of insulin.<sup>91</sup> These capsules were able to deliver insulin to the intestine without undergoing degradation in the acidic environment of the stomach. This example hints at the oral drug delivery administration route as very relevant clinical niche for these vesicle-in-capsule formulations. The capsule shell can serve as a protective barrier for the vesicles and their encapsulated contents against the harsh gastrointestinal environment while en route to the bloodstream via the intestine.

In this study, we also create biopolymer capsules containing liposomes, here through a mechanism of self-assembly. Liquid mixtures of liposomes and chitosan, a cationic biopolymer, are added dropwise into solutions of anionic biopolymer, gellan gum, or surfactant, sodium dodecylbenzene sulfonate (SDBS). Spherical capsules are formed immediately due to electrostatic interaction between the positively and negatively charged structural molecules at the droplet interface. We call these biopolymer capsules containing vesicles “motherships,” as these larger containers are able to retain smaller

intact containers, i.e. “babyships,” within their lumen. An overview of this type of soft structure is shown in **Figure 4.1**. Note that we can create small micro-sized capsules (~200  $\mu\text{m}$ ) by means of employing an electric field beneath a 200  $\mu\text{m}$  nozzle, or we can simply drop chitosan/liposome solution out of a standard pipet and create macro-, or “over-the-counter” sized capsules. To our knowledge, no one has produced chitosan-gellan or chitosan-SDBS capsules containing liposomes.

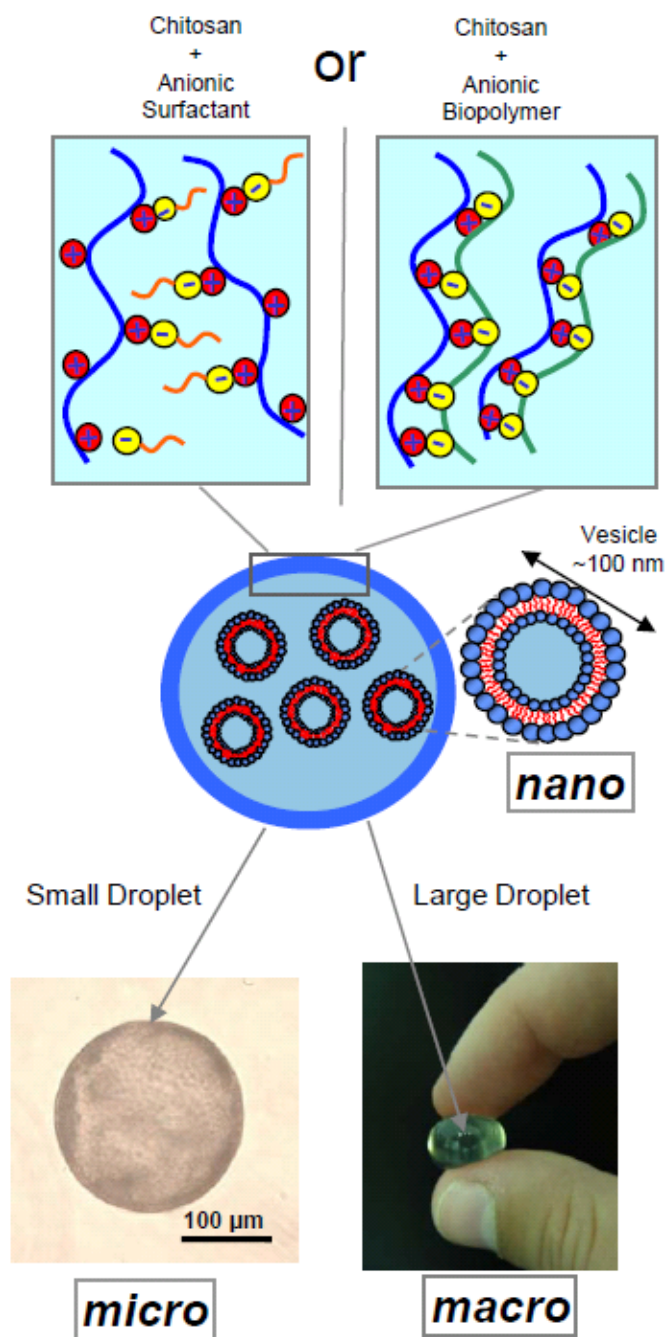


**Figure 4.1. Formation Chitosan ‘mothership’ capsules containing vesicles.** Capsules are formed by dropping a positively-charged amphiphilic biopolymer mixed with vesicles (~100 nm in size) into a solution of negatively charged SDBS surfactant or negatively charged gellan gum biopolymer. Spherical capsules are formed instantaneously. Capsule size is dictated by droplet size and sizes can range from ~100 μm (*micro*) to 10,000 μm (*macro*)



Although many advantages of the combined properties of vesicles and capsules have already been reported in the literature, here we aim to reiterate some of those advantages while extending the potential use of hybrid systems in two key ways. The first is that we explore the ability of these motherships to conduct controlled or triggered release of the vesicles themselves,<sup>92</sup> which is a largely unexplored subtopic within the field of drug delivery. Why is controlled release of vesicles potentially high impact from a therapeutic standpoint? As a first example scenario outlined in **Figure 4.2**, these capsules could be useful for cancer therapy by injecting or implanting them in the vicinity of tumor tissue. An anti-angiogenic drug could be packaged within the lumen of the capsule, whereas a cytotoxic cancer drug could be contained within the vesicles. The anti-angiogenic drug would be released first and subsequently slow or stop the growth of new blood vessels into the tumor tissue.<sup>93</sup> Secondly the capsule would degrade, releasing the drug-loaded vesicles into the blockaded tumor tissue, locally destroying the diseased cells. As a further example, neural circuits are largely dependent upon the triggered release of vesicles carrying neurotransmitters within the neuronal synapse.<sup>94</sup> Creating structures that would allow for triggered release of vesicles may provide a way to build high-level circuitry within soft, ‘squishy’ environments, much like the brain. Of course, these sorts of advances may give important insights on neurodegenerative diseases that involve hindered neuronal signal transmission (e.g. Multiple Sclerosis, Parkinson’s Disease).<sup>95-96</sup>

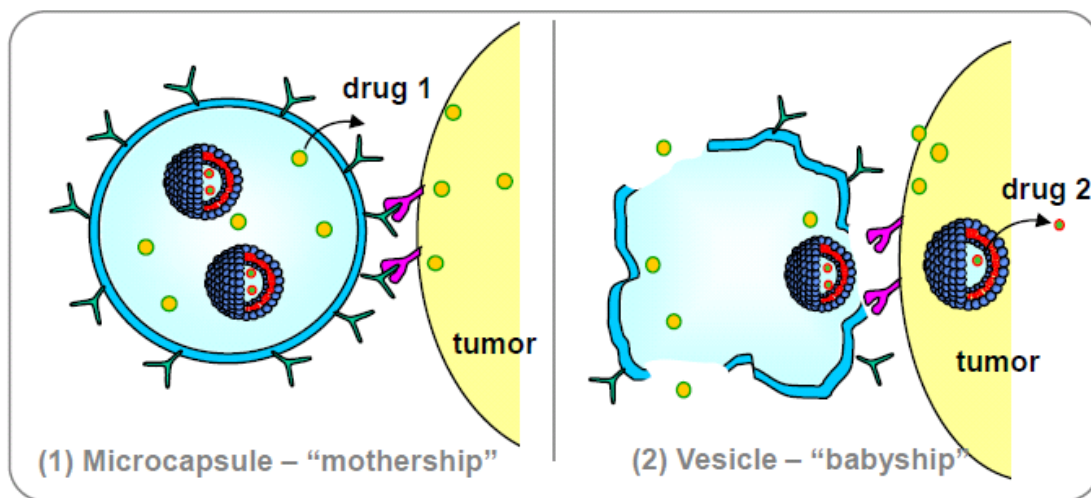


**Figure 4.2. Schematic of Chitosan ‘mothership’ capsules attacking a tumor.** In step (1), the microcapsule “motherships” would be docked at the tumor site using antibodies or magnetic targeting and thereafter release one drug from the capsule lumen (e.g. an anti-angiogenic drug). In step (2), capsule shell would become ruptured due to enzymatic degradation, and “babyship” vesicles carrying cytotoxic drug would escape freely into the tumor tissue.

The second extension upon the vesicle-within-capsule concept presented here is a vesicle-within-(*small*)capsule-within-(*large*)capsule concept. These latter structures are built by the exact same one-step drop method, but instead, utilizing nozzles of different sizes to put smaller capsules containing vesicles within larger sized capsules, and hence provide a simple means of assembling materials display important structural features over a hierarchy of length scales. What advantages or insights could these kinds of hierarchical structures present? Certainly in biology, there are many examples of systems exhibiting important features over a hierarchy of length scales. Cells contain hundreds of smaller enclosed structures within their membrane including, the nucleus, endosomal vesicles, lysosomal vesicles, mitochondria, etc. Interestingly, an encapsulation system containing biological components, such as enzymes, proteins and detoxicants, was originally

proposed in 1964 by Chang *et al* as an “Artificial Cell.”<sup>97</sup> As a next generation of this original theory, the hierarchical capsules shown here could potentially serve as much more advanced cellular mimics. By the described one-step drop procedure, a pre-designed fleet of containers, e.g. one medium-sized capsule containing DNA (nucleus), ~30 smaller capsules stuffed with ATP (mitochondria), and hundreds of vesicles packed with digestive enzymes (lysosomes), could all be housed within one large capsule. Such a structure could be prepared in just minutes using only elementary lab hardware.

## 4.2 Experimental Section

**Materials.** Acetic acid, sodium dodecyl benzenesulfonate (SDBS), n-dodecyl aldehyde, sodium cyanoborohydride, 5,6-Carboxyfluorescein (CF), Triton X-100, rabbit IgG (tagged  $\lambda = 600$  nm emission) and anti-rabbit IgG (tagged  $\lambda = 520$  nm emission), glutaraldehyde (40% in water) and chitosanase from *streptomyces griseus* were all purchased from Sigma-Aldrich chemicals. L- $\alpha$ -phosphatidylcholine (PC) was purchased from Avanti Polar Lipids, Inc. The magnetic nanoparticles ( $\gamma$ -Fe<sub>2</sub>O<sub>3</sub>) were purchased from Alfa Aesar. Their size was specified to be  $32 \pm 18$  nm, and their average surface area was 42 m<sup>2</sup>/g. Magnets were obtained from United Nuclear. All experiments were performed using 18.2 M $\Omega$  DI Water.

**Chitosan.** Chitosan of medium molecular weight (190-310K) and Brookfield viscosity of 286 cps was obtained from Aldrich. The reported degree of deacetylation was about 80%, and this has been verified by NMR (Supplemental Info). The chitosan backbone is thus

mostly composed of D-glucosamine [ $\beta$ -(1,4)-2-deoxy-2-amino-D-glucopyranose] sugars, with a small fraction of *N*-acetyl-D-glucosamine [ $\beta$ -(1,4)-2-deoxy-2-acetamido-D-glucopyranose] sugars as well. Chitosan is pH-sensitive as a result of its amine groups and is soluble only under acidic conditions, that is, at a pH < 6.5. We have used 0.2M acetic acid to control the pH in chitosan solutions.<sup>98</sup> Chitosan acts a cationic polyelectrolyte under these conditions.

**Gellan Gum.** Gelrite<sup>®</sup> Gellan Gum (FW 1,000,000) was obtained from Sigma. Gellan gum is a water-soluble negatively charged polysaccharide with a repeating tetrasaccharide unit consisting of two residues of D-glucose, one residue of L-rhamnose, and one residue of D-glucuronic acid. All units are joined by  $\alpha$ -1,3 glycosidic bonds.

**Synthesis of Hydrophobically-Modified Chitosan (hm-Chitosan).** We attached *n*-dodecyl tails to chitosan by reacting the amine groups with *n*-dodecyl aldehyde. The procedure follows that reported in the literature.<sup>99</sup> Briefly, it involves the addition of aldehyde to an acidic solution in a water-ethanol mixture, followed by addition of sodium cyanoborohydride. The molar ratio of aldehyde to that of the chitosan monomer(s) was fixed at 5% in this study. The hm-chitosan was precipitated by raising the pH and adding ethanol, and the precipitate was purified by washing with ethanol followed by deionized water. The final hm-chitosan precipitate was redissolved in acetic acid solution, and the concentration was recalibrated.

**Preparation of Capsules:** In general, capsules were formed by dropping liquid mixtures of liposomes and chitosan ('feeders') into solutions of either negatively biopolymer (Gellan Gum) or surfactant (SDBS). The size of the capsule is dictated by droplet size. Macro-sized capsules (1000 – 5000  $\mu\text{m}$ ) were made by dispensing chitosan/liposome solution from either a 22G needle via syringe, or by a large aperture fluid transfer pipet. Smaller capsules (200, 400  $\mu\text{m}$ ) were made using a Nisco Engineering Encapsulator Unit (Norway) with the following settings: voltage 6.5 kV, flow rate 20 mL/hr, 0.2 or 0.4 mm (accordingly) needle diameter, needle distance from gellan or SDBS bath 1.3 cm.

**Chitosan-SDBS Capsules.** Chitosan (0.5 wt%) was mixed with PC liposomes (0.5 wt %) as the feeder. This feeder was loaded into a syringe and dispensed via 22G needle into a free-standing solution of 2.5 wt% SDBS. Capsules were allowed to incubate in SDBS solution for 2 min, after which the SDBS solution was dumped from the vial while the capsules were retained via strainer. Capsules were then washed 3 $\times$  with 10 ml of DI water so as to remove any excess SDBS. In another sample preparation, hm-chitosan (0.5 wt%) was used to form the capsules instead of unmodified chitosan.

**Chitosan-Gellan Capsules.** This method of capsule formation largely follows that of Yamamoto *et al.*<sup>100-101</sup> Chitosan (1.5 wt%) was mixed with PC liposomes (0.5 wt%) as the feeder. This feeder was also loaded into syringe and dispensed via 22G needle into a heated solution of gellan gum (60°C) under stirring. Capsules were allowed to incubate in gellan gum solution for 30 min, after which the gellan was dumped from the vial while the capsules were retained via strainer. Capsules were then washed 3 $\times$  with 10 ml of DI water so as to remove any excess gellan. After resuspension in buffer solution, the capsules were kept under light stirring.

**Liposome Preparation.** Liposomes were prepared by an extrusion method, as recommended by the manufacturer (Avanti Polar Lipids). Briefly, dried films of the lipids were hydrated under moderate stirring, freeze-thawed 5 times, and then passed through two double-stacked polycarbonate membrane filters (100 nm pores) using a Lipex pressurized extrusion system. Dye-filled liposomes were prepared in DI water from PC (20 mM) and CF (20 mM) and purified of free CF using the Sephadex G-50 column.

**Optical Microscopy.** The Zeiss Axiovert 135 TV inverted microscope equipped with the Motic Image Plus imaging system has been used for optical microscopy (bright-field). Capsules were imaged with a 2.5X objective.

**Dynamic Light Scattering (DLS).** DLS was used to characterize the sizes of vesicles in solution. A Photocor-FC light scattering instrument with a 5 mW laser source at 633 nm was used at a scattering angle of 90°. A logarithmic correlator was used to measure the intensity autocorrelation function. The hydrodynamic size of the vesicles was extracted from the data using the Stokes-Einstein equation.

**Fluorescence Microscopy.** Photomicrographs of fluorescent electrodeposited materials were taken by a fluorescence stereomicroscope (MZFLIII, Leica) equipped with a digital camera (Spot 32, Diagnostic Instruments). To observe primary IgG antibody fluorescence, the filters were chosen with an excitation wavelength of 560 nm (bandwidth of 40 nm), and an emission filter of 610 nm. To observe secondary anti-IgG antibody fluorescence,

the microscope was set with an excitation wavelength of 480 nm (bandwidth of 40 nm) and a long-pass emission filter at 510 nm.

**Release Profiles.** Lipid vesicles were combined with 25 mM CF dye. To separate unencapsulated dye, the vesicle-dye mixture was passed through a Sephadex G-50 size-exclusion chromatography (SEC) column. The vesicle fraction (with encapsulated dye) was collected and used in preparing the vesicle-loaded capsules. Note that in these experiments, “macrocapsules” approximately 5 mm in diameter were used so as to allow easy collection of external aqueous media. To examine the release of dye, 4 g of phosphate buffer solution (pH 7.4) was added to the capsules after washing. The concentration of CF in the external buffer solution was measured by UV-Vis spectrometry (Cary Bio 50). A control gel (no vesicles) was prepared using an amount of CF equal to that in the encapsulated vesicles. To determine the latter, 2 mL of the vesicle fraction from SEC was analyzed by UV-Vis after the vesicles were disrupted by adding 50  $\mu$ L of Triton-X100.

**Enzymatic Degradation of Capsules.** Chitosanase was added to a Petri dish containing several chitosan-gellan capsules at a concentration of 0.125 units/ml in acetate buffer solution (pH 5). Capsules were then observed under phase contrast microscopy for up to 5 days. Control capsules in acetate buffer solution (pH 5) with no enzyme added were also observed.

## Targetability of Capsules

**Magnetic Capsules.** Chitosan (0.5 wt %) and liposomes (0.5 wt%) were mixed with 0.1% wt  $\gamma\text{-Fe}_3\text{O}_4$  nanoparticles and subsequently dropped into anionic surfactant or biopolymer solution. Capsules were then moved within stagnant fluid in a vial using a large magnet, and then against a flowing aqueous stream within Silicone tubing connected to a pump.

**Antibody Conjugation.** Primary IgG antibody was added in excess to chitosan-SDBS capsules in phosphate buffer solution (pH 7.4) until mild stirring. 100  $\mu\text{l}$  of glutaraldehyde solution was then added to the buffer media under increased stirring. Reaction was allowed to take place for 20 min. The buffer solution was then drained from the vial according to the straining procedure described above. Capsules were washed 3 $\times$  with PBS and then resuspended in PBS. Fluorescence microscopy was used to detect the presence of antibody on the capsule surface. IgG-capsules were then incubated with a secondary antibody, anti-IgG, for a period of 30 min. Capsules again washed according to the above procedure, and imaged in with Fluorescence microscopy.

## 4.3 Results and Discussion

In Figure 4.3, release profiles of model drug, carboxyfluorescein (CF), from these mothership structures are shown. Figure 4.3a shows that chitosan-gellan motherships impregnated with drug-loaded liposomes (red circles) display a sustained release of drug. In contrast, chitosan-gellan control capsules with the same amount of drug freely dispersed inside the capsule lumen shows a classic “dosage dumping” release profile (blue circles). This result is explainable by the additional transport resistance provided by the liposome bilayer in the motherships. While drug inside the control capsules must



only cross 1 barrier, i.e. the capsule shell, the dye inside the motherships must cross two: (1) lipid bilayer and (2) capsule shell. At 3.25 h, a detergent molecule Triton X-100 was added to the external buffer and a spike in dye release for mothership capsules is observed for the remainder of the 4 timeframe. This result gives two key insights into the experiment. Firstly, it demonstrates that the liposomes existed *intact* inside the motherships. Triton X-100 is molecule which rapidly disrupts intact vesicles into mixed micelles, henceforth spilling the contents of the vesicle core into external solution. Thus, the spike in release implies that intact vesicles were broken and the newly escaped drug molecules take on a “dosage dumping” release profile similar to that observed for the control capsules. Secondly, the experiment demonstrates that adequate control capsules which contain an approximately equal amount of dye to the mothership capsules were properly produced.

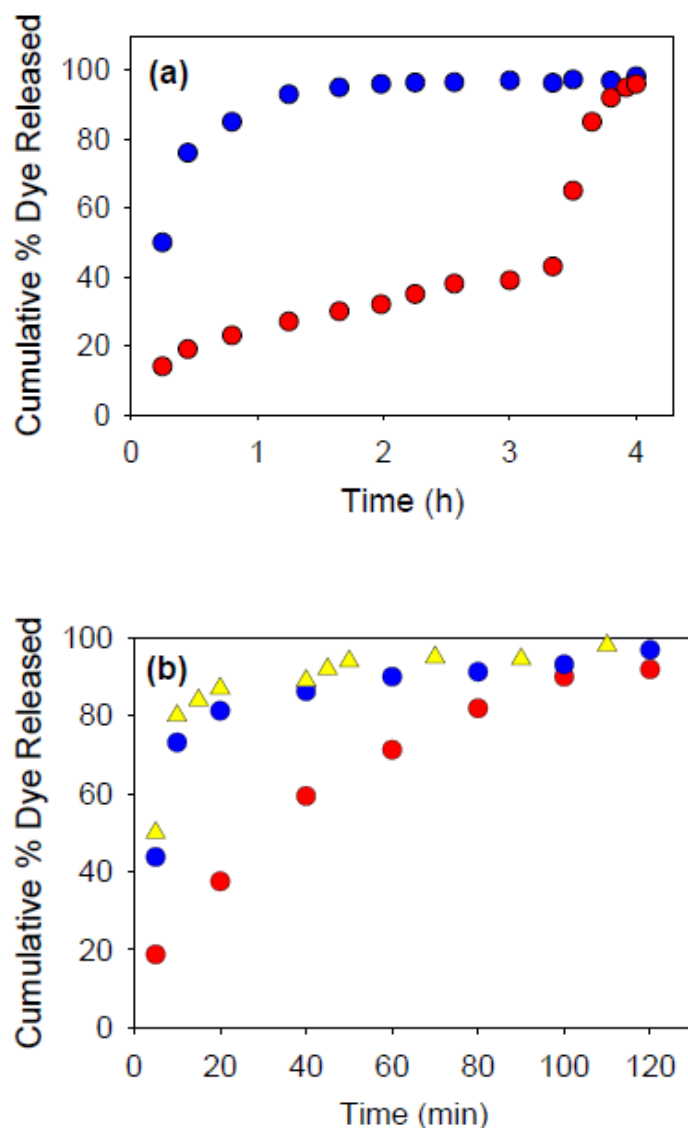


**Figure 4.3. Controlled Release of Dye from ‘Mothership’ Capsules.** In (a), a sustained release is observed for chitosan-gellan capsules impregnated with carboxyfluorescein-loaded liposomes (red circles). Chitosan-gellan control capsules with dye freely dispersed inside the capsule lumen shows a “dosage dumping” release profile (blue circles). Addition of Triton X-100 at 3.25 h shows a spike in dye release for “mothership” capsules, indicating vesicle intactness. In (b), chitosan-SDBS capsules impregnated with CF-loaded liposomes show (blue circles) show a similar release profile to control capsules containing no liposomes (yellow triangles), suggesting potential liposome rupture during capsule formation. In contrast, hm-chitosan capsules formed in SDBS while retaining liposomes, shows a sustained release over a 2 hour interval.

Figure 4.3b shows the release profile of CF from motherships constructed with SDBS surfactant instead of anionic biopolymer. Unexpectedly, the chitosan-SDBS motherships impregnated with CF-loaded liposomes (blue circles) show a similar release profile to control capsules containing no liposomes (yellow triangles). This result suggests potential liposome rupture during capsule formation. Such an outcome is feasible considering high enough concentrations of SDBS molecules are able to rupture liposomes into mixed micelles. Previous work on a similar polyelectrolyte-surfactant system describes the resulting structures as ‘gel beads,’ and suggests that the surfactant quickly diffuses into the entire polyelectrolyte droplet.<sup>102-103</sup> While our own optical microscopy of these capsules displays a distinct “shell” structure of the capsule distinct from the lumen, it is probable that a large number of surfactant molecules infiltrate the droplet core prior to rigid shell formation. In contrast, relative to the unmodified chitosan-SDBS motherships, hydrophobically modified (hm)-chitosan motherships formed in SDBS while retaining liposomes show a sustained release over a 2 hour interval. This could potentially be explained by a delayed diffusion of SDBS into the capsule core due to association with the hydrophobic grafts along the chitosan backbone. This experiment gives some interesting insight into the process of formation of these polyelectrolyte-surfactant complexes, although it also suggests that they are unsuitable carriers of lipid vesicles.

Figures 4.4 and 4.5 outline the potential targetability of these structures via magnetic nanoparticles and antibodies, respectively. In Figure 4.4, magnetically targeted

‘mothership’ capsules via encapsulated  $\gamma\text{-Fe}_3\text{O}_4$  nanoparticles show their magnetic properties in response to a bar magnet. Figure 4.4a displays a magnet collecting a pile of capsules onto the side of the vial. Indeed, this magnet can be used to rapidly move the capsules to any location within the stagnant fluid. Furthermore, as shown in Figure 4.4b, these magnetically-loaded motherships are able to be pulled against a fluid flow within a tube using the magnet. This level of crude targetability is an efficient payoff relative to the simple preparatory work of mixing in the nanoparticles along with the liposomes in the feeder solution prior to capsule formation.

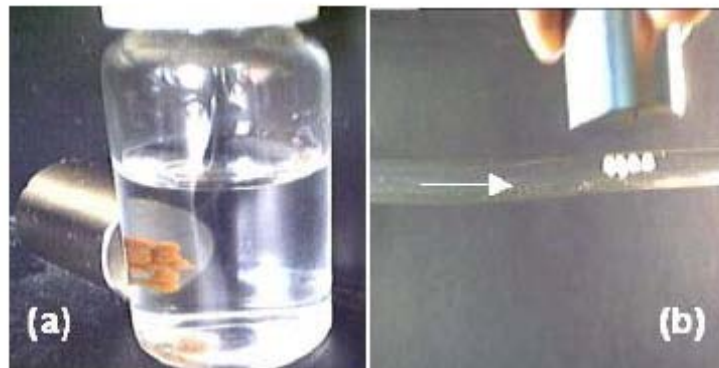


**Figure 4.4.** Magnetically targeted ‘mothership’ capsules via encapsulated ferrite nanoparticles show their magnetic properties in response to a bar magnet. (a) magnet placed near capsules in a vial (b) magnet placed next to a tube in which the capsules are flowing along with the fluid (water) from left to right.

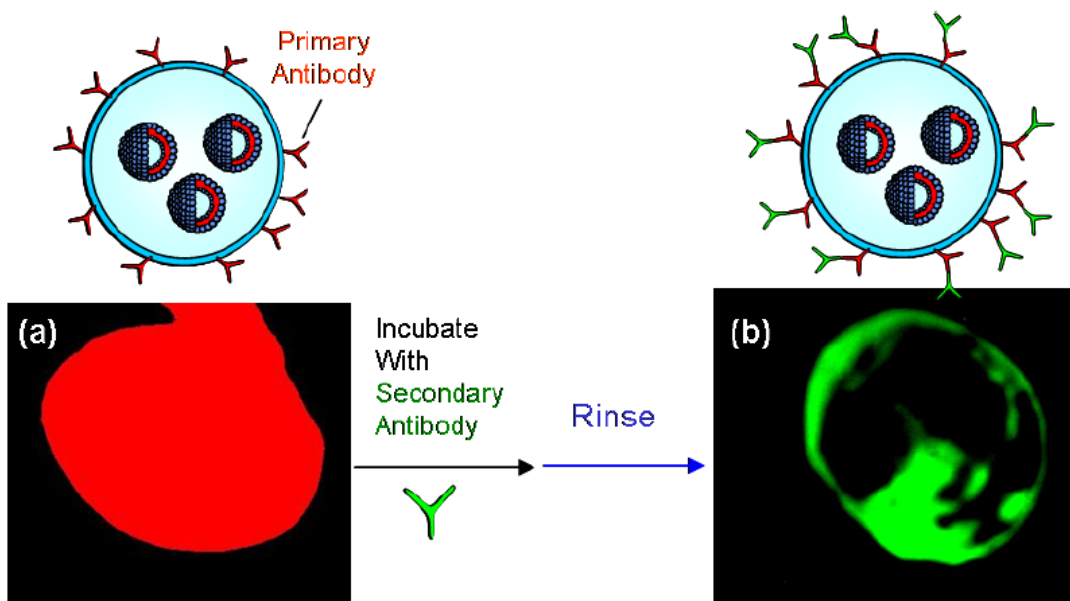


**Figure 4.5. Antibody targeted ‘Motherships.** (a) Fluorescently tagged primary IgG antibody (emission 600 nm) is covalently conjugated to the surface of a Chitosan-SDBS ‘mothership’ capsule as shown by fluorescence micrograph. After incubation with a secondary anti-IgG antibody and subsequent rinsing, fluorescent signal at 520 nm is observed, indicating that a significant amount of primary surface IgG is actively available for ‘lock-and-key’ binding.

Figure 4.5 demonstrates a targetability proof-of-concept via the attachment of fluorescently-labeled mouse IgG antibodies onto the surface of mothership capsules. The synthesis here exploits the plentiful surface amine groups provide by the chitosan molecules. Glutaraldehyde is used as a bifunctional linker, which non-specifically crosslinks moieties bearing amine groups. By adding in glutaraldehyde to a stirring mixture of antibody and capsules, many antibodies become attached to the capsule surface. This linkage is confirmed via fluorescence microscopy (Figure 4.5a) as a uniformly bright red color is observed on the capsule after thorough washing.

To demonstrate functionality of the newly conjugated antibodies, capsules were brought incubated for 20 min with a secondary antibody specific for IgG (FL-anti-mouse-

IgG). After washing several times with buffer, the capsules were examined under fluorescence microscopy as shown in Figure 4.5b. After incubation with a secondary anti-IgG antibody and subsequent rinsing, fluorescent signal at 520 nm is observed, indicating that a significant amount of primary surface IgG is actively available for “lock-and-key” binding, although not with the same level of uniformity observed for the primary antibody. This result suggests that a significant amount of the primary antibody is available for binding and hence applicable for targeting applications. Of course, a remaining portion of the primary antibody is not available for binding, which is not surprising given the crude, non-specific nature of glutaraldehyde chemistry involved.

Next, we explore the triggered rupture of these motherships via enzymatic degradation. Figure 4.6a displays a phase micrograph of an intact chitosan-gellan mothership, approximately 5 mm, in size prior to addition of chitosanase. After enzyme is added to the surrounding media, the progression of mothership degradation over time is shown in Figure 4.6b. At 1 hour, little effect is shown on the capsule shell, i.e. the effect of the enzyme is not immediate. However, after a period of 2 days the capsule shell has clearly shriveled, presumably due to loss of mechanical integrity. Furthermore, after a period of 5 days, the capsules are completely broken and pieces of shell debris are observed floating in the sample. After 7 days, the debris is fully dissolved and clear solution produced. It is important to note that after this 7 day period, the solution scatters light from structures measured at approximately ~100 nm in size by dynamic light scattering (DLS). These structures are presumably intact vesicles, as they closely match the DLS measurements of the same vesicles prior to addition to the feeder solution. Control

capsules to which no enzyme was added show no degradation after the same time period of 5 days. Also, it is worth noting that the chitosanase cannot degrade chitosan capsules formed with SDBS, most likely due to protein denaturing caused by the surfactant.

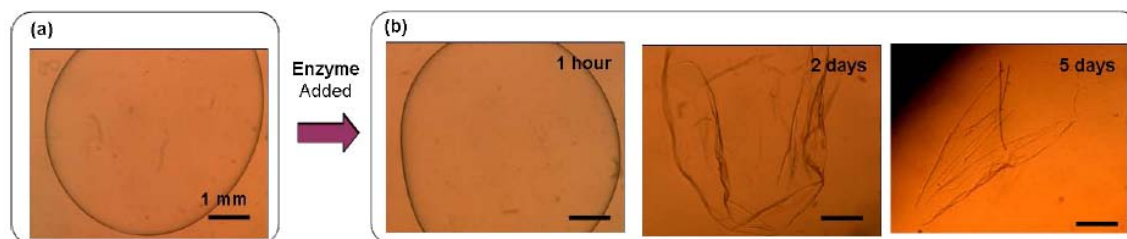


**Figure 4.6. Enzymatic Degradation of ‘Mothership’ Capsules.** (a) Phase contrast micrograph of Chitosan – Gellan capsules formed by standard drop method via 22G syringe needle; (b) 1h, 2d, and 5d micrographs of chitosan-gellan capsule after addition of 10 units/ml of chitosanase in external buffer solution. Capsule appears almost wholly degraded after the studied 5 day interval. Note that the chitosanase cannot degrade chitosan capsules formed with SDBS.

Lastly, we were interested in building hierarchical structures by placing smaller capsules within larger capsules, again employing the same one-step drop method. A schematic of this kind of structure is shown in Figure 4.7. By a simple one-step self-assembly process, structures displaying a hierarchy of length scales, from nano (i.e. vesicles), to micro (microcapsules), to macro (large capsules) can be produced. These structures have the capability to package a wide variety of molecules and targeting agents either on their surface, or within their multi-level lumens. Presumably the release of each of the molecule would differ based upon their original location within the hierarchical structure.

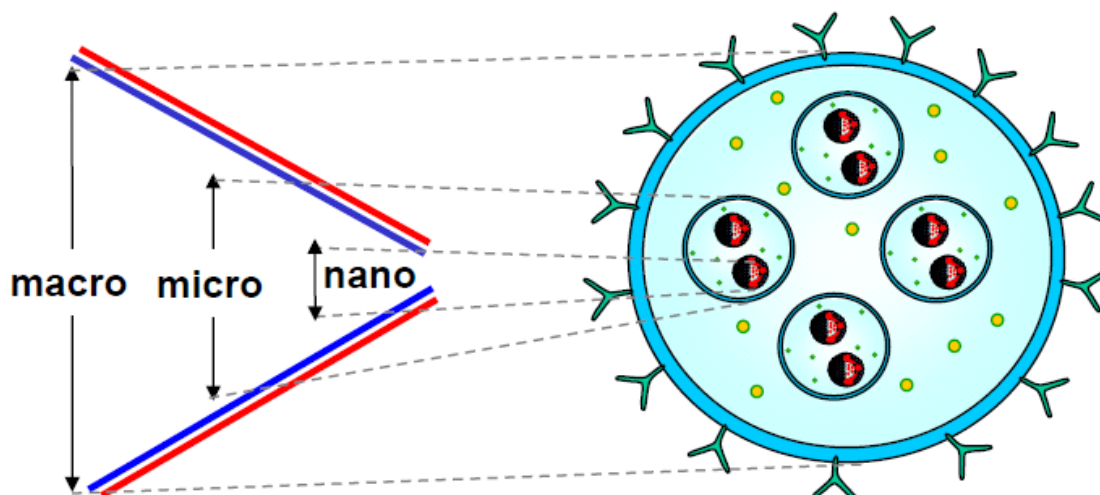


**Figure 4.7. Schematic of hierachical nano-micro-macro ‘motherships.’** By a simple one-step self-assembly process, structures displaying a hierchary of length scales, from nano (i.e. vesicles), to micro (microcapsules), to macro (large capsules) can be produced. These structures can package a wide variety of molecules and targeting agents either on their surface, or within their multi-level lumens.

In Figure 4.8, small chitosan SDBS capsules were formed by the standard drop method via 22G syringe needle. After incubation, capsules were removed from SDBS solution and placed into a fresh chitosan solution. Chitosan solution containing capsules was uptaken by a wide-aperture fluid transfer pipet as a new feeder and dispensed dropwise into a solution of SDBS, thus forming capsule-within-capsule structures. As shown in the micrographs, various numbers of smaller capsules can be placed within these larger capsules. Note that we can create the same sorts of capsule-within-capsule structures with chitosan-gellan, although the inner capsules tend to lose some shell integrity due to pressure from the chitosan in the capsule lumen. Of course, the advantage with the chitosan-gellan system is that we can successfully place intact nanostructures, i.e. vesicles, within the inner capsule lumens.



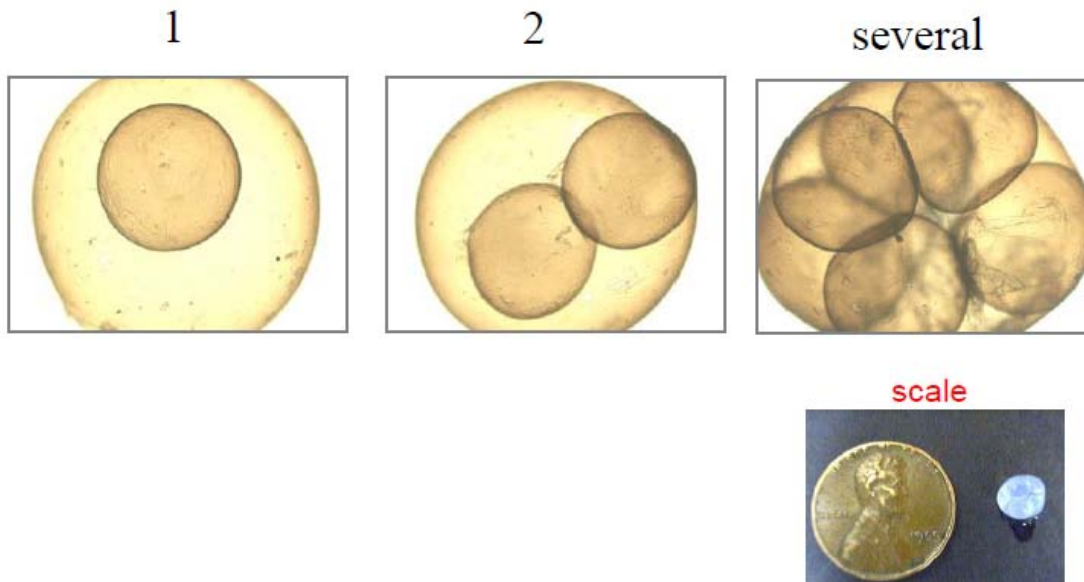


**Figure 4.8. Phase Microscopy (2.5 $\times$ ) of Capsules-within-capsules.** Small Chitosan SDBS capsules were formed by the standard drop method via 22G syringe needle. After incubation, capsules were removed from SDBS solution and placed into a fresh chitosan solution. Chitosan solution containing capsules was uptaken by a wide-aperture fluid transfer pipet and dispensed dropwise into a solution of SDBS, thus forming capsule-within-capsule structures.

Lastly in Figure 4.9, we study the release of dye from capsules-within-capsules using the chitosan-SDBS system. Release of CF dye from smaller capsules packaged with larger capsules (red circles) is significantly sustained over a 30 period relative to the same number of small capsules freely dispersed in aqueous buffer (blue circles). This is expected since the dye molecules experience an added transport barrier of the large capsule shell. Similar results are observed for chitosan-gellan capsules-within-capsules confirming a proof of concept for controlled release from these hierarchical structures.

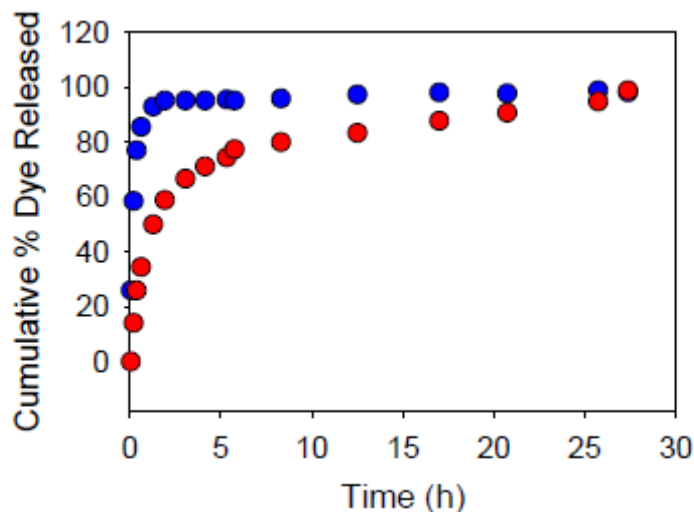


**Figure 4.9. Release of dye from capsules-within-capsules.** Release of carboxyfluorescein dye from smaller capsules packaged with larger capsules (red circles) is significantly sustained over a 24 period relative to the same number of small capsules freely dispersed in aqueous buffer (blue circles).

#### 4.4 Conclusions

We have shown that “motherhip” capsules with hierarchical structural features can be formed by adding droplets of a feeder solution consisting of liposomes and chitosan, a cationic biopolymer, into a solution of anionic biopolymer (gellan gum) or surfactant (SDBS). The resulting structures are spherical capsules; assembly is achieved via electrostatic interactions between oppositely charged polymers/surfactants at the interface of the droplet. Capsule size is simply dictated by drop size. Chitosan-gellan motherhips are able to sustain model drug release due via intact liposomes carrying the drug within the capsule. In contrast, liposomes within chitosan-SDBS motherhips disrupt quickly; this disruption process can be slowed by the covalent addition of hydrophobes to the chitosan backbone prior to capsule formation. The potential for targetability of

motherships was confirmed by (1) by dispersing  $\gamma\text{-Fe}_3\text{O}_4$  nanoparticles within the capsule lumen and (2) attaching IgG antibodies to the capsule surface, a significant portion of which are available for binding secondary antibody. Chitosan-gellan motherships can be degraded by the addition of the enzyme chitosanase; complete degradation occurs over a 7 period, with intact vesicles present in the remaining solution post-degradation. Finally, hierarchical capsule-within-capsule structures can be produced with either chitosan-SDBS or chitosan-gellan systems. Dye release from smaller capsules entrapped within larger capsules undergo sustained drug of a 30 h period.

## Chapter 5

# Vesicle Capture on Patterned Surfaces Coated with Amphiphilic Biopolymers

---

### 5.1 Introduction

Vesicles (or liposomes) are self-assembled “nano-containers” formed by lipids or surfactants in aqueous solution.<sup>104</sup> These structures are ~ 100 nm in size and comprise an aqueous core and a lipid bilayer. The aqueous core can be used to encapsulate hydrophilic molecules such as drugs, proteins, or genes, while hydrophobic and amphiphilic substances can be integrated into vesicle bilayers.<sup>104</sup> Few, if any, other nanostructures demonstrate this level of versatility as carriers of useful payloads. Accordingly, vesicles have been explored and exploited for a myriad of applications, including targeted drug delivery, gene transfection, imaging agents, biosensors, food science, and cosmetics.<sup>105</sup>

Recently, there has been new-found interest into the capture of vesicles on solid substrates, as opposed to vesicles in solution.<sup>106</sup> The motivation for such studies includes: (a) fundamental aspects, e.g., related to vesicles as biological models for adherent cells;<sup>107-109</sup> as well as (b) applied aspects related to the fabrication of biosensors or modified biomaterials.<sup>110-113</sup> In this context, it is to be noted that vesicles usually fuse or rupture into flat bilayers upon approaching a solid surface.<sup>114</sup> This highlights the inherent disconnect between the “soft” nature of vesicles and the “hard” nature of solid surfaces.

However, it is often desirable to capture *intact* vesicles on surfaces.<sup>115-121</sup> If vesicles were intact, their internal volume would be available for entrapping biomolecules, drugs, or fluorescent molecules, which could be useful for sensor and immunoassay applications. In addition, proteins embedded in vesicle bilayers are expected to more closely mimic their *in vivo* function compared to the same proteins in supported planar bilayers.<sup>116,122</sup>

Previous attempts to capture intact vesicles on surfaces have employed DNA tethering,<sup>115-117</sup> covalent binding to gold or polystyrene,<sup>118-119</sup> or biotin-streptavidin linking schemes.<sup>120-121</sup> These methods generally involve labor-intensive experimental procedures and expensive reagents. Furthermore, spatial and temporal control of vesicle capture (i.e., onto specific areas of a given surface at a given time) cannot be easily achieved by these methods. A greater level of control could be advantageous for many applications – for example, vesicle capture at predetermined locations (e.g., “vesicle arrays”) could facilitate the development of new biosensors.<sup>116</sup>

In this study, we explore a simple and inexpensive method to capture vesicles onto solid surfaces with a high degree of spatio-temporal control. Our method exploits two sets of key results from our laboratories over the past several years. The first is the ability to electrodeposit the biopolymer chitosan onto patterned surfaces using electrical signals.<sup>123-126</sup> Chitosan is a widely available cationic biopolymer that has a pH-responsive character (pKa ~ 6.0) – i.e., it transforms from a soluble to an insoluble form upon increasing pH above ca. 10. Accordingly, chitosan films can be deposited on cathode surfaces upon application of a current due to the high local pH near this electrode.<sup>123-125</sup>

Here, we extend the electrodeposition scheme to a derivative of chitosan that is functionalized with hydrophobic tails (Figure 5.1). We term this derivative as “hydrophobically modified chitosan”, or hm-chitosan for short.<sup>99</sup> Previously, we have studied the interaction between hm-chitosan and vesicles in solution.<sup>99,127-128</sup> The key result was that the hydrophobes from this amphiphilic biopolymer tended to insert into the hydrophobic bilayers of vesicles, thus transforming the vesicle solution into a “vesicle gel”, with the vesicles now serving as junction points in a network. Here, we show that the affinity for vesicles also extends to hm-chitosan films. *When a surface coated with hm-chitosan is exposed to a solution of vesicles, the film captures vesicles simply via non-covalent interactions between the vesicles and the polymer hydrophobes* (see schematic in Figure 5.1). Thus, hm-chitosan can act as a “soft” interconnect between vesicles and a hard surface such as a gold electrode.<sup>126</sup> Moreover, our ability to selectively deposit hm-chitosan in predesigned patterns, as shown in Figure 5.1, allows us to create corresponding patterns of immobilized vesicles.

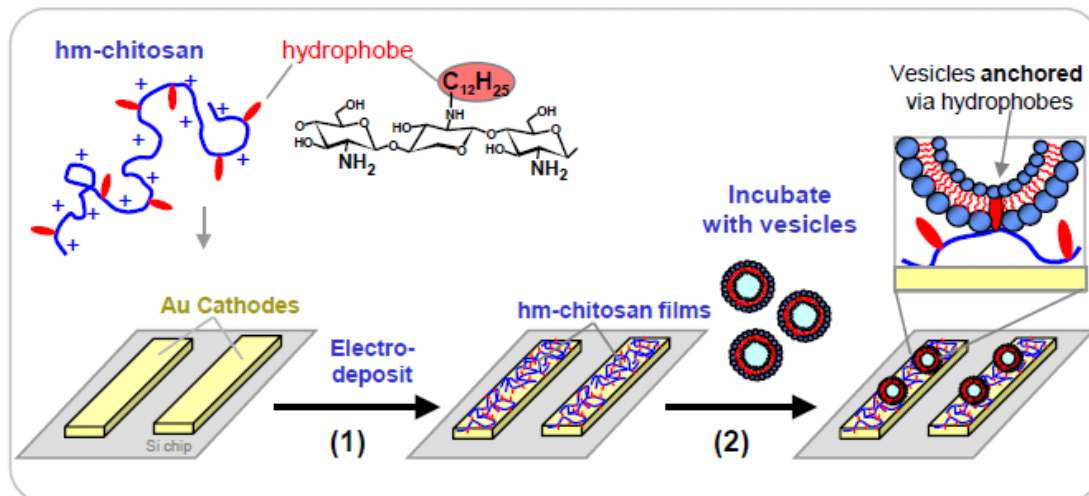


**Figure 5.1.** Schematic showing the spatiotemporal capture of vesicles using hm-chitosan. The structure of hm-chitosan as well as a schematic of its chain are shown in the top left. The chain has a hydrophilic backbone shown in blue and pendant hydrophobes ( $C_{12}$  tails) that are shown in red. In step (1), thin films of hm-chitosan are electrodeposited onto gold cathodes that are patterned on a silicon chip. Next, in step (2), the chip is incubated with a solution of vesicles. Intact vesicles become spontaneously anchored onto the polymer films. The inset shows the likely mechanism for such anchoring, which is via non-covalent interaction between the hydrophobes on the polymer and vesicle bilayers.

It is worth emphasizing certain features of our approach as well as some potential applications. Our approach (Figure 5.1) involves deposition of hm-chitosan followed by capture of vesicles on the surfaces of these films. The advantage is that the vesicles remain accessible to the external environment, which facilitates their use as sensors. (The accessibility of vesicles is more problematic if the vesicles are simply co-deposited with the polymer, as has been done earlier.<sup>129</sup>) We will also present several pieces of evidence to show that the vesicles are indeed intact, i.e., they are not being ruptured into flat lipid bilayers within the hm-chitosan film. Thus, the payload within the vesicles is expected to remain available for future use. The latter aspect is important in considering potential applications for vesicle-polymer hybrid films in drug delivery or wound healing. For

example, in the case of chronic-wound healing, macroscopic films of hm-chitosan could be therapeutically functionalized with vesicles housing several types of growth factors (i.e., proteins that promote wound healing). These films could then be used to cover chronic wounds while protecting them from exudation or infection (chitosan is known also for its anti-bacterial properties). In turn, the controlled release of the growth factors from the vesicles attached to the films would enhance and sustain the wound-healing process. Note also that the bioactivity of growth factors is likely to be maintained when they are within vesicles; in contrast, growth factors embedded directly within polymer films may lose some of their activity.<sup>130</sup> In sum, vesicle-polymer hybrids can have interesting applications, and the present study shows how these materials can be readily assembled via non-covalent hydrophobic interactions.

## 5.2 Experimental Section

**Materials.** Chitosan of medium molecular weight (190-310K) and Brookfield viscosity of 286 cps was obtained from Sigma-Aldrich. The reported degree of deacetylation was about 80%. Chitosan is soluble only under acidic conditions (pH < 6.5) and here it was dissolved in 0.2 M acetic acid. The phospholipids L- $\alpha$ -phosphatidylcholine (PC) and biotinylated phosphatidylethanolamine (PE-biot), and the fluorescent lipid 1'-dioctadecyl-3,3,3',3'-tetramethylindocarbocyanine perchlorate (DiI) were purchased from Avanti Polar Lipids. The surfactants cetyltrimethylammonium tosylate (CTAT), sodium dodecyl benzenesulfonate (SDBS), and Triton X-100, the dye 5,6-carboxyfluorescein (CF), and the reagent *n*-dodecyl aldehyde were purchased from Sigma-Aldrich. Streptavidin bound



to fluorescein isothiocyanate (FITC-streptavidin) and the succinimidyl ester of CF (NHS-fluorescein) were purchased from Fluka. All experiments were performed using distilled-deionized (DI) water.

**Synthesis of Chitosan Derivatives.** The hm-chitosan was synthesized by attaching *n*-dodecyl tails to the chitosan backbone via reaction with *n*-dodecyl aldehyde. The procedure has been reported in our earlier paper<sup>99</sup> and follows that described in the literature.<sup>17,98,131</sup> The degree of hydrophobic substitution follows the reaction stoichiometry and in this study it was fixed at *ca.* 2.5 mol% of the available amine groups. Fluorescently-labeled chitosan and hm-chitosan were synthesized by reacting the polymers with NHS-fluorescein, as previously reported in the literature.<sup>124</sup>

**Vesicle and Liposome Preparation.** Both surfactant vesicles and lipid vesicles (liposomes) have been used in this study. Catanionic surfactant vesicles<sup>12,132</sup> were prepared by mixing 0.7 wt% of the cationic surfactant CTAT and 0.3 wt% of anionic surfactant SDBS (~ 2:1 molar ratio) in DI water and gently stirring overnight. Dye-filled catanionic vesicles were prepared by combining 1 mM of CF with the CTAT/SDBS mixture, followed by separation of vesicles from free dye using a Sephadex G-50 column (from Roche). Liposomes were prepared by an extrusion method, as recommended by the manufacturer (Avanti Polar Lipids). Briefly, dried films of the lipids were hydrated under moderate stirring, freeze-thawed 5 times, and then passed through two double-stacked polycarbonate membrane filters (100 nm pores) using a Lipex pressurized extrusion system. Dye-filled liposomes were prepared in DI water from PC (20 mM) and CF (15

mM) and purified of free CF using the Sephadex G-50 column. Fluorescently labeled liposomes were prepared in DI water by combining the lipid PC (13 mM) with trace amounts (13  $\mu$ M) of the fluorescent lipid DiI. For the streptavidin binding assay, biotinylated liposomes were prepared by combining PC and PE-Biotin in a molar ratio of 9:1, with a total lipid concentration of 1 wt%. Vesicle sizes in all cases were measured using a Photocor-FC dynamic light scattering (DLS) instrument.

**Preparation of Giant Unilamellar Vesicles (GUVs).** The GUVs were prepared by electroformation, as described in the literature.<sup>133-134</sup> The lipids (1 mg/mL) and DiI (7.7  $\mu$ g/ml) were dissolved in chloroform. One drop of this solution (5  $\mu$ L) was deposited onto the conducting side of an indium tin-oxide (ITO)-coated glass slide. The solvent was removed first under desiccation for 1 h, and then freeze-drying for 3 h. A chamber was then made by creating an O-ring out of Seal-Ease and then pressing a second ITO-coated slide, conducting side facing downward, above the original slide. The chamber was hydrated with a solution of 100 mM sucrose in DI water via injection needle through the Seal-Ease; after injection, the needle was removed and the hole closed by Seal-Ease. Alligator clips were connected to both glass slides as well as a function generator (BK Precision 10 MHz Sweep/Function Generator 4017) via a BNC connector. An electric field of AC 1.5 V at 10 Hz was applied for 2 h at 55°C; the frequency was then dropped to 1 Hz for an additional 50 min. The fluid in the chamber now consisted of GUVs.

**Electrodeposition.** Electrodeposition was performed on “chips” fabricated from silicon wafers with deposited micropatterns of gold (Figure 5.2). Fabrication procedures have been described in detail in our earlier papers.<sup>123-125</sup> Electrodeposition was performed by

negatively biasing a specific lead on the chip while it was partially immersed in an aqueous solution containing 1 wt% of either chitosan or hm-chitosan at a pH ~ 5. A DC power supply (model 6641C, Agilent Technologies) was used to supply a constant current to the chip and counter electrode over a 2 min period. Photomicrographs of fluorescent electrodeposited materials were taken by a fluorescence stereomicroscope (MZFLIII, Leica) equipped with a digital camera (Spot 32, Diagnostic Instruments). To observe CF or FITC fluorescence, the microscope was set with an excitation wavelength of 480 nm (bandwidth of 40 nm) and a long-pass emission filter at 510 nm. To observe DiI fluorescence, the filters were chosen with an excitation wavelength of 560 nm (bandwidth of 40 nm), and an emission filter of 610 nm. In all cases, Image J1.34S software from NIH was used to analyze images and quantify fluorescence intensity.

**Cryo-TEM.** C-FLAT holey carbon grids with a hole size of 1.2  $\mu\text{m}$  were purchased from Electron Microscopy Sciences. Grids bearing hm-chitosan and surfactant vesicles were plunged into liquid ethane ( $-183^\circ\text{C}$ ) using a Gatan CryoPlunge3, so as to form vitrified specimens and thereby preserve any molecular assemblies present. The samples were thereafter imaged on a JEOL-2100 LaB6 TEM at liquid nitrogen temperature.

### 5.3 Results and Discussion

**Vesicle Capture on hm-chitosan Films.** The first step in our approach involves electrodeposition of hm-chitosan films onto gold electrodes. These films are then to be used to capture vesicles. In the context of vesicle capture, it is useful to compare hm-chitosan with the native chitosan (no hydrophobes). Electrodeposition of native chitosan was first demonstrated in our laboratories in 2002;<sup>123</sup> the present study is the first to extend this capability to hm-chitosan. For our initial studies, we used the two-electrode chip shown in Figure 5.2. As mentioned earlier, the chip substrate is a silicon wafer, on which gold electrodes are deposited in a specific pattern. We then conducted sequential electrodeposition of hm-chitosan and chitosan (both tagged with the green fluorescent dye, NHS-fluorescein) on the left and right electrodes, respectively. This was done as follows: first, the right electrode was connected to the power supply and the other unconnected while the chip was immersed in a solution of chitosan. The connections were then switched (only left electrode connected) and the chip was immersed in a solution of hm-chitosan. After deposition, the electrodes were disconnected from the power supply, and the chips were rinsed several times with DI water. Figure 5.3 (top) shows the results of the experiment: the green color on both electrodes in the two fluorescence images indicates successful deposition of both hm-chitosan and chitosan.

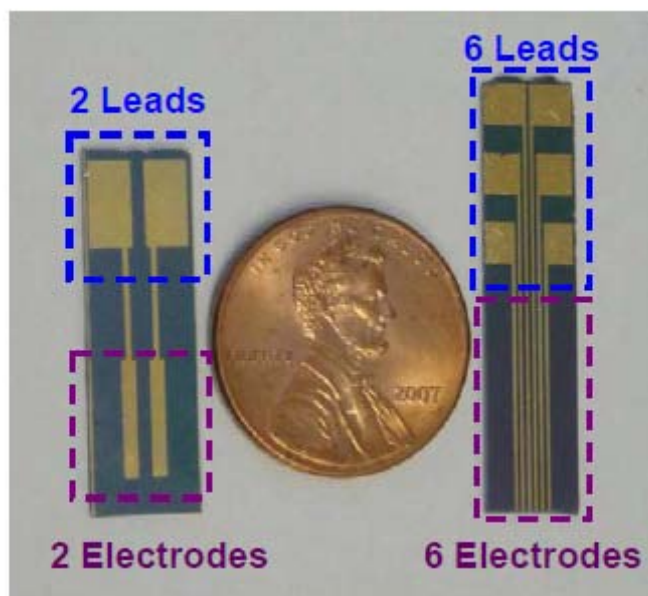


**Figure 5.2.** Photograph of micropatterned chips used in this study. The leads and electrodes are formed by depositing gold on a silicon wafer using lithographic techniques. On the left is a 2-electrode chip and on the right a 6-electrode chip. A US penny is shown for size comparison.

Next we examined the relative capabilities of hm-chitosan and chitosan to capture vesicles from solution. These experiments were conducted with both surfactant vesicles as well as lipid vesicles (liposomes). The cationic surfactant vesicles (70/30 CTAT/SDBS, total 1 wt%) had an average diameter around 120 nm, as measured by DLS. The liposomes of PC were made by extrusion through 100 nm membrane filters and had an average diameter around 110 nm from DLS. Both the vesicles and the liposomes were tagged with the fluorescent lipid DiI, which incorporates into the bilayer membranes of the above structures. Note that DiI exhibits a red fluorescence, i.e., a distinct color compared to the green signal from the chitosan and hm-chitosan. We incubated the chip on the left with surfactant vesicles and the one on the right with the liposomes, both for 10 min. The chips were then rinsed three times with DI water to remove weakly adsorbed structures and then imaged under the fluorescence microscope using red filters. The

resulting images (Figure 5.3, bottom) show a significantly higher red fluorescent signal from the hm-chitosan side compared to the chitosan-side – and this is the case for both the surfactant vesicles and the liposomes. These results show that hm-chitosan is considerably more effective at capturing vesicles than chitosan. We believe this is because hydrophobes from hm-chitosan chains can get inserted into vesicle bilayers through non-covalent hydrophobic interactions (as depicted in Figure 5.1). Such interactions enable a tight anchoring of the vesicles to the polymer film.

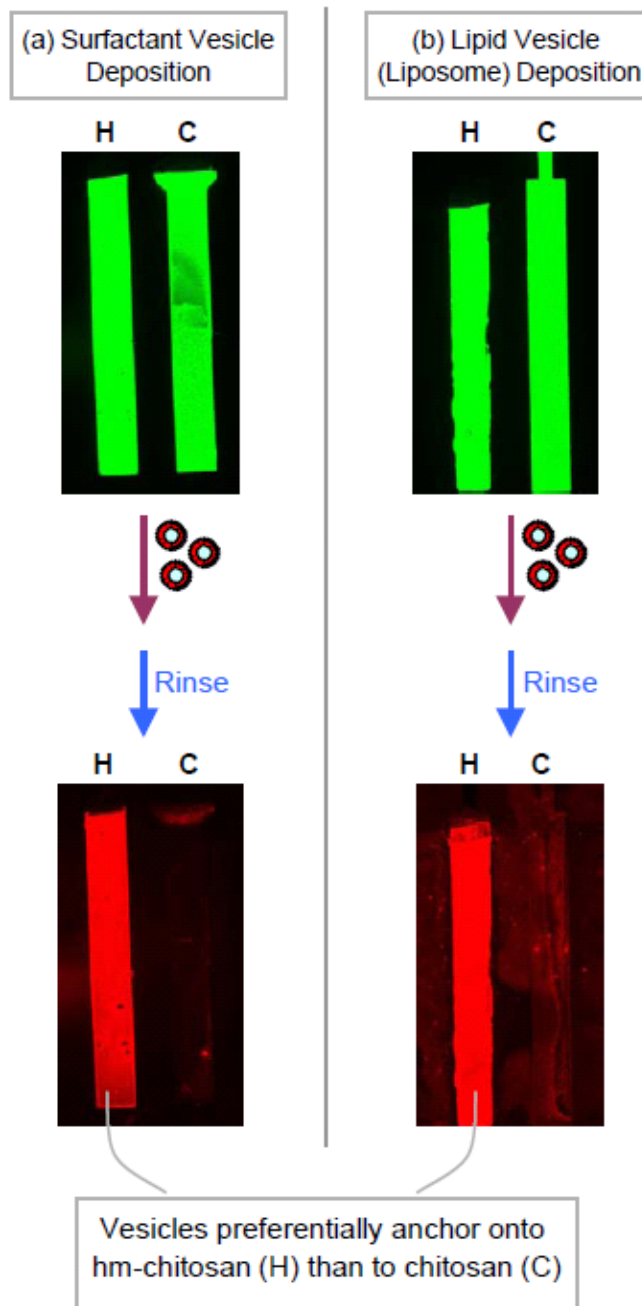


**Figure 5.3:** Comparison of hm-chitosan (H) and chitosan (C) films in terms of their ability to capture vesicles. *Top images:* Green-filtered fluorescence micrographs showing deposition of NHS-tagged hm-chitosan on the left electrode and NHS-tagged chitosan on the right electrode of a two-electrode chip. The chips are then incubated with vesicles for 10 min, followed by rinsing with DI water. *Bottom images:* Red-filtered fluorescence micrographs showing the presence of DiI-tagged vesicles on the electrodes. The results in (a) (left-column) are obtained with cationic surfactant vesicles, while those in (b) (right-column) are obtained with liposomes. In both cases, the vesicles are anchored preferentially to the hm-chitosan film than to the chitosan one.

The superior effectiveness of hm-chitosan in capturing vesicles is a robust result and this is further proven by experiments with varying vesicle incubation times. For these experiments, surfactant vesicles were used and the time of chip incubation in the vesicle solution was varied from 5 to 10 to 20 min. All other experimental variables, including rinsing times and image exposure time were kept constant. The results in Figure 5.4 show an increase in red fluorescence from the hm-chitosan electrode with increasing incubation time – the increase is quite significant between 5 and 10 min and slight between 10 and 20 min. In all cases, the signal from the hm-chitosan side dwarfs that from the chitosan side. Similar results were obtained for macroscopic films of chitosan and hm-chitosan simply dried onto glass slides and incubated with tagged surfactant vesicles for various time intervals (data not shown). These results suggest that vesicle capture on hm-chitosan proceeds by surface diffusion of vesicles until they connect with free hydrophobes from the polymer, whereupon the vesicles get strongly bound. As the free hydrophobes get used up, fewer vesicles are able to bind strongly and the binding capacity of the film becomes saturated.



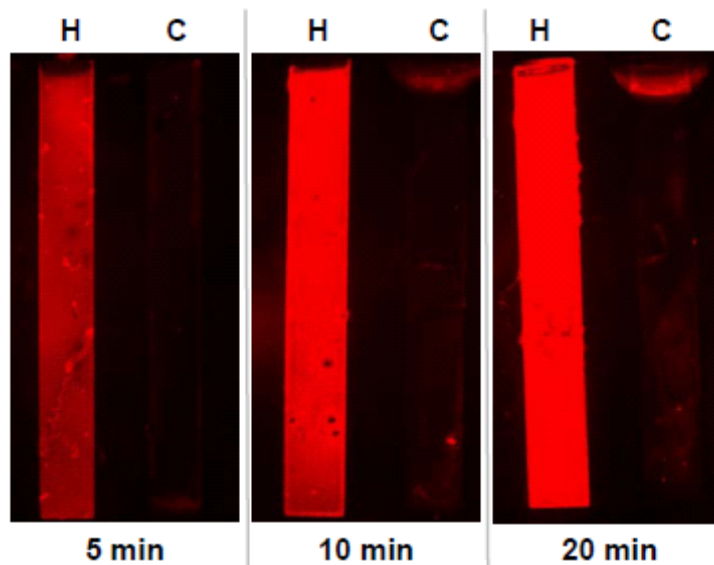


**Figure 5.4:** Variation in the extent of vesicle capture based on the time of chip incubation with a vesicle solution. Hm-chitosan (H) and chitosan (C) are deposited on the left and right electrodes, respectively. The chip is incubated with a solution of surfactant vesicles for different lengths of time and then imaged by fluorescence microscopy. The images are red-filtered fluorescence micrographs showing DiI-tagged vesicles on the electrodes. A constant exposure time of 20 s at the excitation wavelength was used to obtain each image. The results show increasing capture of vesicles on the H side and negligible capture on the C side.

**Intactness of Captured Vesicles.** Next we tackle the question of whether the vesicles captured on hm-chitosan films are intact or whether the red fluorescent signal reflects fragments of vesicle bilayers. Figure 5.5 is a first piece of evidence to demonstrate intactness of vesicles. In this case, we prepared a solution of fluorescently tagged giant unilamellar vesicles (GUVs) of phospholipids. Optical microscopy (not shown) revealed that the GUVs ranged in size from 10 to 50  $\mu\text{m}$ , which is typical of GUVs made via electroformation. We then incubated a chip bearing hm-chitosan in the GUV solution for 10 min, rinsed the chip and observed it under a fluorescence microscope. Note the red fluorescent “hot spots” on the hm-chitosan film – these are shown at two different levels

of magnification in Figures 5.5. The spot sizes compare well with the sizes of GUVs and therefore it is likely that the spots correspond to intact GUVs. Thus, large microsized GUVs are shown to remain intact when immobilized on an hm-chitosan film.

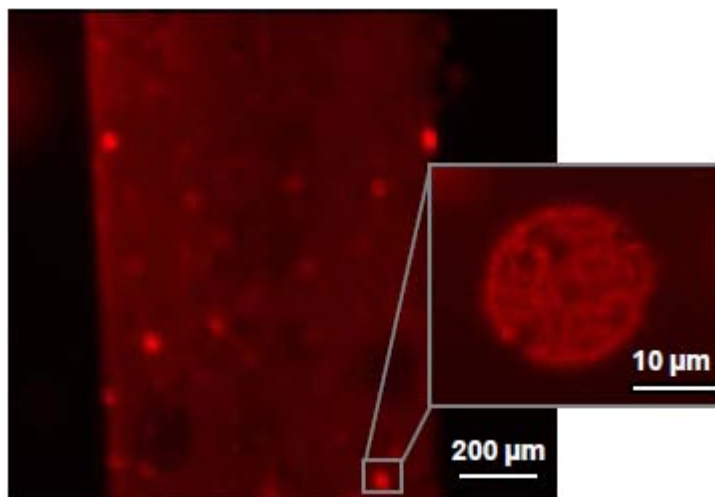


**Figure 5.5:** Immobilization of giant unilamellar vesicles (GUVs) on an hm-chitosan film. After 10 min incubation with DiI-tagged GUVs, multiple red-fluorescent ‘hot spots’ appear on the electrode bearing hm-chitosan. A zoomed-in image of a ‘hot-spot’ shows an intact GUV of ca. 20 µm diameter.

Returning to the nanosized vesicles and liposomes, we present evidence to show that these are also captured intact by hm-chitosan. In this experiment, we prepared liposomes containing the hydrophilic dye CF. We ensured that the dye was present only inside liposomal cores; free (unencapsulated) dye was removed via size-exclusion chromatography, as described in the Experimental Section. The biopolymers were left untagged for this experiment to avoid overlap with the green fluorescence from the CF. Again, hm-chitosan was deposited on the left electrode and chitosan on the right. The chip was then incubated with the CF-filled liposomes followed by rinsing with DI water. At this stage, Figure 5.6a shows a strong green signal only on the hm-chitosan side,

implying that the liposomes preferentially attached there. The only alternate explanation is that the fluorescence comes from free CF dye stuck to the hm-chitosan, i.e., that the liposomes had already been disrupted. To rule out this possibility, we added the detergent Triton X-100 into the solution above the chip. This detergent is known for its ability to disrupt liposomes into mixed micelles, whereupon dye in the liposomal cores would be released into solution (this is illustrated by the schematics in Figure 5.6). After detergent addition and subsequent rinsing, Figure 5.6b shows that the green signal has vanished from the hm-chitosan film. The loss of signal after detergent treatment necessarily implies that the liposomes were initially *intact* on the hm-chitosan surface in Figure 5.6a.

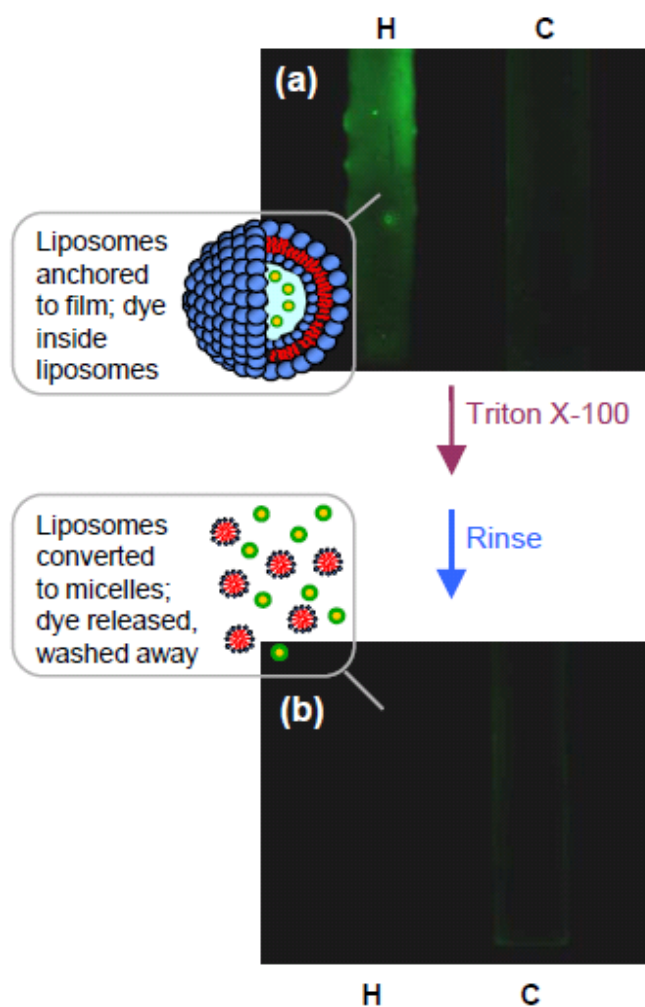


**Figure 5.6:** Evidence for intact capture of liposomes on hm-chitosan films. (a) Green-filtered fluorescence image showing preferential binding of liposomes (filled with the hydrophilic dye CF) to the hm-chitosan (H) side relative to the chitosan (C) side. The chip is then exposed to the detergent Triton X-100 and rinsed. The detergent disrupts the liposomes into micelles, as shown by the schematics, and the encapsulated dye is thus released and washed away. (b) Fluorescence image of the rinsed chip shows nearly complete loss of fluorescent signal, confirming disruption of originally intact liposomes.

Further evidence for the intact capture of nanosized surfactant vesicles is provided by cryo-TEM. For these experiments, we deposited hm-chitosan directly on holey-carbon TEM grids. These grids were then incubated with surfactant vesicles, followed by a rinsing step with DI water to remove weakly adsorbed vesicles. The rinsed grids were

maintained in an aqueous environment at room temperature. These grids were then prepared in the usual way for cryo-TEM (see Experimental Section) by plunging into liquid ethane. Observation of the vitrified specimens showed the presence of numerous spherical structures of 100-150 nm diameter (Figure 5.7). These are evidently the surfactant vesicles and they all seem whole – no breaks or holes can be found on the vesicle shells. Thus, once again, the vesicles appear to have been captured intact.

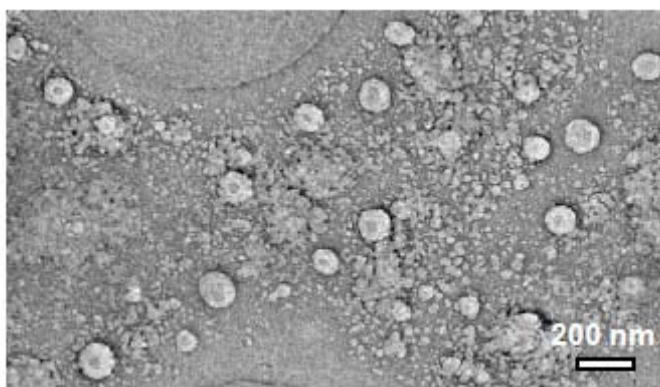


**Figure 5.7:** Cryo-TEM image of vesicles on an hm-chitosan film. The hm-chitosan was deposited on the TEM grid and then used to capture surfactant vesicles from solution. The image shows numerous spherical objects of ~ 100–150 nm diameter, which are presumably intact vesicles.

**Spatiotemporal Control of Vesicle Capture.** We now demonstrate the capability to create specific microscale patterns of vesicles on the chip. Towards this end, we used two 6-electrode chips with a view towards engineering two specific patterns of vesicles. On one chip we deposited hm-chitosan (H) and unmodified chitosan (C) in an alternating pattern, i.e., HCHCHC, on the 6 electrodes (Figure 5.8a). After incubating the film with a solution of DiI-tagged surfactant vesicles, the red signal indicative of vesicles is observed

only on the hm-chitosan (H) electrodes (Figure 5.8b). Next, on the other chip, we deposited the polymers in an ‘outside-inside’ pattern, i.e., HCHHCH (Figure 5.8c). Incubation of the chip with the same tagged vesicles again results in a red signal *only* on the hm-chitosan (H) electrodes (Figure 5.8d). Thus, in both cases, pre-determined patterns of vesicles were successfully created. Such patterning can be easily extended to more complex designs and with finer resolution. Previous work with chitosan has indicated the resolution limits of electrodeposition to be on the order of 1  $\mu\text{m}$ .<sup>124</sup> We view this work as a step towards the construction of “vesicle arrays” that could prove to be a useful tool for probing the properties of biomolecules such as membrane proteins.

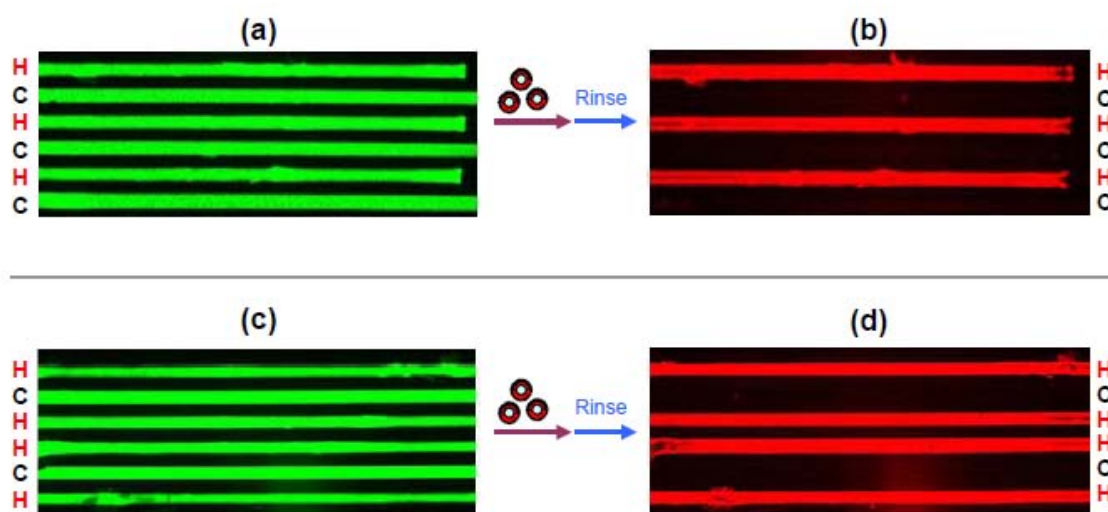


**Figure 5.8:** Patterning of vesicles on 6-electrode chips. (a) NHS-tagged hm-chitosan (H) and chitosan (C) are electrodeposited in an alternating pattern, HCHCHC. (b) Following contact with DiI-tagged surfactant vesicles and rinsing, the red fluorescence indicative of vesicles is found only on the H electrodes. (c) H and C are electrodeposited in an ‘outside-inside’ pattern, HCHHCH. (d) Once again, DiI-tagged surfactant vesicles are found anchored only on the H electrodes.

**Accessibility of Captured Vesicles.** Lastly, for immobilized vesicles to be useful in biosensing or binding assays, the vesicles should be able to access ligands from the external solution. To evaluate this aspect, we studied the interaction between surface-

bound biotinylated liposomes and streptavidin in the surrounding solution. The experiment is depicted schematically in Figure 5.9a. Biotinylated liposomes were prepared by combining PC and PE-biot in a molar ratio of 9:1. These liposomes were then contacted with a chip bearing hm-chitosan (H) and chitosan (C) films on adjacent electrodes. The chip was then rinsed with DI water and exposed to a solution containing fluorescently tagged streptavidin, a protein that non-covalently binds to biotin with extremely high specificity. The results show a significantly higher fluorescent signal from streptavidin on the hm-chitosan electrode than the chitosan electrode (Figure 5.9b). The signals are quantified in the plot shown in Figure 5.9c – the fluorescence is approximately 6 times higher on the hm-chitosan side ( $9.3 \pm 0.8$  gray value) relative to the chitosan side ( $1.6 \pm 0.3$  gray value) . The high signal on the hm-chitosan side is evidently due to the binding of streptavidin to the biotinylated liposomes captured on that film. The binding of streptavidin to the chitosan side is not zero presumably because streptavidin (a negatively charged protein) can bind non-specifically to the positively charged chitosan. Nevertheless, this is an encouraging result because it does confirm the ability of immobilized vesicles to sense reporter molecules from the surrounding environment.

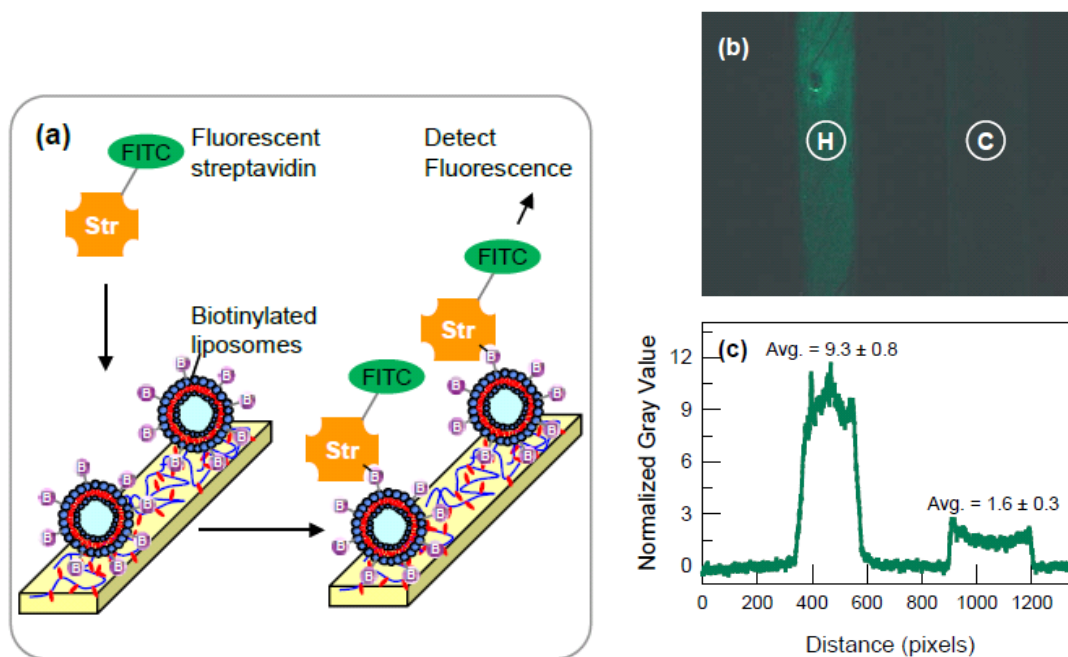


**Figure 5.9:** Protein sensing via vesicles anchored to an hm-chitosan film. (a) Schematic of the experiment: biotin-decorated liposomes are first immobilized, then the chip is contacted with the fluorescently labeled protein, FITC-streptavidin. The binding of the protein is then detected by fluorescence microscopy. (b) Fluorescence image showing a strong signal from the hm-chitosan (H) electrode compared to the chitosan (C) electrode. The strong signal is indicative of protein binding to the biotins on the anchored liposomes. (c) Analysis of the intensities in (b). The average gray values for each electrode area are listed above the corresponding regions.

## 5.4 Conclusions

We have shown that vesicles and liposomes can be captured on electrodeposited films of hm-chitosan. Hm-chitosan is significantly superior in its capability for vesicle capture compared to unmodified chitosan, which implies that vesicle capture on hm-chitosan is promoted by the non-covalent binding of polymer hydrophobes to the hydrophobic interiors of vesicle bilayers. We have presented a range of evidence to show that the vesicles bound to hm-chitosan are intact structures. The evidence includes direct visualization of captured vesicles – by optical microscopy in the case of microscale GUVs and by cryo-TEM in the case of nanoscale vesicles. Additionally, key indirect



evidence for vesicle intactness comes from a study on dye-filled vesicles – upon detergent treatment, a loss of fluorescence from the film is observed, which can only be attributed to the detergent-induced disruption of intact vesicles. We have also confirmed the ability of biotinylated vesicles bound to hm-chitosan to conjugate with the protein streptavidin from the surrounding solution. A particular utility of using hm-chitosan as a “soft” interconnect between “hard” surfaces and vesicles is the prospect of creating patterns of immobilized vesicles. It is straightforward to electrodeposit hm-chitosan in a variety of predesigned patterns with micron-scale resolution; subsequently, vesicles can be readily captured on the patterned regions without the need for further chemistry (i.e., solely by non-covalent hydrophobic interactions). The simplicity of this approach should make it attractive for researchers to create new biosensors and bioassays using vesicles.

## Chapter 6

# Gelling Blood with an Amphiphilic Biopolymer: A Route to Improved Hemorrhage Control

---

### 6.1 Introduction

The blood coagulation cascade is an enormously complex orchestration of small molecules, proenzymes, proteins and cells that ultimately results in the self-assembly (“polymerization”) of fibrinogen molecules into an elastic fibrin network.<sup>135</sup> Fibrinogen is a small globular protein, and its assembly into fibrin chains is catalyzed by the protein thrombin. The fibrin network forms the hemostatic “plug” or the physical barrier that prevents further loss of freely-flowing blood from the site of injury. The coagulation cascade is effective at arresting blood loss from small wounds, but when the injuries are severe, such as gunshot or knife wounds suffered by soldiers in the battlefield, alternate tools and strategies are required for the achievement of hemostasis.<sup>136-137</sup> Additionally, there are many types of coagulopathic conditions (hemophilia, Von Willebrand disease, liver disease) that require medical treatment even for minor bleeding.<sup>138-140</sup>

Although the need for better hemostats has existed throughout human history, it was not until the mid-twentieth century that major advances in the field began to develop beyond standard cotton gauze or tourniquets. During World War II, fibrin-based materials (glues, foams, adhesives) were some of the first proposed materials for advanced hemorrhage control.<sup>141</sup> These products generally contain extremely high concentrations

of fibrinogen and thrombin, which work to mimic the final stages of the natural coagulation cascade. Early versions of these materials often demonstrated negative side effects such as immunogenic responses or disease transmission;<sup>142</sup> however, improved processing techniques allowed for a great deal of the advancement in fibrin-based hemostats in the early 1990s.<sup>143-144</sup> The approach during that period began to shift toward a dry powdered mixture of human fibrinogen and thrombin packed onto a solid bandage backing.<sup>145</sup> By firmly pressing this dressing onto a bleeding injury, the bandage instantly forms a strong fibrin seal at the point of injury as bodily fluid brings the powder into solution in high concentration. Despite the efficacy of the fibrin sealant (FS) bandage, practical issues have severely limited its contributions to trauma medicine. Specifically, human fibrinogen and thrombin are highly expensive molecules that are scarce in supply. As such, they are extremely costly and largely unable to meet clinical demand.<sup>141,146</sup>

Over the last decade, a myriad of other solutions have been posed to the problem of severe hemorrhage.<sup>147-148</sup> Many of these employ biomolecules involved in the clotting cascade (e.g. factor VIIa, Factor VIII, factor XIII, prothrombin complex concentrates). Unfortunately, these approaches remain costly and some have been shown to evoke immunogenic responses.<sup>149</sup> Other solutions involve materials that work by means other than self-assembly. First in this category are powders (zeolite or mineral) that rapidly absorb fluid and, as a result, concentrate clotting factors at the site of injury.<sup>150</sup> Secondly, there are bandages (chitosan, cellulose, gelatin) that help to either initiate clotting, absorb fluid, provide backpressure against flow of blood, or some combination thereof. However, all of these lower-cost solutions have drawbacks of either inadequate effectiveness or

dangerous side effects (e.g. tissue/nerve damage and embolism).<sup>151-152</sup> Furthermore, they all have demonstrated a great deal of user variability, particularly in uncontrolled environments where they are most needed.<sup>152</sup>

One research group, Ellis-Benhke *et al.*, has employed the concept of self-assembly, independent of the natural coagulation cascade, in order to achieve hemostasis.<sup>153</sup> They used an amphiphilic synthetic peptide (RADA16) which is able to quickly self-assemble into nanofibers upon their introduction into biological solution.<sup>154</sup> While this system has only displayed efficacy in small animal models, the benefits of using a self-assembled material are displayed clearly in their study. Allowing the material itself to build a hemostatic barrier in a “bottom-up” fashion, from nano- to macro-scale, is an approach likely to eliminate the user variability that plagues other proposed solutions to hemorrhage control.<sup>152</sup> Of course, for practical application, such a material should be low cost and easily produced, which are challenging issues for these synthetic peptides.

In this Chapter, we describe the use of an amphiphilic biopolymer that can transform liquid blood into a gel, and thereby serve as a hemostatic sealant even for severe wounds in large animals. The native biopolymer is chitosan, which is a material already of great interest in the field of wound care due to its inherent anti-microbial properties,<sup>155-156</sup> its biocompatibility<sup>157</sup> and wide availability from natural sources.<sup>158</sup> We modify the backbone of chitosan with a limited number of hydrophobic tails (2.5 mol % of available amines), so as to create a ‘comb-graft’ associating polymer that remains soluble in water (schematic in Figure 6.1). While native chitosan has been used in several

applications as a hemostatic material,<sup>159-162</sup> this hydrophobic modification greatly enhances the capability of chitosan to control hemorrhage. Like fibrinogen polymerization and nanofiber assembly via the RADA16 peptide, the mechanism of action for this hydrophobically-modified (hm) chitosan also occurs via self-assembly; however, in this case, the blood cells take an active role in the formation of gel networks, as opposed to passively filling space in between actively polymerizing chains. Based on our previous work on hm-chitosan with vesicles<sup>99</sup> (self-assembled nano-containers, which can be conceptualized as ‘empty’ cells), we hypothesize that the networks are formed by insertion of the hydrophobes into cell bilayers and subsequent bridging of cells by the biopolymer. This hypothesis is outlined in Figure 6.1. We probe the hemostatic mechanism of hm-chitosan via studies on blood using dynamic and steady-shear rheology, and by application to small (murine) and large animal (porcine) injury models.

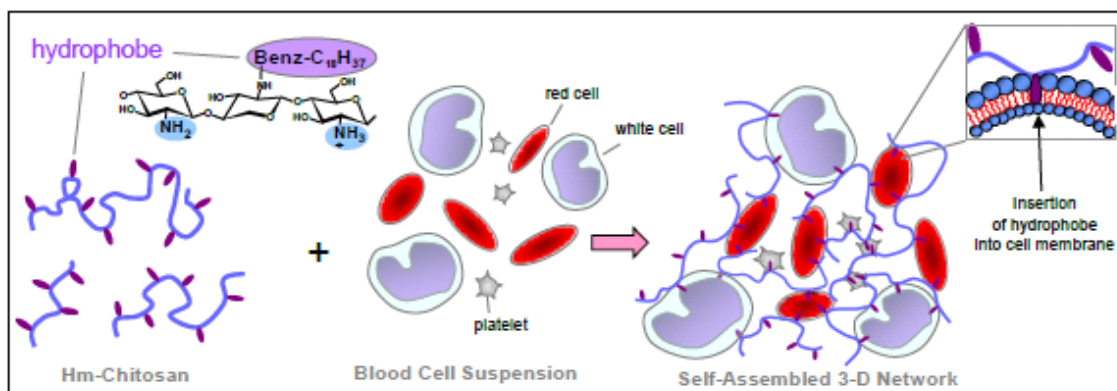


**Figure 6.1. Schematic of hydrophobically-modified (hm)-chitosan as a self-assembling hemostat.** When adding hm-chitosan to a whole blood cell suspension, the resulting mixture self-assembles into a 3-dimensional network. This self-assembly is driven by insertion of hydrophobes into blood cell membranes and the subsequent physical crosslinking of adjacent cells.

## 6.2 Experimental Section

**Materials.** Chitosan of medium molecular weight (190-310K) and Brookfield viscosity of 286 cps was obtained from Sigma-Aldrich. The reported degree of deacetylation was about 80%. Chitosan was dissolved in 0.15 M D-Lactic Acid (LA) so as to mimic physiological ionic strength. D-Lactic Acid and sodium cyanoborohydride were purchased from Sigma-Aldrich. 4-octadecylbenzaldehyde and  $\alpha$ -cyclodextrin were purchased from TCI International. Hank's Balanced Salt Solution (HBSS) was purchased from Lonza. BD Vacutainers<sup>®</sup> were purchased from Becton Dickinson.

**Synthesis of Chitosan Derivatives.** The hm-chitosan was synthesized by attaching benzene-*n*-octadecyl tails to the chitosan backbone via reaction with 4-octadecylbenzaldehyde. The same procedure, but instead using a dodecylaldehyde as the reactant, has been reported in our earlier paper<sup>99</sup> and it also follows those described in the literature.<sup>17,98,131</sup> The degree of hydrophobic substitution follows the reaction stoichiometry and in this study it was fixed at *ca.* 2.5 mol% of the available amine groups. The degree of hydrophobic substitution follows the reaction stoichiometry and in this study it was fixed at *ca.* 2.5 mol% of the available amine groups.

**Manufacture of hm-chitosan Sponges.** 0.5 wt% hm-chitosan in 0.15 M Lactic Acid was poured into trays of dimensions 10 cm (length)  $\times$  10 cm (width)  $\times$  4 cm (height). Trays were filled only up to 2 cm in height with polymer solution. Samples were then frozen to -40°C in a pilot-scale freeze drier, and then placed under vacuum of 50  $\mu$ bar for a period of 5 days in order to remove all water. After drying, a Tegaderm<sup>®</sup> medical tape backing

was placed on the back side of the sponges for unhindered compression of the sponge during surgery.

**Obtaining Blood.** 5 human subjects volunteered to have 20 ml of blood drawn by registered nurse at the University of Maryland School Medicine. Subjects were healthy adults ranging age from 20 to 40 years of age (4 males, 1 female). 10 ml intervals of blood were drawn into BD Vacutainers<sup>®</sup> containing 143 USP units of Sodium Heparin. The protocol was approved by the Institutional Research Board (IRB) at the University of Maryland.

**Rheology of Chitosan-Blood Mixtures:** Steady and dynamic rheological experiments were performed on a Rheometrics AR2000 stress-controlled rheometer. A cone-and-plate geometry of 40 mm diameter and 4° cone angle was used and samples were run at physiological temperature 37°C. Dynamic frequency spectra were obtained in the linear viscoelastic regime of the samples, as determined by dynamic strain sweep experiments.

**Murine Injury Models.** Surgical procedures were approved by the Institutional Animal Care and Use Committee of the University of Maryland. Fasted male Long-Evans rats (n = 15, 250–275 g; Harlan, Indianapolis, IN) were anesthetized (60 mg/kg ketamine and 7.5 mg/kg xylazine given IP) and allowed to breathe air spontaneously. Animals were maintained under pathogen-free conditions in 12 h diurnal cycles, with water and food ad libitum. Animal rooms were kept at 21±3 °C with several changes of air per hour. All husbandry and animal procedures were in accordance of humane animal handling

practices under the guidance of the Unit for laboratory Animal Medicine at the University of Maryland School of Medicine. At the end of each procedure, all animals were humanely sacrificed by ketamine administration.

Using a scalpel, the femoral vein was transected and allowed to bleed for 30 seconds, after a unilateral groin incision was made over the femoral canal. Exposure and isolation of at least 1 cm of the femoral vein was performed. 1 ml of test material was then be dispensed onto 5 randomly selected animals via syringe (with 22 G needle) after wiping away excess blood from the site of injury via cotton gauze. Bleeding time was measured via stopwatch with the start time corresponding to the application of sample and end time corresponding to visual observation of halted bloodflow. Test materials studied were (1) Saline Buffer, (2) 0.5 wt% Chitosan and (3) 0.5 wt% hm-chitosan.

**Pig Injury Models.** 3 Yorkshire crossbred swine, age 2.5 months and weighing 39.6 kg-42.8 kg, were used. A veterinarian screened all animals. Animals were allowed free access to water and to commercial food, which was withheld the night before the study. All animals were maintained in an Association for Assessment and Accreditation of Laboratory Animal Care International–accredited facility, and all experimental manipulations were performed in accordance with the National Research Council’s Guide for the Care and Use of Laboratory Animals. The protocol was approved by the Institutional Animal Care and Use Committee. The swine were anesthetized with 6 mg/kg of Telazol (Fort Dodge Animal Health, Fort Dodge, IA, USA) and 0.01 mg/kg of glycopyrrolate intramuscularly. They were intubated and placed on mechanical ventilation at a tidal volume 12 mL/kg, a rate of 10 respirations per minute, and 100%



oxygen. Anesthesia was maintained using isoflurane and ventilatory parameters were maintained to attain an end-tidal pCO<sub>2</sub> of 40 mm Hg.

The animals underwent midline laparotomy, and a unilateral groin incision was made over the femoral canal. Exposure and isolation of at least 5 cm of the femoral artery was performed. Using a 4.4 mm aortic punch, the femoral artery was punctured and free bleeding was allowed for 45 seconds. Blood loss was collected by suction for this period and was designated pretreatment total blood loss. Dry hm-chitosan sponges (bandages were cut to optimal sizes for wound approach) were applied via 2 min direct compression onto the injury site. Animals were observed under anesthesia for 180 minutes, at which point they were then be euthanized with Pentobarbital IV 100-200 mg/kg.

### 6.3. Results and Discussion

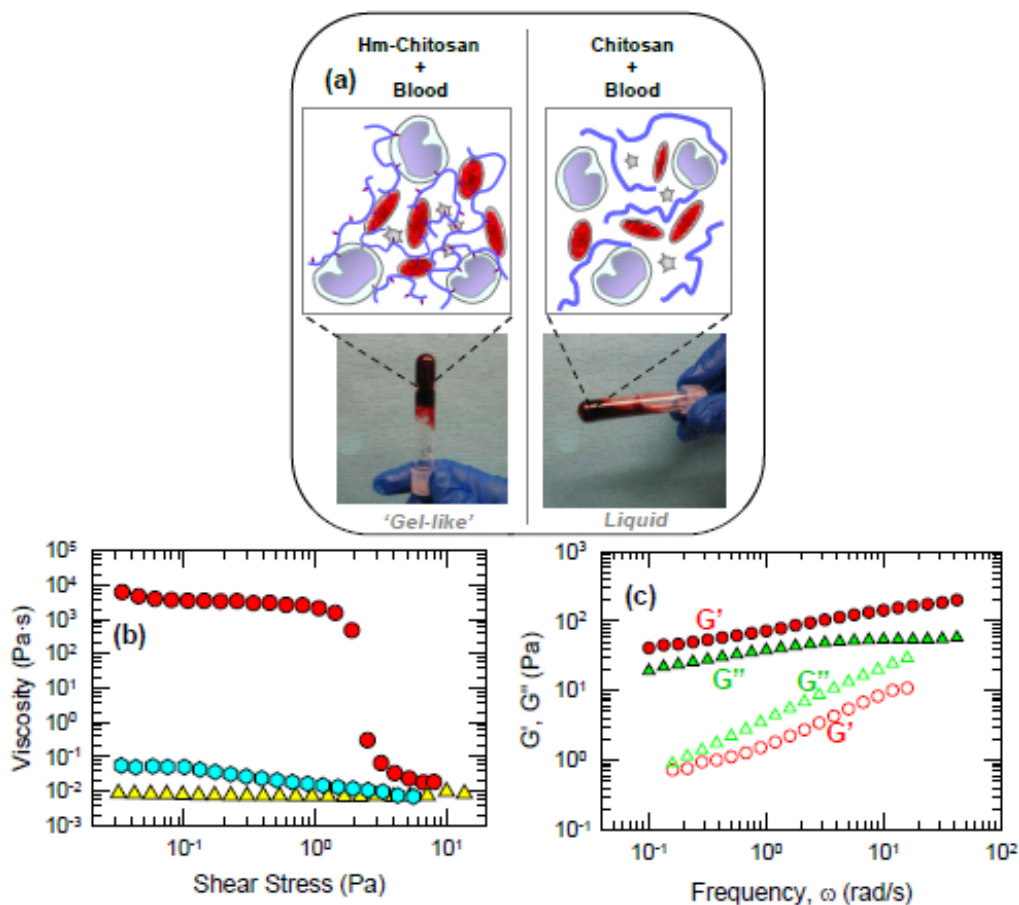


**Figure 6.2. Comparison of the native and hydrophobically-modified polymers with regard to their physical influence on blood.** In (a), photographs show hm-chitosan at 0.25 wt% mixed with heparinized human whole blood (50 wt %) is able to hold its weight upon test tube inversion, whereas unmodified chitosan at 0.25 wt% mixed with heparinized human whole blood (50 wt %) remains as a liquid. A cartoon of the proposed “bridging” effect of hm-chitosan on blood cells is shown above the left photograph; a contrasting schematic of unmodified chitosan mixed with blood is above the right photograph. In (b), steady shear rheology displays a dramatically increased ( $\sim O(10^5)$ ) zero-shear viscosity of the hm-chitosan-blood mixture (red circles), relative to both hm-chitosan (0.25 wt%) with no blood (cyan hexagons) and chitosan-blood (yellow triangles) controls. In (c), dynamic rheology of the hm-chitosan blood mixture ( $G'$ , closed red circles,  $G''$  closed green triangles) is that of gel-like elastic material which relaxes slightly over time, whereas rheology of the unmodified chitosan/blood mixture ( $G''$ , open green triangles,  $G'$ , open red circles) is that of a viscous sol

**Results on Gelling Blood.** Figure 6.2 compares hm-chitosan and unmodified chitosan with regard to their affect on a heparinized (14.3 units/mL) suspension of human whole blood. First, we note that visual observation of these samples show the blood mixed with hm-chitosan holds its own weight upon vial inversion (Figure 6.2a). A similar visual result has been observed in a mixture of citrate-stabilized blood and a polyethyleneoxide (PEO) polymer modified with cholesterol groups at either end.<sup>163</sup> In contrast, unmodified chitosan at the same concentration mixed with heparinized human whole blood (50 wt %) remains as a freely flowing liquid. A cartoon of the proposed “bridging” effect of hm-chitosan on blood cells is shown above the left photograph; a contrasting schematic of unmodified chitosan mixed with blood is above the right photograph. In Figure 6.2b, steady shear rheology displays a dramatic (~ million-fold) increase in the zero-shear viscosity of the hm-chitosan-blood mixture, relative to both hm-chitosan (0.25 wt%) with no blood (cyan hexagons) and chitosan (0.25 wt%)-blood (yellow triangles) controls.

In Figure 6.2c, dynamic rheology gives us information about the microstructure of these samples. Note that the key parameters given by dynamic rheology are the elastic modulus,  $G'$  (i.e. the elastic or solid like character of the material) and the viscous modulus,  $G''$ , (i.e. the viscous or liquid-like character of the material). Both moduli are measured as a function of oscillatory shear frequency, and as a result, give us information about the viscoelastic character over a wide range of timescales. Dynamic rheology of the hm-chitosan blood mixture is that of a gel-like elastic material with  $G'$  higher than  $G''$  over the range of practical frequencies (100 rad/s to 0.1 rad/s) and with both moduli showing a weak frequency dependence. No crossover of  $G'$  and  $G''$  is observed,

indicating that the sample does not relax over long time scales (this is consistent with the sample-spanning network structure shown in Figure 6.2a).<sup>164-165</sup> In contrast, rheology of the unmodified chitosan/blood mixture ( $G''$ , open green triangles,  $G'$ , open red circles) is that of a viscous sol. That is, in this case,  $G''$  exceeds  $G'$  over the frequency range and both moduli are strong functions of frequency.

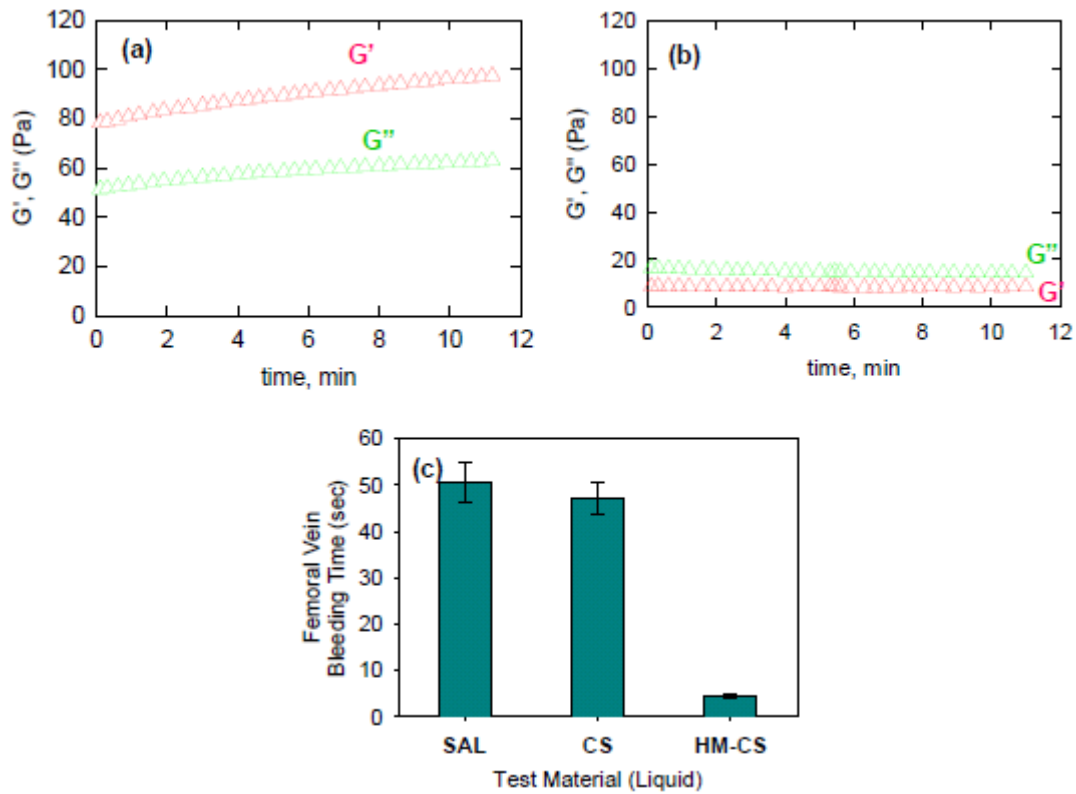


**Figure 6.3. Time-to-gelation of hm-chitosan/blood mixtures.** In (a), a time-sweep of an hm-chitosan (0.25%)/blood (50%) mixture displays the characteristics of an elastic material ( $G'$  [red triangles]  $>$   $G''$  [green triangles]) over the studied interval of 11 min.  $G' > G''$  immediately at  $t = 0$  min for this sample. In (b), unmodified chitosan (0.25%)/blood (50%) mixture shows that the sample remains as a viscous sol ( $G''$  [green triangles]  $>$   $G'$  [red triangles]) over the same interval. Lastly, in (c), a sample comparison in a rat femoral vein injury model demonstrates that hm-chitosan (HM-CS) solution (0.5%) significantly decreases bleeding time relative to saline buffer (SAL) and native chitosan (CS) solution (0.5%) controls.

In Figures 6.3a and 6.3b, we probe the issue of time to gelation. This is again a rheological comparison between hm-chitosan/blood and chitosan/blood mixtures using a time sweep at a constant frequency of 10 rad/s. The experiments were done by mixing a given polymer and blood and quickly loading into the rheometer. For the hm-chitosan/blood mixture,  $G'$  exceeds  $G''$  immediately at  $t = 0$ , and thereafter there is a small increase in  $G'$  over the studied time interval of 11 min. In contrast, the unmodified/blood mixture displays much lower values of  $G'$  and  $G''$ , with  $G''$  exceeding  $G'$  throughout the studied time interval of 11 min. This suggests that hm-chitosan gels blood rapidly upon application. It also highlights the fact that the hydrophobes grafted to the chitosan backbone significantly enhance the hemostatic ability of the polymer.

**Results from Animal Injury Models.** Figure 6.3c displays a bleeding time study on a minor injury model in a small animal. Femoral vein injuries were created in Long-Evans adult rats ( $n = 5$  per sample) via scalpel. Bleeding times were measured for all injuries. All materials were applied to the injury via a 22 G needle syringe. One mL of a saline control achieved hemostasis in  $50 \pm 4$  s; an equal volume of an unmodified chitosan control (0.5 wt%) showed a similar time to hemostasis of  $47 \pm 3$  sec. In contrast, 1 mL of an hm-chitosan solution, also at 0.5 wt%, achieved hemostasis in a period of  $4.5 \pm 0.6$  sec. The hm-chitosan was also able to control bleeding from a porcine femoral vein injury in a comparable period of time ( $5.6 \pm 0.7$  s). Hence, this amphiphilic chitosan displays promise over unmodified chitosan as a hemostat for minor wounds in animals.

In order to treat high-pulsatile injuries in large animals, we produced freeze-dried bandages of this hm-chitosan. 150 mL of a 0.8 wt% hm-chitosan solution was prepared and then cast into a plastic container of dimensions 4'' × 4'' × 0.5''. The solution was frozen at -40°C and vacuumed at  $50 \times 10^{-6}$  mbar for several days. Similar bandages of unmodified chitosan have been used commercially, particularly for US troops in the conflicts in Iraq and Afghanistan.<sup>146,166</sup> While these unmodified chitosan bandages generally provide adequate initial first aid, they fail to maintain hemostasis for a period of longer than 1.6 h, and they allow secondary bleedings to occur.<sup>167</sup> This is likely due to loss of tissue adhesion during the studied timeframe as the bandages become saturated with liquid blood, thus displacing key electrostatic interactions between chitosan and soft tissue.

We have performed an evaluation of the effectiveness of the hm-chitosan bandages on a pig femoral artery injury model ( $n = 3$ ). Figure 6.4 displays photographs from a representative application of the bandage to a femoral artery puncture (4.4 mm punch), which is fatal within 15 minutes left untreated. Figure 6.4a displays the blood pooling with the open cavity after puncture, Figure 6.4b displays the application of the bandage, Figure 6.4c displays the bandage successfully halting bleeding after 2 min of compression, and Figure 6.4d shows the arterial puncture successfully clotted after removal of the bandage (3 h after application). All pigs survived for the duration of the experiment, after which they were euthanized according to protocol. In sum, the bandage was highly effective at treating a severe bleeding injury in pigs, no secondary bleedings occurred during the studied timeframe, and no toxicity was observed.

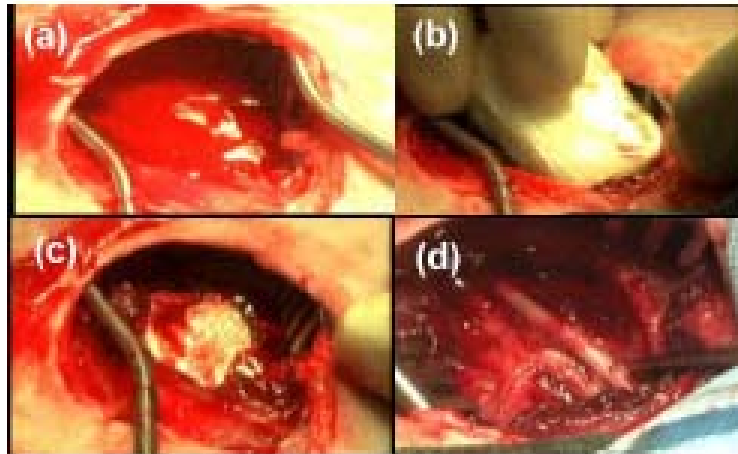


**Figure 6.4. Application of an hm-chitosan sponge to a porcine femoral artery puncture.** In (a) the injury was created in the femoral artery, resulting in high-pulsatile flow. An hm-chitosan is then applied to the injury in (b) by direct compression. After 2 min of compression, the bandage is observed in (c) to be attached to the wound site and providing hemostasis. The bandage is removed after 180 min (d) with no rebleeding during the studied interval.

We believe that a dual effect is occurring during the use of the hm-chitosan bandage on severe injuries. First, the hm-chitosan that comes in direct contact with the blood dissolves slightly, and in turn, helps gel the blood in the manner highlighted in Figure 6.2a. Because the blood in the vicinity of the bandage gets gelled, it does not soak up the bandage readily, and the gelled blood presumably acts as a barrier to blood loss through the puncture. (This is similar to the postulated action of solid fibrin bandages, as discussed in the Introduction.) Secondly, the parts of the bandage that come in direct contact with the tissue are able to adhere much more strongly to the tissue than an unmodified chitosan bandage. Indeed, *in vitro* tissue adhesion studies have shown that increasing the level of hydrophobic modification along the chitosan backbone enhances the peel strength of the chitosan in a linear fashion (data not shown). The improved

adhesion decreases the likelihood of bandage delamination and thereby the possibility of secondary bleeding. We believe the improved adhesion of hm-chitosan to tissue may also be a consequence of hydrophobic interactions between polymer hydrophobes and the underlying tissue cells. Although these hydrophobic interactions are non-covalent and hence weak individually, they sum up to a significantly large interaction over the entire surface area of the tissue. As such, the bandage acts like a nano-scale Velcro material in its interaction with soft tissue, i.e. it adheres strongly due to many nano-scale interactions, but yet it can be conveniently removed with no damage to underlying tissue or nerves since each individual interaction is weak.

**Probing the Mechanism for Blood Gelling.** In order to probe the mechanism of gel formation, we separated blood plasma from the hemotacrit via centrifugation. The cells were resuspended in an equal volume of Hank's Balanced Salt Solution and then mixed with hm-chitosan. Figure 6.5 shows the dynamic rheology of 0.25% hm-chitosan with 50% diluted blood cell suspension. The rheology mirrors that of the whole blood mixed with the same concentration hm-chitosan quite closely, with  $G' > G''$  over the entire range of frequencies. Also, it is observed visually that the mixture, like whole blood, holds its own weight upon vial inversion. In contrast, the mixture of 0.25% hm-chitosan with 50% diluted plasma shows  $G'' > G'$  over the range of frequencies, and visually appears to flow freely. This set of results shows that the cells play a key role in the gelation process.



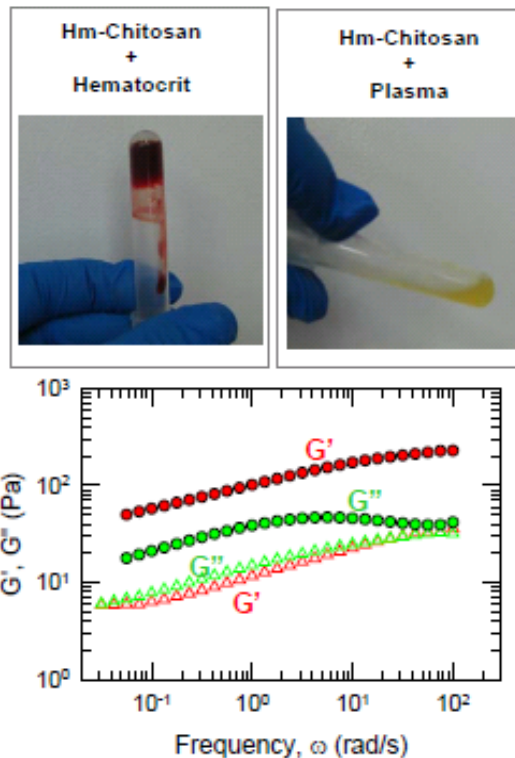


**Figure 6.5. Dynamic rheology of hm-polymer mixed with separated blood hematocrit and plasma.** The hm-chitosan concentration is maintained at 0.25%. Hematocrit was resuspended in isotonic buffer after centrifugation; plasma was removed and stored for use. Visual observation of an hm-chitosan-hematocrit mixture shows that the sample can hold its weight upon vial inversion, whereas an hm-chitosan-plasma mixture flows freely as a viscous liquid. Dynamic rheology confirms the visual evidence, as the hematocrit mixed with polymer ( $G'$  [closed red circles] and  $G''$  [closed green circles]) is that of a gel-like elastic material which relaxes slightly over long times. In contrast, the rheology of the plasma mixed with polymer ( $G'$  [open red triangles] and  $G''$  [open green triangles]) is close to that of a sol-gel transition.

**Reversal of Blood Gelling.** While new hemostatic technologies have advanced rapidly over the past 15 years, there always exists a concern of undesired embolism formation from a new hemostat. In our probing of the mechanism of blood gelation via hm-chitosan, we have incidentally discovered a means of mitigating concerns of blood vessel embolization. Cyclodextrins (CDs) are a class of supramolecules known for their ability to modulate hydrophobic interactions between associating polymers.<sup>33,38</sup> CDs are

biologically safe molecules often used frequently in foods, pharmaceutical excipients, etc. Of the three major cyclodextrins (CDs), (1)  $\alpha$ -CD, (2)  $\beta$ -CD, and (3)  $\gamma$ -CD, it is  $\alpha$ -CD that shows a strong affinity for single-tailed hydrophobes. In a rheological study previously reported from our group, all three cyclodextrins were added to aqueous solutions of telechelic polyethylene oxide with single tailed n-alkyl grafts on either end.<sup>168</sup> The  $\alpha$ -CD decreased the viscosity of the polymer solution much more rapidly than the other two CD species.  $\alpha$ -CD has also been used in several other studies as a viscosity reducer for associating biopolymers. This phenomenon is thought to occur due to the molecular architecture of the  $\alpha$ -CD.  $\alpha$ -CD is a barrel shaped supramolecule; the exterior of the barrel is very hydrophilic, allowing solubility in water, whereas the center of the barrel is hydrophobic. The diameter of the barrel is 5.4 Å, which in contrast to that of  $\beta$ -CD and  $\gamma$ -CD, is optimal for associating with single-tailed alkyl chains. In this way, the barrels are able to “cap” the hydrophobes along the backbone of the polymer, and hence screen their hydrophobic interactions from one another, in effect reducing the apparent viscosity of a bulk solution of hydrophobically-modified polymer.

Because of  $\alpha$ -CD's ability to eliminate hydrophobic interactions among neighboring polymer chains, we hypothesized that given enough concentration of  $\alpha$ -CD in solution, this supramolecule would be able to displace existing interactions between the hydrophobes and the bilayers of blood cell membranes. A schematic of this  $\alpha$ -CD “screening” hypothesis is shown above in Figure 6.6a. The key concept here is that the addition of  $\alpha$ -CD in aqueous media to an hm-chitosan/blood gel, triggers a “self-disassembly” of the elastic 3-dimensional network into a freely flowing fluid. In Figure

6.6b, dynamic rheology confirms this hypothesis as a hm-chitosan (0.25%)/blood (50%) displays gel-like characteristics with  $G'$  exceeding  $G''$  for the studied range of frequencies, whereas the same mixture hm-chitosan (0.25%)/blood (50%) with 3 wt%  $\alpha$ -CD included displays the rheology of a freely-flowing liquid, with  $G''$  exceeding  $G'$  over the range of frequencies and significantly lower moduli values.

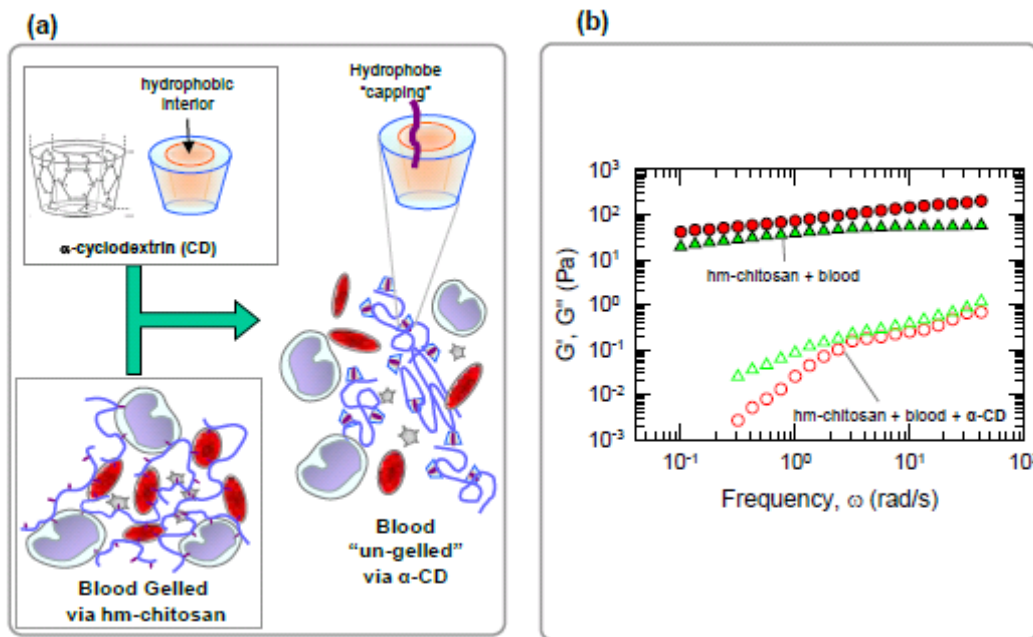


**Figure 6.6. Reversal of blood-gelation via  $\alpha$ -cyclodextrin (CD).** In (a), a cartoon of  $\alpha$ -CD displays its supramolecular barrel-shaped structure, with hydrophobic core and hydrophilic exterior. A schematic hypothesis shows that by adding these molecules together with hm-chitosan-blood mixtures, the samples become liquefied due to “capping” of hydrophobes by the  $\alpha$ -CD molecules. In (b), dynamic rheology confirms this hypothesis as a hm-chitosan (0.25%)/blood (50%) displays gel-like characteristics ( $G'$  [closed red circles] and  $G''$ [closed green triangles]), whereas a hm-chitosan (0.25%)/blood (50%)/ $\alpha$ -CD (3%) mixture displays the rheology of a freely-flowing liquid ( $G'$  [open red circles] and  $G''$ [open green triangles]).

The results of this experiment have two important implications. The first is a practical one. That is, this gelation process, or “artificial clotting,” is reversible by the

addition of a low-cost, biocompatible molecule,  $\alpha$ -CD. This is a key mitigation against embolization potentially caused by this system. Although neither dangerous clotting nor toxicity were observed during our animal studies, it is useful to have the capability to reverse the action of a hemostatic agent. The second implication is a further insight into the mechanism of gelation. Because the  $\alpha$ -CD has been shown to negate the interaction of the hydrophobes within associating biopolymer solutions in water, we can conclude that the hydrophobes must play an important role in the blood gelation process.

## 6.4. Conclusions

We have shown that the amphiphilic biopolymer, hm-chitosan, can act as an effective hemostatic agent. It has the ability to transform whole liquid blood into a gel, and it quickly stops bleeding from both minor and severe injuries in small and large animals. The parent polymer, chitosan, is itself commercially used as a material for hemostatic bandages, presumably because of its cationic nature and anti-microbial properties. However, chitosan does not change the physical character of liquid blood, i.e., a mixture of chitosan and blood remains a sol. In contrast, the addition of hm-chitosan converts liquid blood into an elastic gel with a sufficient yield stress so as to hold its weight in an inverted tube. The gelling mechanism evidently arises due to the hydrophobes on the hm-chitosan chain; we postulate that the hydrophobes anchor in blood cell membranes and thereby bridge the cells into a 3-dimensional network. The cells are thus active components (nodes or junction points) in the network rather than being physically trapped in a polymer mesh. The gelling ability of hm-chitosan is similar to that of fibrin-based sealants, but at a much lower cost and wider availability. A further

unique aspect of hm-chitosan is that its gelling effect on blood can be reversed by addition of supramolecule  $\alpha$ -CD. The reversal occurs because  $\alpha$ -CD molecules sequester the hydrophobes and prevent them from attaching to blood cells. In sum, we suggest that amphiphilic biopolymers (hydrophobes attached to a hydrophilic backbone) represent a revolutionary paradigm in hemostatic technologies.

# Chapter 7

## Conclusions and Recommendations

---

### 7.1. Conclusions

The goal of building nano-machines for improving human health from the nano-scale upward is a noble and ambitious one. Progress in the area of nanomedicine will hinge upon a fundamental understanding and embracing of the soft and “sticky” environment which exists at the biological nano-scale. Taking inspiration from the cell as the ultimate “soft machine,” one which is able to work beautifully at the nano-scale, we have blueprinted 4 self-assembled soft-material systems which display advanced functionalities with applications in the areas of controlled drug delivery, tissue engineering, and wound care.

We have shown that nanoscale vesicles of NaOA can be entrapped within gelatin hydrogels. The resulting vesicle-gel hybrids exhibit the pH-responsive properties of the NaOA vesicles. Specifically, when exposed to a pH 10 buffer, the vesicles within the gel become transformed into micelles. Vesicle disruption can be done in a controlled manner at specific locations within a gel. Gels can thus be “patterned” to have vesicle-rich and micelle-rich domains in predetermined arrangements. The utility of entrapping pH-responsive structures within the gel is in the area of controlled release of hydrophilic solutes. We show that the release of calcein dye out of a vesicle-gel into the external

solution is accelerated when the solution pH is raised to 10. This increase is attributed to a pH-induced vesicle to micelle transition within the gel, which reduces the transport resistance to dye diffusion.

We have shown that “mothership” capsules with hierarchical structural features can be formed by adding droplets of a feeder solution consisting of liposomes and chitosan, a cationic biopolymer, into a solution of anionic biopolymer (gellan gum) or surfactant (SDBS). The resulting structures are spherical capsules; assembly is achieved via electrostatic interactions between oppositely charged polymers/surfactants at the interface of the droplet. Capsule size is simply dictated by drop size. Chitosan-gellan motherships are able to sustain model drug release due via intact liposomes carrying the drug within the capsule. Chitosan-gellan motherships can be degraded by the addition of the enzyme chitosanase; complete degradation occurs over a 7 period, with intact vesicles present in the remaining solution post-degradation. Finally, hierarchical capsule-within-capsule structures were produced with either chitosan-SDBS or chitosan-gellan systems.

We have shown that vesicles and liposomes can be captured on electrodeposited films of hm-chitosan. Hm-chitosan is significantly superior in its capability for vesicle capture compared to unmodified chitosan, which implies that vesicle capture on hm-chitosan is promoted by the non-covalent binding of polymer hydrophobes to the hydrophobic interiors of vesicle bilayers. We have presented a range of evidence to show that the vesicles bound to hm-chitosan are intact structures. The evidence includes direct visualization of captured vesicles – by optical microscopy in the case of microscale

GUVs and by cryo-TEM in the case of nanoscale vesicles. Additionally, key indirect evidence for vesicle intactness comes from a study on dye-filled vesicles – upon detergent treatment, a loss of fluorescence from the film is observed, which can only be attributed to the detergent-induced disruption of intact vesicles.

Finally, we have shown that hm-chitosan, an amphiphilic biopolymer, can act as an effective hemostatic agent. It has the ability to transform whole liquid blood into a gel, and it quickly stops bleeding from both minor and severe injuries in small and large animals. The parent polymer, chitosan, does not change the physical character of liquid blood, i.e., a mixture of chitosan and blood remains a sol. The gelling mechanism evidently arises due to the hydrophobes on the hm-chitosan chain; we postulate that the hydrophobes anchor in blood cell membranes and thereby bridge the cells into a 3-dimensional network. A further unique aspect of hm-chitosan is that its gelling effect on blood can be reversed by addition of supramolecule  $\alpha$ -CD. The reversal occurs because  $\alpha$ -CD molecules sequester the hydrophobes and prevent them from attaching to blood cells.

## **7.2. Recommendations for Future Work**

Spatio-temporal control of the transition of fatty acid vesicles to micelles with the gels presented in Chapter 3 would have some interesting implications. For example, we could make potential build different gelatin gel “sections” adjacent to one another that contain different types of model drugs. It would be nice to have a way to selective choose when to release a certain kind of drug into a surrounding buffer solution. This would be



feasible with a spatiotemporal pH-trigger. There is a commercially available photobase generator called MGC which produced  $\text{OH}^-$  ion upon UV irradiation.<sup>169</sup> By incorporating this molecule into the bilayer of the vesicles prior to embedding them within the gels, we could subsequently use UV lasers to point at different spots within the gels where we want a vesicle-to-micelle transition to occur. A schematic of MGC generation of hydroxide ion is shown in figure 5.1 below:

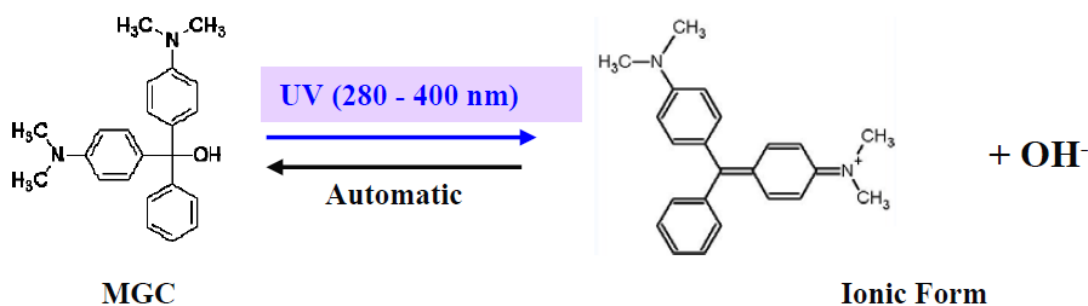


**Figure 7.1.** Photolysis of MGC, a photobase generator (PBG). Upon UV irradiation, the molecule dissociates and releases  $\text{OH}^-$ .

The “mothership” systems described in Chapter 4 have some interesting implications with regard to developmental biology or origin of life studies. For example, a water-soluble glycol chitosan could be dissolved in cell culture media along with a suspension of cells, for example, Human Umbilical Vein Endothelial Cells (HUVECs). Another set of capsules could contain a suspension of proteins, Vascular Endothelial Growth Factor. This would allow us to do very simple, but intriguing experiments where we could take one capsule containing cells and another capsule containing growth factor, then place the two within the same capsules via the one-step drop capsule-within-capsule method described in Chapter 4. It is possible that the cells may be able to escape their capsule and form a primitive blood vessel in the vicinity of the VEGF capsule. This

hypothetical scenario expresses the type of isolated signaling that can take place during embryo formation or tumor growth. More generally, a range of different packaging and release experiments could be done with these systems, and many could yield interesting results.

We remain on the subject of growth factors with regard to future work on the vesicle-biopolymer films described in Chapter 5. Certain growth factors, such as platelet-derived growth factor (PDGF) and epidermal growth factor (EGF), have been shown to accelerate the healing of chronic wounds, however their bolus administration can be problematic and costly.<sup>170</sup> The vesicle hm-chitosan films provide a simple way to therapeutically functionalize the films with both of these growth factors, and presumably would release the factors in a sustained fashion in aqueous media. (1) Proteins could be packaged inside the vesicles, (2) the vesicles could then be attached to the films, (3) and the films could then be removed from the electrodes and (4) finally placed in buffer so as to test the release of protein. Additionally, it would be worth making these films with the active component inside the vesicle and try out the films on chronic wounds in diabetic mice, relative to unmodified chitosan controls and bolus PDGF. Any progress in that regard could be very exciting.

With regard to the use of amphiphilic polymers for gelling blood, many more experiments can and should be tried. It would be instructive to try out a range of amphiphilic polymers, e.g. hm-alginate, hm-gelatin, hm-hyaluronic acid, etc., on the blood samples to determine if there are a few samples that work particularly well with

regard to gel strength and gelation time. These “winners” could then move on to small and large animal studies in head-to-head tests with fibrin-based products which dominant much of the clinical hemostat space. Of course, more large animal studies should be completed for the bandages that were presented in pig models in Chapter 6 and some key controls should be tested in those models. On a grander scheme, it would interesting to try to correlate the rheology of a given hemostat mixed with heparinized blood *in vitro* with the performance of the hemostat in important *in vivo* bleeding models. Because rheology experiments are much less expensive than animal studies, the existence of any positive correlation between *in vitro* and *in vivo* could be very valuable.

Lastly, it would be interesting to develop an hm-chitosan which is able to dissolve in cell culture media at pH 7.4, so that it could potentially gel healthy soft tissue cells. In this way, the hm-chitosan could function as a useful delivery vehicle for cells used as therapeutics (e.g. stem cell therapy for damaged heart tissue). “Cellular therapy” refers to the use of cells themselves as therapeutic agents, as opposed to small molecules or proteins as the sole active agent. A major drawback in the field of cellular therapy is lack of effective delivery mechanisms for the cells, and an associating biopolymer could potentially fill this void.<sup>171</sup>

## 8. References

- [1] Lipids, A. P. Preparation of Liposomes. **2010**.
- [2] Luisi, P. L. *Giant Vesicles*; Wiley: New York, 2000.
- [3] Howe, R. T.; Muller, R. S. "Polycrystalline silicon micromechanical beams." *Journal of the Electrochemical Society* **1983**, *130*, 1420-1423.
- [4] Freitas, R. A. "What is nanomedicine?" *Dm Disease-a-Month* **2005**, *51*, 325-341.
- [5] Freitas, R. A. "Current status of nanomedicine and medical nanorobotics." *Journal of Computational and Theoretical Nanoscience* **2005**, *2*, 1-25.
- [6] Purcell, E. M. "Life at low reynolds-number." *American Journal of Physics* **1977**, *45*, 3-11.
- [7] Luisi, P. L.; de Souza, T. P.; Stano, P. "Vesicle Behavior: In Search of Explanations." *Journal of Physical Chemistry B* **2008**, *112*, 14655-14664.
- [8] Pornpattananankul, D.; Olson, S.; Aryal, S.; Sartor, M.; Huang, C. M.; Vecchio, K.; Zhang, L. "Stimuli-Responsive Liposome Fusion Mediated by Gold Nanoparticles." *Acs Nano* **2010**, *4*, 1935-1942.
- [9] Ashraf, J.; Feix, J. B.; Butterfield, D. A. "Membrane Fluidity and Myotonia - Effects of Cholesterol and Desmosterol on Erythrocyte-Membrane Fluidity in Rats with 20,25-Diazacholesterol-Induced Myotonia and on Phospholipid Liposomes." *Bioscience Reports* **1984**, *4*, 115-120.
- [10] Evans, D. F. W., H. *The Colloidal Domain: Where Physics, Chemistry, Biology and Technology Meet*; Wiley-VCH: New York, 2001.
- [11] Lasic, D. D. *Liposomes: From Physics to Applications*; Elsevier: Amsterdam, 1983.
- [12] Kaler, E. W.; Murthy, A. K.; Rodriguez, B. E.; Zasadzinski, J. A. N. "Spontaneous Vesicle Formation in Aqueous Mixtures of Single-Tailed Surfactants." *Science* **1989**, *245*, 1371-1374.
- [13] Israelachvili, J. N. *Intermolecular and Surface Forces*; Academic Press: New York, 1992.
- [14] Hanczyc, M. M.; Fujikawa, S. M.; Szostak, J. W. "Experimental models of primitive cellular compartments: Encapsulation, growth, and division." *Science* **2003**, *302*, 618-622.

- [15] Hargreaves, W. R.; Deamer, D. W. "Liposomes from ionic, single-chain amphiphiles." *Biochemistry* **1978**, *17*, 3759-3768.
- [16] Annable, T.; Buscall, R.; Ettelaie, R.; Whittlestone, D. "The rheology of solutions of associating polymers - comparison of experimental behavior with transient network theory." *Journal of Rheology* **1993**, *37*, 695-726.
- [17] Desbrieres, J.; Martinez, C.; Rinaudo, M. "Hydrophobic derivatives of chitosan: Characterization and rheological behaviour." *International Journal of Biological Macromolecules* **1996**, *19*, 21-28.
- [18] Menchen, S.; Johnson, B.; Winnik, M. A.; Xu, B. "Flowable networks as DNA sequencing media in capillary columns." *Electrophoresis* **1996**, *17*, 1451-1459.
- [19] Alberts, B. e. a. *Molecular Biology of the Cell*; Garland Publishing: New York, 1994.
- [20] Skjak-Braek, G. A., T.; Sandford, P. *Chitin and Chitosan: Sources, Chemistry, Biochemistry, Physical Properties, and Applications*; Elsevier: London, 1988.
- [21] Illum, L. "Chitosan and its use as a pharmaceutical excipient." *Pharmaceutical Research* **1998**, *15*, 1326-1331.
- [22] Kumar, M. "A review of chitin and chitosan applications." *Reactive & Functional Polymers* **2000**, *46*, 1-27.
- [23] Miyazaki, S.; Ishii, K.; Nadai, T. "The use of chitin and chitosan as drug carriers." *Chemical & Pharmaceutical Bulletin* **1981**, *29*, 3067-3069.
- [24] Uchegbu, I. F.; Schatzlein, A. G.; Tetley, L.; Gray, A. I.; Sludden, J.; Siddique, S.; Mosha, E. "Polymeric chitosan-based vesicles for drug delivery." *Journal of Pharmacy and Pharmacology* **1998**, *50*, 453-458.
- [25] Aberg, C. M.; Chen, T. H.; Olumide, A.; Raghavan, S. R.; Payne, G. F. "Enzymatic grafting of peptides from casein hydrolysate to chitosan. potential for value-added byproducts from food-processing wastes." *Journal of Agricultural and Food Chemistry* **2004**, *52*, 788-793.
- [26] Bernkop-Schnurch, A. "Chitosan and its derivatives: potential excipients for peroral peptide delivery systems." *International Journal of Pharmaceutics* **2000**, *194*, 1-13.
- [27] Chen, T. H.; Kumar, G.; Harris, M. T.; Smith, P. J.; Payne, G. F. "Enzymatic grafting of hexyloxyphenol onto chitosan to alter surface and rheological properties." *Biotechnology and Bioengineering* **2000**, *70*, 564-573.

- [28] Yalpani, M.; Hall, L. D. "Some chemical and analytical aspects of polysaccharide modifications .3. formation of branched-chain, soluble chitosan derivatives." *Macromolecules* **1984**, *17*, 272-281.
- [29] Hirano, S.; Ohe, Y.; Ono, H. "Selective N-acylation of chitosan." *Carbohydrate Research* **1976**, *47*, 315-320.
- [30] Domszy, J. G.; Roberts, G. A. F. "Evaluation of infrared spectroscopic techniques for analyzing chitosan." *Makromolekulare Chemie-Macromolecular Chemistry and Physics* **1985**, *186*, 1671-1677.
- [31] Le Tien, C.; Lacroix, M.; Ispas-Szabo, P.; Mateescu, M. A. "N-acylated chitosan: hydrophobic matrices for controlled drug release." *Journal of Controlled Release* **2003**, *93*, 1-13.
- [32] Galant, C.; Wintgens, W.; Amiel, C.; Auvray, L. "A reversible polyelectrolyte involving a beta-cyclodextrin polymer and a cationic surfactant." *Macromolecules* **2005**, *38*, 5243-5253.
- [33] Szejtli, J. "Introduction and general overview of cyclodextrin chemistry." *Chemical Reviews* **1998**, *98*, 1743-1753.
- [34] Abdala, A. A.; Tonelli, A. E.; Khan, S. A. "Modulation of hydrophobic interactions in associative polymers using inclusion compounds and surfactants." *Macromolecules* **2003**, *36*, 7833-7841.
- [35] Burckbuchler, V.; Kjoniksen, A. L.; Galant, C.; Lund, R.; Amiel, C.; Knudsen, K. D.; Nystrom, B. "Rheological and structural characterization of the interactions between cyclodextrin compounds and hydrophobically modified alginate." *Biomacromolecules* **2006**, *7*, 1871-1878.
- [36] Karlson, L.; Thuresson, K.; Lindman, B. "Cyclodextrins in hydrophobically modified poly(ethylene glycol) solutions: Inhibition of polymer-polymer associations." *Langmuir* **2002**, *18*, 9028-9034.
- [37] Liao, D.; Dai, S.; Tam, K. C. "Rheological properties of hydrophobic ethoxylated urethane (HEUR) in the presence of methylated beta-cyclodextrin." *Polymer* **2004**, *45*, 8339-8348.
- [38] Tonelli, A. E. "Nanostructuring and functionalizing polymers with cyclodextrins." *Polymer* **2008**, *49*, 1725-1736.
- [39] Challa, R.; Ahuja, A.; Ali, J.; Khar, R. K. "Cyclodextrins in drug delivery: An updated review." *Aaps Pharmscitech* **2005**, *6*.

- [40] Macosko, C. W. *Rheology: Principles, Measurements and Applications*; VCH Publishers: New York, 1994.
- [41] Zemb, T. L., P. *Neutron, X-Ray and Light Scattering: Introduction to an Investigative Tool for Colloidal and Polymeric Systems*; Elsevier: Amsterdam, 1991.
- [42] Brown, W. *Dynamic Light Scattering: The Method and some Applications*; Clarendon Press: Oxford, 1993.
- [43] Roy, I.; Gupta, M. N. "Smart polymeric materials: Emerging biochemical applications." *Chemistry & Biology* **2003**, *10*, 1161-1171.
- [44] Alarcon, C. D. H.; Pennadam, S.; Alexander, C. "Stimuli responsive polymers for biomedical applications." *Chemical Society Reviews* **2005**, *34*, 276-285.
- [45] Peppas, N. A.; Hilt, J. Z.; Khademhosseini, A.; Langer, R. "Hydrogels in biology and medicine: From molecular principles to bionanotechnology." *Advanced Materials* **2006**, *18*, 1345-1360.
- [46] Ulijn, R. V.; Bibi, N.; Jayawarna, V.; Thornton, P. D.; Todd, S. J.; Mart, R. J.; Smith, A. M.; Gough, J. E. "Bioresponsive hydrogels." *Materials Today* **2007**, *10*, 40-48.
- [47] Djabourov, M. "Architecture of gelatin gels." *Contemporary Physics* **1988**, *29*, 273-297.
- [48] Lasic, D. D. *Liposomes: From Physics to Applications*; Elsevier: Amsterdam, 1993.
- [49] Gregoriadis, G. "Engineering liposomes for drug delivery: Progress and problems." *Trends in Biotechnology* **1995**, *13*, 527-537.
- [50] Lian, T.; Ho, R. J. Y. "Trends and developments in liposome drug delivery systems." *Journal of Pharmaceutical Sciences* **2001**, *90*, 667-680.
- [51] Weiner, A. L.; Carpentergreen, S. S.; Soehngen, E. C.; Lenk, R. P.; Popescu, M. C. "Liposome collagen gel matrix - a novel sustained drug delivery system." *Journal of Pharmaceutical Sciences* **1985**, *74*, 922-925.
- [52] Takagi, I.; Shimizu, H.; Yotsuyanagi, T. "Application of alginate gel as a vehicle for liposomes .1. Factors affecting the loading of drug-containing liposomes and drug release." *Chemical & Pharmaceutical Bulletin* **1996**, *44*, 1941-1947.
- [53] DiTizio, V.; Karlgard, C.; Lilge, L.; Khoury, A. E.; Mittelman, M. W.; DiCosmo, F. "Localized drug delivery using crosslinked gelatin gels containing liposomes:

- Factors influencing liposome stability and drug release." *Journal of Biomedical Materials Research* **2000**, *51*, 96-106.
- [54] Paavola, A.; Kilpelainen, I.; Yliruusi, J.; Rosenberg, P. "Controlled release injectable liposomal gel of ibuprofen for epidural analgesia." *International Journal of Pharmaceutics* **2000**, *199*, 85-93.
- [55] Glavas-Dodov, M.; Goracinova, K.; Mladenovska, K.; Fredro-Kumbaradzi, E. "Release profile of lidocaine HCl from topical liposomal gel formulation." *International Journal of Pharmaceutics* **2002**, *242*, 381-384.
- [56] Ruel-Gariepy, E.; Leclair, G.; Hildgen, P.; Gupta, A.; Leroux, J. C. "Thermosensitive chitosan-based hydrogel containing liposomes for the delivery of hydrophilic molecules." *Journal of Controlled Release* **2002**, *82*, 373-383.
- [57] Cistola, D. P.; Hamilton, J. A.; Jackson, D.; Small, D. M. "Ionization and phase-behavior of fatty-acids in water - application of the Gibbs phase rule." *Biochemistry* **1988**, *27*, 1881-1888.
- [58] Deamer, D. W. "The first living systems: a bioenergetic perspective." *Microbiology and Molecular Biology Reviews* **1997**, *61*, 239-&.
- [59] Szostak, J. W.; Bartel, D. P.; Luisi, P. L. "Synthesizing life." *Nature* **2001**, *409*, 387-390.
- [60] Drummond, D. C.; Zignani, M.; Leroux, J. C. "Current status of pH-sensitive liposomes in drug delivery." *Progress in Lipid Research* **2000**, *39*, 409-460.
- [61] Hoffman, A. S. "Hydrogels for biomedical applications." *Advanced Drug Delivery Reviews* **2002**, *54*, 3-12.
- [62] Lee, K. Y.; Mooney, D. J. "Hydrogels for tissue engineering." *Chemical Reviews* **2001**, *101*, 1869-1879.
- [63] Pedersen, J. S. "Analysis of small-angle scattering data from colloids and polymer solutions: modeling and least-squares fitting." *Advances in Colloid and Interface Science* **1997**, *70*, 171-210.
- [64] Kucerka, N.; Kiselev, M. A.; Balgavy, P. "Determination of bilayer thickness and lipid surface area in unilamellar dimyristoylphosphatidylcholine vesicles from small-angle neutron scattering curves: a comparison of evaluation methods." *European Biophysics Journal with Biophysics Letters* **2004**, *33*, 328-334.
- [65] Peppas, N. A. "Analysis of Fickian and non-Fickian drug release from polymers." *Pharmaceutica Acta Helvetiae* **1985**, *60*, 110-111.



- [66] Ritger, P. L.; Peppas, N. A. "A simple equation for description of solute release I. Fickian and non-Fickian release from non-swellable devices in the form of slabs, spheres, cylinders or discs." *Journal of Controlled Release* **1987**, *5*, 23-36.
- [67] Lin, C. C.; Metters, A. T. "Hydrogels in controlled release formulations: Network design and mathematical modeling." *Advanced Drug Delivery Reviews* **2006**, *58*, 1379-1408.
- [68] Breiter, M.; Hoffmann, K. "Bestimmung der diffusionskoeffizienten DH<sub>2</sub>, DH<sub>+</sub> und DOH- mit der platin-scheibenelektrode." *Zeitschrift Fur Elektrochemie* **1960**, *64*, 462-467.
- [69] Sharma, J.; Aswal, V. K.; Goyal, P. S.; Bohidar, H. B. "Small-angle neutron scattering studies of chemically cross-linked gelatin solutions and gels." *Macromolecules* **2001**, *34*, 5215-5220.
- [70] Mohanty, B.; Aswal, V. K.; Kohlbrecher, J.; Bohidar, H. B. "Length scale hierarchy in sol, gel, and coacervate phases of gelatin." *Journal of Polymer Science Part B-Polymer Physics* **2006**, *44*, 1653-1665.
- [71] Kost, J.; Langer, R. "Responsive polymeric delivery systems." *Advanced Drug Delivery Reviews* **2001**, *46*, 125-148.
- [72] Bala, K.; Vasudevan, P. "Polymeric microcapsules for drug delivery." *Journal of Macromolecular Science-Chemistry* **1981**, *A16*, 819-827.
- [73] Thies, C. "Microcapsules as drug delivery devices." *Crc Critical Reviews in Biomedical Engineering* **1982**, *8*, 335-383.
- [74] Caruso, F.; Caruso, R. A.; Mohwald, H. "Nanoengineering of inorganic and hybrid hollow spheres by colloidal templating." *Science* **1998**, *282*, 1111-1114.
- [75] Pastine, S. J.; Okawa, D.; Zettl, A.; Frechet, J. M. J. "Chemicals On Demand with Phototriggerable Microcapsules." *Journal of the American Chemical Society* **2009**, *131*, 13586-+.
- [76] Ranjha, N. M.; Khan, I. U.; Naseem, S. "Encapsulation and characterization of flurbiprofen loaded poly(N"-caprolactone)-poly(vinylpyrrolidone) blend microspheres by solvent evaporation method." *Journal of Sol-Gel Science and Technology* **2009**, *50*, 281-289.
- [77] Jalil, R.; Nixon, J. R. "Biodegradable poly(lactic acid) and polymer (lactide-co-glycolide) microcapsules - problems associated with preparative techniques and release properties." *Journal of Microencapsulation* **1990**, *7*, 297-325.
- [78] Lasic, D. D. "Liposomes." *Recherche* **1989**, *20*, 904-913.

- [79] Lasic, D. D.; Papahadjopoulos, D. "Liposomes and biopolymers in drug and gene delivery." *Current Opinion in Solid State & Materials Science* **1996**, *1*, 392-400.
- [80] Lasic, D. D.; Needham, D. "The "Stealth" liposome: A prototypical biomaterial." *Chemical Reviews* **1995**, *95*, 2601-2628.
- [81] Ishida, T.; Kojima, H.; Harashima, H.; Kiwada, H. "Biodistribution of liposomes and C3 fragments associated with liposomes: evaluation of their relationship." *International Journal of Pharmaceutics* **2000**, *205*, 183-193.
- [82] Zhao, H.; Wang, J. C.; Sun, Q. S.; Luo, C. L.; Zhang, Q. "RGD-based strategies for improving antitumor activity of paclitaxel-loaded liposomes in nude mice xenografted with human ovarian cancer." *Journal of Drug Targeting* **2009**, *17*, 10-18.
- [83] Zhang, Q.; Huang, X. E.; Gao, L. L. "A clinical study on the premedication of paclitaxel liposome in the treatment of solid tumors." *Biomedicine & Pharmacotherapy* **2009**, *63*, 603-607.
- [84] Kibat, P. G.; Igari, Y.; Wheatley, M. A.; Eisen, H. N.; Langer, R. "Enzymatically Activated Microencapsulated Liposomes Can Provide Pulsatile Drug Release." *Faseb Journal* **1990**, *4*, 2533-2539.
- [85] Cohen, S.; Bernstein, H.; Hewes, C.; Chow, M.; Langer, R. "The pharmacokinetics of, and humoral responses to, antigen delivered by microencapsulated liposomes." *Proceedings of the National Academy of Sciences of the United States of America* **1991**, *88*, 10440-10444.
- [86] Peniche, C.; Arguelles-Monal, W.; Peniche, H.; Acosta, N. "Chitosan: An attractive biocompatible polymer for microencapsulation." *Macromolecular Bioscience* **2003**, *3*, 511-520.
- [87] Machluf, M.; Apte, R. N.; Regev, O.; Cohen, S. "Enhancing the immunogenicity of liposomal hepatitis B surface antigen (HBsAg) by controlling its delivery from polymeric microspheres." *Journal of Pharmaceutical Sciences* **2000**, *89*, 1550-1557.
- [88] Machluf, M.; Regev, O.; Peled, Y.; Kost, J.; Cohen, S. "Characterization of microencapsulated liposome systems for the controlled delivery of liposome-associated macromolecules." *Journal of Controlled Release* **1997**, *43*, 35-45.
- [89] Feng, S. S.; Ruan, G.; Li, Q. T. "Fabrication and characterizations of a novel drug delivery device liposomes-in-microsphere (LIM)." *Biomaterials* **2004**, *25*, 5181-5189.

- [90] Dhoot, N. O.; Wheatley, M. A. "Microencapsulated Liposomes in controlled drug delivery: Strategies to modulate drug release and eliminate the burst effect." *Journal of Pharmaceutical Sciences* **2003**, *92*, 679-689.
- [91] Ramadas, M.; Paul, W.; Dileep, K. J.; Anitha, Y.; Sharma, C. P. "Lipoinulin encapsulated alginate-chitosan capsules: intestinal delivery in diabetic rats." *Journal of Microencapsulation* **2000**, *17*, 405-411.
- [92] Stenekes, R. J. H.; Loebis, A. E.; Fernandes, C. M.; Crommelin, D. J. A.; Hennink, W. E. "Controlled release of liposomes from biodegradable dextran microspheres: A novel delivery concept." *Pharmaceutical Research* **2000**, *17*, 690-695.
- [93] Glade-Bender, J.; Kandel, J. J.; Yamashiro, D. J. "VEGF blocking therapy in the treatment of cancer." *Expert Opinion on Biological Therapy* **2003**, *3*, 263-276.
- [94] Bahler, M.; Benfenati, F.; Valtorta, F.; Czernik, A. J.; Greengard, P. "Characterization of synapsin-I fragments produced by cysteine-specific cleavage - a study of their interactions with F-actin." *Journal of Cell Biology* **1989**, *108*, 1841-1849.
- [95] Liu, Y. J.; Edwards, R. H. "The role of vesicular transport proteins in synaptic transmission and neural degeneration." *Annual Review of Neuroscience* **1997**, *20*, 125-156.
- [96] Volz, T. J.; Farnsworth, S. J.; Hanson, G. R.; Fleckenstein, A. E. Methylphenidate-Induced Alterations in Synaptic Vesicle Trafficking and Activity Functional Consequences and Therapeutic Implications. In *Drug Addiction: Research Frontiers and Treatment Advances*; Kuhar, M. J., Ed., 2008; Vol. 1139; pp 285-290.
- [97] Chang, T. M. S. "Semipermeable microcapsules." *Science* **1964**, *146*, 524-&.
- [98] Kjoniksen, A. L.; Iversen, C.; Nystrom, B.; Nakken, T.; Palmgren, O. "Light scattering study of semidilute aqueous systems of chitosan and hydrophobically modified chitosans." *Macromolecules* **1998**, *31*, 8142-8148.
- [99] Lee, J. H.; Gustin, J. P.; Chen, T. H.; Payne, G. F.; Raghavan, S. R. "Vesicle-biopolymer gels: Networks of surfactant vesicles connected by associating biopolymers." *Langmuir* **2005**, *21*, 26-33.
- [100] Fujii, T.; Ogiwara, D.; Ohkawa, K.; Yamamoto, H. "Alkaline phosphatase encapsulated in gellan-chitosan hybrid capsules." *Macromolecular Bioscience* **2005**, *5*, 394-400.

- [101] Yamamoto, H.; Senoo, Y. "Polyion complex fiber and capsule formed by self-assembly of chitosan and gellan at solution interfaces." *Macromolecular Chemistry and Physics* **2000**, *201*, 84-92.
- [102] Lapitsky, Y.; Eskuchen, W. J.; Kaler, E. W. "Surfactant and polyelectrolyte gel particles that swell reversibly." *Langmuir* **2006**, *22*, 6375-6379.
- [103] Babak, V. G.; Merkovich, E. A.; Desbrieres, J.; Rinaudo, M. "Formation of an ordered nanostructure in surfactant-polyelectrolyte complexes formed by interfacial diffusion." *Polymer Bulletin* **2000**, *45*, 77-81.
- [104] Lasic, D. D. "Novel applications of liposomes." *Trends in Biotechnology* **1998**, *16*, 307-321.
- [105] Lasic, D. D.; Papahadjopoulos, D. "Liposomes revisited." *Science* **1995**, *267*, 1275-1276.
- [106] Lipowsky, R.; Seifert, U. "Adhesion of Vesicles and Membranes." *Molecular Crystals and Liquid Crystals* **1991**, *202*, 17-25.
- [107] McConnell, H. M.; Watts, T. H.; Weis, R. M.; Brian, A. A. "Supported Planar Membranes in Studies of Cell-Cell Recognition in the Immune-System." *Biochimica Et Biophysica Acta* **1986**, *864*, 95-106.
- [108] Naumann, R.; Baumgart, T.; Graber, P.; Jonczyk, A.; Offenhausser, A.; Knoll, W. "Proton transport through a peptide-tethered bilayer lipid membrane by the H<sup>+</sup>-ATP synthase from chloroplasts measured by impedance spectroscopy." *Biosensors & Bioelectronics* **2002**, *17*, 25-34.
- [109] Puu, G.; Gustafson, I.; Artursson, E.; Ohlsson, P. A. "Retained Activities of Some Membrane-Proteins in Stable Lipid Bilayers on a Solid Support." *Biosensors & Bioelectronics* **1995**, *10*, 463-476.
- [110] Fisher, M. I.; Tjarnhage, T. "Structure and activity of lipid membrane biosensor surfaces studied with atomic force microscopy and a resonant mirror." *Biosensors & Bioelectronics* **2000**, *15*, 463-471.
- [111] Nikolelis, D. P.; Pantoulis, S. "A minisensor for the rapid screening of sucralose based on surface-stabilized bilayer lipid membranes." *Biosensors & Bioelectronics* **2000**, *15*, 439-444.
- [112] Rongen, H. A. H.; Bult, A.; vanBennekom, W. P. "Liposomes and immunoassays." *Journal of Immunological Methods* **1997**, *204*, 105-133.

- [113] Szymanska, I.; Radecka, H.; Radecki, J.; Kikut-Ligaj, D. "Fullerene modified supported lipid membrane as sensitive element of sensor for odorants." *Biosensors & Bioelectronics* **2001**, *16*, 911-915.
- [114] Cremer, P. S.; Boxer, S. G. "Formation and spreading of lipid bilayers on planar glass supports." *Journal of Physical Chemistry B* **1999**, *103*, 2554-2559.
- [115] Hook, F.; Stengel, G.; Dahlin, A. B.; Gunnarsson, A.; Jonsson, M. P.; Jonsson, P.; Reimhult, E.; Simonsson, L.; Svedhem, S. "Supported lipid bilayers, tethered lipid vesicles, and vesicle fusion investigated using gravimetric, plasmonic, and microscopy techniques." *Biointerphases* **2008**, *3*, FA108-FA116.
- [116] Yoshina-Ishii, C.; Boxer, S. G. "Arrays of mobile tethered vesicles on supported lipid bilayers." *Journal of the American Chemical Society* **2003**, *125*, 3696-3697.
- [117] Yoshina-Ishii, C.; Chan, Y. H. M.; Johnson, J. M.; Kung, L. A.; Lenz, P.; Boxer, S. G. "Diffusive dynamics of vesicles tethered to a fluid supported bilayer by single-particle tracking." *Langmuir* **2006**, *22*, 5682-5689.
- [118] Lunelli, L.; Pasquardini, L.; Pederzoli, C.; Vanzetti, L.; Anderle, M. "Covalently anchored lipid structures on amine-enriched polystyrene." *Langmuir* **2005**, *21*, 8338-8343.
- [119] Sofou, S.; Thomas, J. L. "Stable adhesion of phospholipid vesicles to modified gold surfaces." *Biosensors & Bioelectronics* **2003**, *18*, 445-455.
- [120] Boukobza, E.; Sonnenfeld, A.; Haran, G. "Immobilization in surface-tethered lipid vesicles as a new tool for single biomolecule spectroscopy." *Journal of Physical Chemistry B* **2001**, *105*, 12165-12170.
- [121] Jung, L. S.; Shumaker-Parry, J. S.; Campbell, C. T.; Yee, S. S.; Gelb, M. H. "Quantification of tight binding to surface-immobilized phospholipid vesicles using surface plasmon resonance: Binding constant of phospholipase A(2)." *Journal of the American Chemical Society* **2000**, *122*, 4177-4184.
- [122] Patel, A. R.; Frank, C. W. "Quantitative analysis of tethered vesicle assemblies by quartz crystal microbalance with dissipation monitoring: Binding dynamics and bound water content." *Langmuir* **2006**, *22*, 7587-7599.
- [123] Wu, L. Q.; Gadre, A. P.; Yi, H. M.; Kastantin, M. J.; Rubloff, G. W.; Bentley, W. E.; Payne, G. F.; Ghodssi, R. "Voltage-dependent assembly of the polysaccharide chitosan onto an electrode surface." *Langmuir* **2002**, *18*, 8620-8625.
- [124] Wu, L. Q.; Yi, H. M.; Li, S.; Rubloff, G. W.; Bentley, W. E.; Ghodssi, R.; Payne, G. F. "Spatially selective deposition of a reactive polysaccharide layer onto a patterned template." *Langmuir* **2003**, *19*, 519-524.

- [125] Fernandes, R.; Wu, L. Q.; Chen, T. H.; Yi, H. M.; Rubloff, G. W.; Ghodssi, R.; Bentley, W. E.; Payne, G. F. "Electrochemically induced deposition of a polysaccharide hydrogel onto a patterned surface." *Langmuir* **2003**, *19*, 4058-4062.
- [126] Payne, G. F.; Raghavan, S. R. "Chitosan: a soft interconnect for hierarchical assembly of nano-scale components." *Soft Matter* **2007**, *3*, 521-527.
- [127] Lee, J. H.; Agarwal, V.; Bose, A.; Payne, G. F.; Raghavan, S. R. "Transition from unilamellar to bilamellar vesicles induced by an amphiphilic biopolymer." *Physical Review Letters* **2006**, *96*.
- [128] Zhu, C.; Lee, J. H.; Raghavan, S. R.; Payne, G. F. "Bioinspired vesicle restraint and mobilization using a biopolymer scaffold." *Langmuir* **2006**, *22*, 2951-2955.
- [129] Zhu, C.; Wu, L. Q.; Wang, X.; Lee, J. H.; English, D. S.; Ghodssi, R.; Raghavan, S. R.; Payne, G. F. "Reversible vesicle restraint in response to spatiotemporally controlled electrical signals: A bridge between electrical and chemical signaling modes." *Langmuir* **2007**, *23*, 286-291.
- [130] Li, H.; An, J. H.; Park, J. S.; Han, K. "Multivesicular liposomes for oral delivery of recombinant human epidermal growth factor." *Archives of Pharmacal Research* **2005**, *28*, 988-994.
- [131] Esquenet, C.; Terech, P.; Boue, F.; Buhler, E. "Structural and rheological properties of hydrophobically modified polysaccharide associative networks." *Langmuir* **2004**, *20*, 3583-3592.
- [132] Kaler, E. W.; Herrington, K. L.; Murthy, A. K.; Zasadzinski, J. A. N. "Phase-Behavior and Structures of Mixtures of Anionic and Cationic Surfactants." *Journal of Physical Chemistry* **1992**, *96*, 6698-6707.
- [133] Angelova, M. I.; Dimitrov, D. S. "Liposome electroformation." *Faraday Discussions* **1986**, *81*, 303-+.
- [134] Mathivet, L.; Cribier, S.; Devaux, P. F. "Shape change and physical properties of giant phospholipid vesicles prepared in the presence of an AC electric field." *Biophysical Journal* **1996**, *70*, 1112-1121.
- [135] Macfarlane, R. G. "Enzyme Cascade in Blood Clotting Mechanism + Its Function as Biochemical Amplifier." *Nature* **1964**, *202*, 498-&.
- [136] Champion, H. R.; Bellamy, R. F.; Roberts, C. P.; Leppaniemi, A. "A profile of combat injury." *Journal of Trauma-Injury Infection and Critical Care* **2003**, *54*, S13-S19.

- [137] Stewart, R. M.; Myers, J. G.; Dent, D. L.; Ermis, P.; Gray, G. A.; Villarreal, R.; Blow, O.; Woods, B.; McFarland, M.; Garavaglia, J.; Root, H. D.; Pruitt, B. A. "Seven hundred fifty-three consecutive deaths in a level trauma center: The argument for injury prevention." *Journal of Trauma-Injury Infection and Critical Care* **2003**, *54*, 66-70.
- [138] Cattaneo, M. "Review of clinical experience of desmopressin in patients with congenital and acquired bleeding disorders." *European Journal of Anaesthesiology* **1997**, *14*, 10-14.
- [139] Gill, J. C. "Treatment of urgent bleeding in von Willebrand disease." *Thrombosis Research* **2007**, *120*, S21-S25.
- [140] Peyvandi, F.; Kaufman, R. J.; Seligsohn, U.; Salomon, O.; Bolton-Maggs, P. H. B.; Spreafico, M.; Menegatti, M.; Palla, R.; Siboni, S.; Mannucci, P. M. "Rare bleeding disorders." *Haemophilia* **2006**, *12*, 137-142.
- [141] Neuffer, M. C.; McDivitt, J.; Rose, D.; King, K.; Cloonan, C. C.; Vayer, J. S. "Hemostatic dressings for the first responder: A review." *Military Medicine* **2004**, *169*, 716-720.
- [142] Reiss, R. F.; Oz, M. C. "Autologous fibrin glue: Production and clinical use." *Transfusion Medicine Reviews* **1996**, *10*, 85-92.
- [143] Holcomb, J. B.; Pusateri, A. E.; Hess, J. R.; Hetz, S. P.; Harris, R. A.; Tock, B. B.; Drohan, W. N.; MacPhee, M. J. "Implications of new dry fibrin sealant technology for trauma surgery." *Surgical Clinics of North America* **1997**, *77*, 943-&.
- [144] Saltz, R.; Sierra, D.; Feldman, D.; Saltz, M. B.; Dimick, A.; Vasconez, L. O. "Experimental and Clinical-Applications of Fibrin Glue." *Plastic and Reconstructive Surgery* **1991**, *88*, 1005-1015.
- [145] Larson, M. J.; Bowersox, J. C.; Lim, R. C.; Hess, J. R. "Efficacy of a Fibrin Hemostatic Bandage in Controlling Hemorrhage from Experimental Arterial Injuries." *Archives of Surgery* **1995**, *130*, 420-422.
- [146] Pusateri, A. E.; Holcomb, J. B.; Kheirabadi, B. S.; Alam, H. B.; Wade, C. E.; Ryan, K. L. "Making sense of the preclinical literature on advanced hemostatic products." *Journal of Trauma-Injury Infection and Critical Care* **2006**, *60*, 674-682.
- [147] Kheirabadi, B. S.; Scherer, M. R.; Estep, J. S.; Dubick, M. A.; Holcomb, J. B. "Determination of Efficacy of New Hemostatic Dressings in a Model of

- Extremity Arterial Hemorrhage in Swine." *Journal of Trauma-Injury Infection and Critical Care* **2009**, *67*, 450-460.
- [148] Arnaud, F.; Teranishi, K.; Tomori, T.; Carr, W.; McCarron, R. "Comparison of 10 hemostatic dressings in a groin puncture model in swine." *Journal of Vascular Surgery* **2009**, *50*, 632-639.
- [149] Teitel, J. M. "Recombinant factor VIIa versus aPCCs in haemophiliacs with inhibitors: treatment and cost considerations." *Haemophilia* **1999**, *5*, 43-49.
- [150] Alam, H. B.; Uy, G. B.; Miller, D.; Koustova, E.; Hancock, T.; Inocencio, R.; Anderson, D.; Llorente, O.; Rhee, P. "Comparative analysis of hemostatic agents in a swine model of lethal groin injury." *Journal of Trauma-Injury Infection and Critical Care* **2003**, *54*, 1077-1082.
- [151] Cox, E. D.; Schreiber, M. A.; McManus, J.; Wade, C. E.; Holcomb, J. B. "New hemostatic agents in the combat setting." *Transfusion* **2009**, *49*, 248S-255S.
- [152] Kheirabadi, B. S.; Edens, J. W.; Terrazas, I. B.; Estep, J. S.; Klemcke, H. G.; Dubick, M. A.; Holcomb, J. B. "Comparison of New Hemostatic Granules/Powders With Currently Deployed Hemostatic Products in a Lethal Model of Extremity Arterial Hemorrhage in Swine." *Journal of Trauma-Injury Infection and Critical Care* **2009**, *66*, 316-328.
- [153] Ellis-Behnke, R. G.; Liang, Y.-X.; Tay, D. K. C.; Kau, P. W. F.; Schneider, G. E.; Zhang, S.; Wu, W.; So, K.-F. "Nano hemostat solution: immediate hemostasis at the nanoscale." *Nanomedicine: Nanotechnology, Biology and Medicine* **2006**, *2*, 207-215.
- [154] Zhang, S. G.; Holmes, T.; Lockshin, C.; Rich, A. "Spontaneous Assembly of a Self-Complementary Oligopeptide to Form a Stable Macroscopic Membrane." *Proceedings of the National Academy of Sciences of the United States of America* **1993**, *90*, 3334-3338.
- [155] Dai, T. H.; Tegos, G. P.; Burkatovskaya, M.; Castano, A. P.; Hamblin, M. R. "Chitosan Acetate Bandage as a Topical Antimicrobial Dressing for Infected Burns." *Antimicrobial Agents and Chemotherapy* **2009**, *53*, 393-400.
- [156] Burkatovskaya, M.; Tegos, G. P.; Swietlik, E.; Demidova, T. N.; Castano, A. P.; Hamblin, M. R. "Use of chitosan bandage to prevent fatal infections developing from highly contaminated wounds in mice." *Biomaterials* **2006**, *27*, 4157-4164.
- [157] Kean, T.; Thanou, M. "Biodegradation, biodistribution and toxicity of chitosan." *Advanced Drug Delivery Reviews*, *62*, 3-11.



- [158] Pillai, C. K. S.; Paul, W.; Sharma, C. P. "Chitin and chitosan polymers: Chemistry, solubility and fiber formation." *Progress in Polymer Science* **2009**, *34*, 641-678.
- [159] Acheson, E. M.; Kheirabadi, B. S.; Deguzman, R.; Dick, E. J.; Holcomb, J. B. "Comparison of hemorrhage control agents applied to lethal extremity arterial hemorrhages in swine." *Journal of Trauma-Injury Infection and Critical Care* **2005**, *59*, 865-874.
- [160] Fischer, T. H.; Connolly, R.; Thatte, H. S.; Schwaitzberg, S. S. "Comparison of structural and hemostatic properties of the poly-N-acetyl glucosamine Syvek Patch with products containing chitosan." *Microscopy Research and Technique* **2004**, *63*, 168-174.
- [161] Millner, R. W. J.; Lockhart, A. S.; Bird, H.; Alexiou, C. "A New Hemostatic Agent: Initial Life-Saving Experience With Celox (Chitosan) in Cardiothoracic Surgery." *Annals of Thoracic Surgery* **2009**, *87*, E13-E14.
- [162] Valentine, R.; Athanasiadis, T.; Moratti, S.; Hanton, L.; Robinson, S.; Wormald, P. J. "The efficacy of a novel chitosan gel on hemostasis and wound healing after endoscopic sinus surgery." *American Journal of Rhinology & Allergy*, *24*, 70-75.
- [163] Meier, W.; Hotz, J.; GuntherAusborn, S. "Vesicle and cell networks: Interconnecting cells by synthetic polymers." *Langmuir* **1996**, *12*, 5028-5032.
- [164] Geerligs, M.; Peters, G. W. M.; Ackermans, P. A. J.; Oomens, C. W. J.; Baaijens, F. P. T. "Linear viscoelastic behavior of subcutaneous adipose tissue." *Biorheology* **2008**, *45*, 677-688.
- [165] Kiss, M. Z.; Varghese, T.; Hall, T. J. "Viscoelastic characterization of in vitro canine tissue." *Physics in Medicine and Biology* **2004**, *49*, 4207-4218.
- [166] Wedmore, I.; McManus, J. G.; Pusateri, A. E.; Holcomb, J. B. "A special report on the chitosan-based hemostatic dressing: Experience in current combat operations." *Journal of Trauma-Injury Infection and Critical Care* **2006**, *60*, 655-658.
- [167] Kheirabadi, B. S.; Acheson, E. M.; Deguzman, R.; Sondeen, J. L.; Ryan, K. L.; Delgado, A.; Dick, E. J.; Holcomb, J. B. "Hemostatic efficacy of two advanced dressings in an aortic hemorrhage model in swine." *Journal of Trauma-Injury Infection and Critical Care* **2005**, *59*, 25-34.
- [168] Kumar, R.; Raghavan, S. R. "Thermothickening in Solutions of Telechelic Associating Polymers and Cyclodextrins." *Langmuir*, *26*, 56-62.
- [169] Irie, M. "Light-induced reversible pH change." *Journal of the American Chemical Society* **1983**, *105*, 2078-2079.

- [170] Ulubayram, K.; Cakar, A. N.; Korkusuz, P.; Ertan, C.; Hasirci, N. "EGF containing gelatin-based wound dressings." *Biomaterials* **2001**, 22, 1345-1356.
- [171] Drury, J. L.; Boontheeku, T.; Mooney, D. J. "Cellular cross-linking of peptide modified hydrogels." *Journal of Biomechanical Engineering-Transactions of the Asme* **2005**, 127, 220-228.